Polyethylene Wear Modeling in Modular Total Knee Replacements using Finite Element Simulation

By

Sean Tyler O'Brien

A thesis submitted to
the Faculty of Graduate Studies
in partial fulfilment of
the requirements for the degree of
Master of Science

Department of Mechanical Engineering
Faculty of Engineering
University of Manitoba
Winnipeg, Manitoba

October 2011

Abstract

A computational model for the prediction of articular and backside polyethylene (PE) wear of total knee replacements (TKRs) could enable the optimization of TKRs for the reduction of polyethylene wear, thereby improving the long term success of TKRs. A finite element model was developed for the TKR and the results were implemented in a computational wear model to assess PE wear. The wear factors of Archard's wear law were identified by implementing the finite element simulation results along with knee simulator wear test results. Archard's wear law was found to have insufficient accuracy for the purpose of optimization. Therefore, a novel computational wear model was developed by the author based on a theoretical understanding of the molecular behavior of PE. The model predicted result fell within the standard deviation of the independent knee simulator wear test results, indicating a high level of accuracy for the novel computational wear model.

Acknowledgments

Firstly, I would like to thank my advisors, Dr. Christine Wu, Dr. Yunhua Luo and Dr. Jan Brandt. I greatly appreciate their guidance and support throughout my studies. Their extensive knowledge and mentorship have made this research possible.

I would like to thank DePuy Orthopedics (Warsaw, IN) for providing the manufacturing drawings of the AMK femoral and tibial tray components, as well as the CAD model of the AMK tibial insert.

I would also like to thank Matrix Biomedical, the Orthopaedic Innovation Centre (OIC) and the Mathematics of Information Technology and Complex Systems (MITACS) for the funding which has enabled this research to be completed. In addition, the computationally intensive finite element models of this thesis could not have been completed without the use of the 48 compute core cluster of the OIC. I would like to thank the OIC for the use of their cluster as well as for the use of their ShapeGrabber Laser Scanner, Solidworks License and Abaqus License.

I would also like to thank, the Concordia Joint Replacement Group (CJRG), for providing an excellent connection to the application of orthopaedic engineering. I would like to thank the research engineers Martin Petrak, and Dr. Urs Wyss for their guidance on this project, as well as sharing their knowledge and experience with me. I would like to thank my fellow engineering students and all the staff at CJRG, it has been a pleasure to

work with all of you. I would also like to thank the orthopaedic surgeons Dr. Eric Bohm, Dr. Tom Turgeon, Dr. Colin Burnell, and Dr. David Hedden, for sharing their knowledge of orthopaedics with me.

I would like to thank my parents, Shirl and Gord O'Brien, for all their support and encouragement throughout my education. I greatly appreciate all that you have done for me. I would also like to thank my parent in-laws Gail and Laurie Hall for their encouragement and enthusiasm in my research work.

Lastly I would like to thank my wife and best friend, Laura Hall, for her outstanding encouragement, support, interest and excitement in my research. Thank you for your unwavering excitement and encouragement no matter how much time I spent on this thesis.

Dedication

To Laura Hall

Contents

List of Tables

List of Figures

List of Symbols

P	Contact Pressure
E	Young's Modulus
ν	Poisson's Ratio
d	Surface Overclosure Distance
h	Thickness
W_{depth}	Wear Depth
V_{wear}	Wear Volume
k	Wear Factor
S	Sliding Distance
CS	Cross Shear
$W_{cross\text{-}shear}$	Proportion of Work for which the Shear Force is in the Direction Perpendicular to the Principal Molecular Orientation
W_{total}	Total Work
A	Distance of Sliding Direction 1
B	Distance of Sliding Direction 2
σ	Stress
t	Time
ε	Strain

μm	Micromotion
R_w	Material Resistance to Wear
C_w	Current Work
M_{mc}	Molecular Chain Mobility
NA	Nodal Area
μ	Coefficient of Friction
B_w	Work Required to Reach the Current Cross Shear Angle at Initiation
CSA	Cross Shear Angle
CSA_i	Cross Shear Angle at Initiation of Time Step
CSA_e	Cross Shear Angle at End of Time Step
EA	Element Area
NN	Number of Nodes Associated with an Element
CD	Creep Deformation
MM	Wear Mode and Mechanism Correction Factor

List of Abbreviations

TKR	Total Knee Replacement
PE	Ultra High Molecular Weight Polyethylene
TKA	Total Knee Arthroplasty
AP	Anterior-Posterior Direction
ML	Medial-Lateral Direction
IE	Internal-External Rotation Axis
CoCr	Cobalt Chromium Molybdenum
Ti	Titanium (Ti6Al4V)
CR	Cruciate Retaining
PS	Posterior Stabilized
GA	Gamma-Air Sterilization Environment
MO	Molecular Orientation (Direction of Orientated Crystalline Lamella)
POD	Pin-on-Disk
BOF	Ball-on-Flat
FE	Finite Element
MBD	Multibody Dynamics
EF	Elastic Foundation
AMK	Anatomic Modular Knee

Mc	Million Cycles
gR	Shear Relaxation Modulus
σ	Stress
ε	Strain
DVRT	Differential Variable Reluctance Transducers
PFC	Press-Fit Condylar
PMO	Primary Molecular Orientation (the average, time independent, direction of sliding)
CMO	Current Molecular Orientation (the current, time dependant, direction of sliding)
CS	Cross Shear
CSA	Cross Shear Angle (angle between the current shear force vector and the CMO)
MM	Mode and Mechanism Factor

Chapter 1

Introduction

1.1 Total Knee Replacements

The healthy human knee joint consists of cartilage covered articulating surfaces, operating in the presence of synovial fluid, controlled and constrained by ligaments, tendons and muscles (Figure 1). The knee joint can become damaged as a result of trauma or diseases such as arthritis, thus causing pain and limiting the mobility of the patient. TKRs are used to replace the damaged articulating surfaces of the knee. Approximately 450,000 primary total knee replacement surgeries (referred to as total knee arthroplasty, TKA) were performed within the United States in 2005 [1], and 60,000 were performed in Canada [2]. The number of primary TKA procedures is projected to exceed 4 million per a year within the United States by 2030 [1].

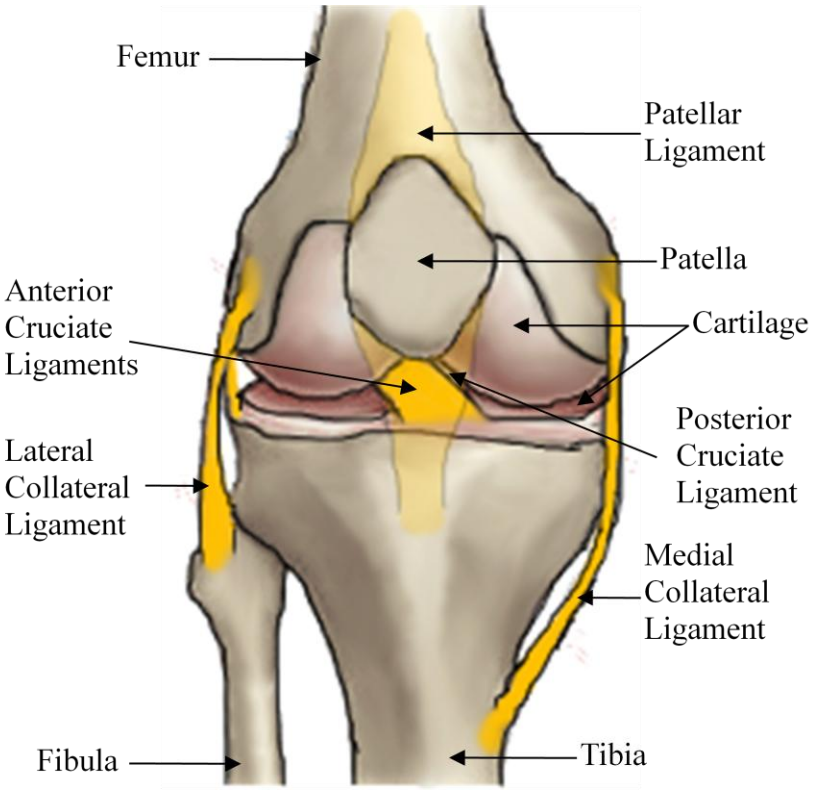

Figure 1: The Human Knee

The kinematics of the knee are complex. The femoral articular surface not only rotates relative to the tibia articular surface, resulting in flexion, but also translates in the anterior-posterior (AP) and medial-lateral (ML) directions. In addition to flexion and translation, the femoral articular surface also undergoes internal-external (IE) rotation and abduction-adduction relative to the tibial articular surface (Figure 2).

The modular fixed bearing TKR remains one of the most common and widely used design for the treatment of damaged cartilage [3]. Modular TKRs include a femoral component, PE tibial insert, tibial tray and typically a patella resurfacing component (Figure 2). The femoral component resurfaces the femur and is typically comprised of a cobalt

The modular fixed bearing TKR remains one of the most common and widely used

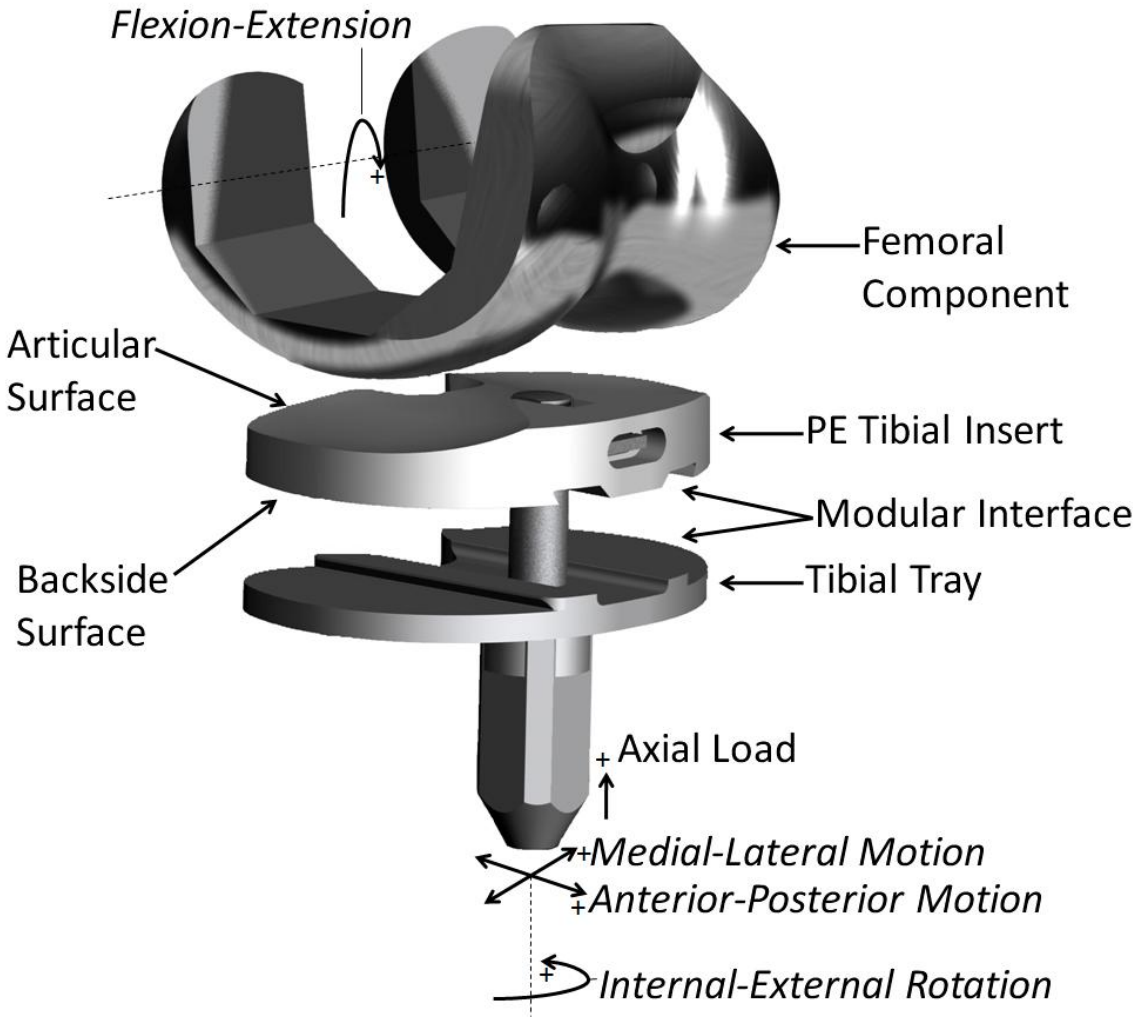

Figure 2: Motion of a Total Knee Replacement

design for the treatment of damaged cartilage [3]. Modular TKRs include a femoral component, PE tibial insert, tibial tray and typically a patella resurfacing component (Figure 2). The femoral component resurfaces the femur and is typically comprised of a cobalt chromium molybdenum alloy (CoCr, ASTM-F75), although other materials such as Oxinium (oxidized zirconium) are also used. The PE insert is comprised of ultra high molecular weight polyethylene and is attached to the tibial tray by some form of locking

mechanism. The tibial tray resurfaces the tibia and is typically comprised of a titanium alloy (Ti, Ti6Al4V) or of CoCr alloy. The patella is typically resurfaced with a dome shaped component comprised of PE, which articulates along the patellar grove of the femoral component. The components can be attached to the bone by either cemented or cementless fixation.

The TKR includes designs which preserve cruciate ligaments (Figure 3), referred to as cruciate retaining (CR), and designs which require the removal of the cruciate ligament (Figure 4), referred to as posterior stabilized (PS). The CR design retains the anatomical conditions of the knee to a greater extent than the PS design, and well functioning cruciate ligaments provide additional constraint resulting in more natural kinematics [3]. Alternatively, the PS design enables the geometric resurfacing of the entire end of the tibia, thereby improving tibial fixation. In addition the cruciate ligaments are not always functional in elderly patients, or may have been previously damaged, and therefore the sacrifice of the cruciate ligaments and the implementation of a PE post to constrain the kinematics of the knee may be favourable over a CR design.

An alternative to a TKR is a unicondylar knee replacement. Unicondylar knee replacements replace only one condyle of the knee, and are typically used for patients with unicondylar disease (osteoarthritis) [4-5]. TKRs are currently more common than unicondylar knee replacements, and include fixed bearing (Figure 3 and Figure 4) and mobile bearing varieties. Fixed bearing knees replace all articulating surfaces of the knee and are available in modular (Figure 3 and Figure 4) and non-modular designs. The PE tibial insert of non-modular designs is either permanently fixed to a metallic backing tray,

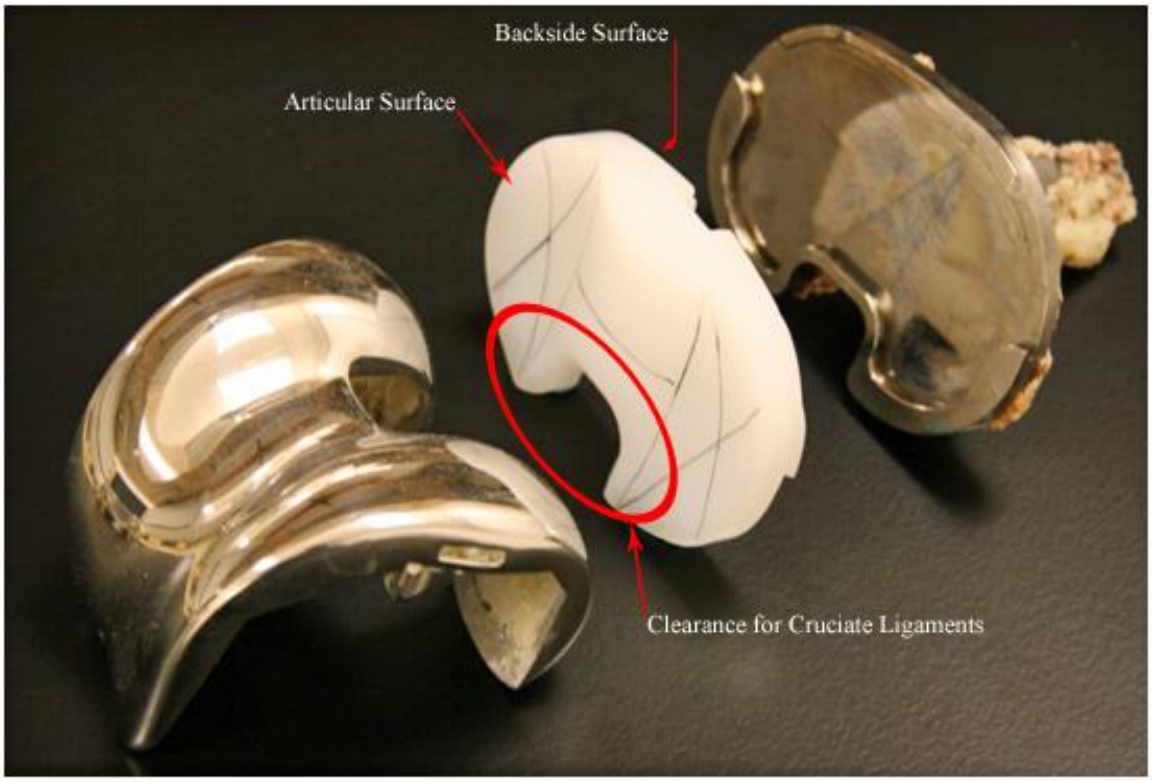

Figure 3: Cruciate Retaining Modular Fixed Bearing Total Knee Replacement

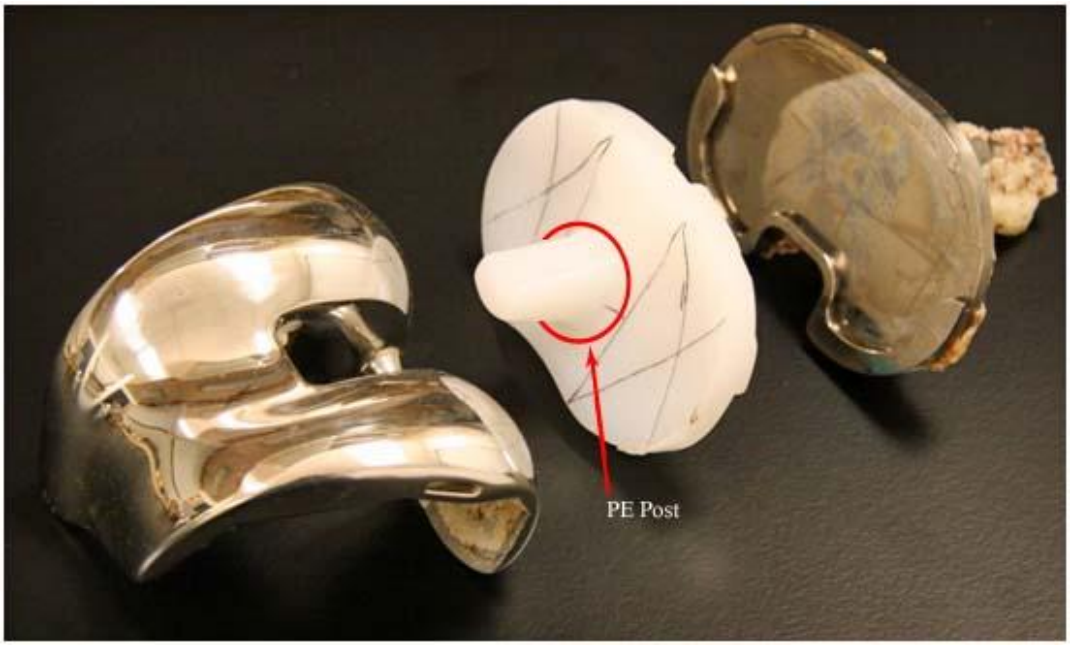

Figure 4: Posterior Stabilized Modular Fixed Bearing Total Knee Replacement

or is directly attached to the tibia without a tibial tray (all-polyethylene tibial components). All-polyethylene tibial components of non-modular designs, have the disadvantage of poor fixation to the tibia [6], as well as the high stress, and uneven distribution of the loads into the subchondral bone [7-8]. Non-modular designs have the advantage of removing the modular connection which has been shown to be a source of clinically relevant wear particles [9-16]. Yet, both forms of the non-modular designs, complicate the revision of the components, as the PE component cannot be revised without removing the entire tibial assembly, which may necessitate the removal of a well fixed component and the loss of valuable bone stock. Modular designs feature a modular connection between the metallic tibial tray and the PE tibial insert, enabling the revision of the PE tibial insert without any modification to the tibial tray. The modular design introduces an additional interface which may be subject to wear. Modular designs include both mobile bearing designs and fixed bearing designs. Mobile bearing designs include two sets of intended articulation surfaces. The insert articulates against both a polished femoral component as well as a polished tibial tray. Mobile bearings include both meniscal bearings and rotating platform designs. Meniscal bearing designs feature two separate PE components which are constrained by the tibial tray to only allow articulation in the AP directions against the tibial tray. Rotating platform designs typically consist of a single PE component which is constrained by the tibial tray to only permit IE rotation. The objective of the mobile bearing design was to enable highly conforming articular pairs to be used (which

results in decreased contact pressure) by providing an additional articular pair to prevent over constraining the knee and enable the natural knee kinematics.

1.2 Total Knee Replacement Wear

The failure of TKRs necessitates costly revision surgery, as well as exposes the patient to additional risk of infection and pain. PE wear has been identified as one of the factors currently limiting the long term success of total knee replacements [17-19]. The PE wear particles released into the synovium can stimulate an immune response which may initiate a cascade of adverse tissue responses leading to osteolysis (bone resorption), and the subsequent loosening of the implant [20]. PE wear particles are generated as a result of the relative movement between contacting components. Wear occurs at the articular (topside) surface [3], the distal (backside) surface of modular designs [9-16], the post of posterior stabilized designs [21] and at the articular surface of patella resurfacing components [3]. Wear in TKRs depends upon multiple factors, including contact pressure [22], sliding distance [22], surface finish [23], material properties [24], temperature [25], lubrication effects [26] [27], tractive rolling [28], sliding velocity [29], repeated loading effects [30], sterilization method [3] and directional PE strain hardening [22]. Therefore, the development of a TKR design for reduced wear is a complex task due to the large number of variables governing the interaction.

1.2.1 Articular Wear

A large portion of wear particles are generated at the articular surface of the tibial insert. The articulation between the femoral component and the PE tibial insert results in the generation of wear particles which are released into the synovium. Adhesive/abrasive wear particles originating from the articular surface are usually less than 1 micron in size [31]. The large varieties of TKR designs on the market indicate a lack of consensus as to which design is optimal for the reduction of wear while still maintaining physiologically relevant kinematics.

1.2.2 Backside Wear of Modular Total Knee Replacements

Although the majority of wear particles originate from the articular surface, the PE wear particles generated at the backside surface of modular TKRs have been considered most insidious, as osteolysis has not be reported for non-modular components [32]. The loading and motion of the femoral component relative to the PE insert causes deformation of the insert and relative movement (micromotion) between the distal (backside) surface of the PE insert and the tibial tray of modular TKR's [14, 33]. The micromotion at the backside interface can generate PE wear particles which have been shown to be smaller in size than wear particles from the articulating surface [33-35]. Therefore, PE particles originating from backside wear have an increased biological activity, resulting in an increased potential for osteolysis in comparison to articular surface wear particles [36-37]. Backside wear has been shown to make a significant contribution to osteolysis [13-16] and has been correlated with tibial osteolysis [16]. The wear of the backside surface has been

shown to account for up to 30% of total PE insert volume wear for some TKR designs [38].

The influence of the tibial tray surface finish and locking mechanism design on wear is of particular interest for the design of implants with reduced backside wear. Components retrieved from patients have been analyzed to assess the effect of various design parameters on backside wear [9-10, 12-16, 39]. The retrieval studies of Azzam et al. [10], Akisue et al. [9] and Brandt et al. [39] present evidence that partial-peripheral locking mechanisms reduce backside damage over central locking mechanisms. Grit-blasted surface finishes were shown to result in a greater amount of backside damage by the retrieval study of Brandt et al. [39]. The in vitro knee simulator experiments of McNulty and Swope [40] demonstrated that grit-blasted surfaces increase wear by as much as 38% as a result of their higher roughness. In addition, gamma-air (GA) sterilization of PE components, and shelf ageing of GA sterilized components, has been shown to increase backside damage [39, 41-42].

1.2.3 Additional Sources of Clinically Relevant Wear

The posts of PS designs are additional sources of wear [43]. The articulation of the femoral component against the post has been shown to result in adhesive, abrasive and fatigue wear [43]. In addition patella resurfacing components are also a source of wear particles, resulting from the articulation of the patella component against the femoral component [44].

1.2.4 Optimizing TKRs for the Reduction of Wear

The optimization of TKRs for the reduction of wear is complicated by the large number of factors upon which wear depends. Knee wear simulators are the current standard for evaluating implant bearing materials and designs. While knee simulators are invaluable for the assessment of TKRs, the cost and time requirements of knee simulators may make the parametric analysis of the design variables unfeasible [45]. Therefore, the development and utilization of a computational model for the prediction of PE wear, in combination with knee simulator experiments, could potentially enable the analysis of a greater number of variables to be studied than is currently possible with knee simulators alone. The development of a computational model for the prediction of wear may also provide greater insight into the factors affecting wear, such as contact pressures, sliding distances and cross-shear.

1.3 Thesis Objectives and Outline

The development of an efficient and accurate computational wear prediction method could enable the efficient evaluation of a broader range of TKR designs and enable design optimization for the reduction of wear. A review of TKR wear and the *in vitro* simulation of wear are given in Sections 2.1 and 2.2 respectively. The proposed wear modeling method requires contact pressure and sliding displacement vectors, as well as a computational wear model. The first objective of this research was to develop a FE model for the prediction of contact pressures and relative sliding displacement between all compo-

nents in contact with the PE tibial insert (Section 3.2) A deformable model with three different constitutive models was considered for prediction of contact pressure and sliding distances for the articular and backside surfaces (Sections 3.2.1 and 3.2.2), while three rigid body FE models were considered for the articular surface (Section 3.2.3). The FE models accuracy was verified by the comparison of the FE models predicted relative sliding displacements of the backside surface (backside micromotion) to those of knee simulator wear tests, and the model was used to investigate the effects of various design parameters on backside micromotion (Section 3.3). The second objective was to utilize the FE simulation results along with knee simulator results to identify the wear factors of Archard's wear law relevant to the articular and backside surfaces of the TKR (Section 3.4). The final objective was to develop and assess the accuracy of a new, novel wear model based upon a theoretical understanding of the molecular structure of PE (Section 3.5). The results of the research are presented and discussed in Section 4, conclusions are given in Section 0 and future work is discussed in Section 1. The flow chart of Figure 5 displays the overall research process.

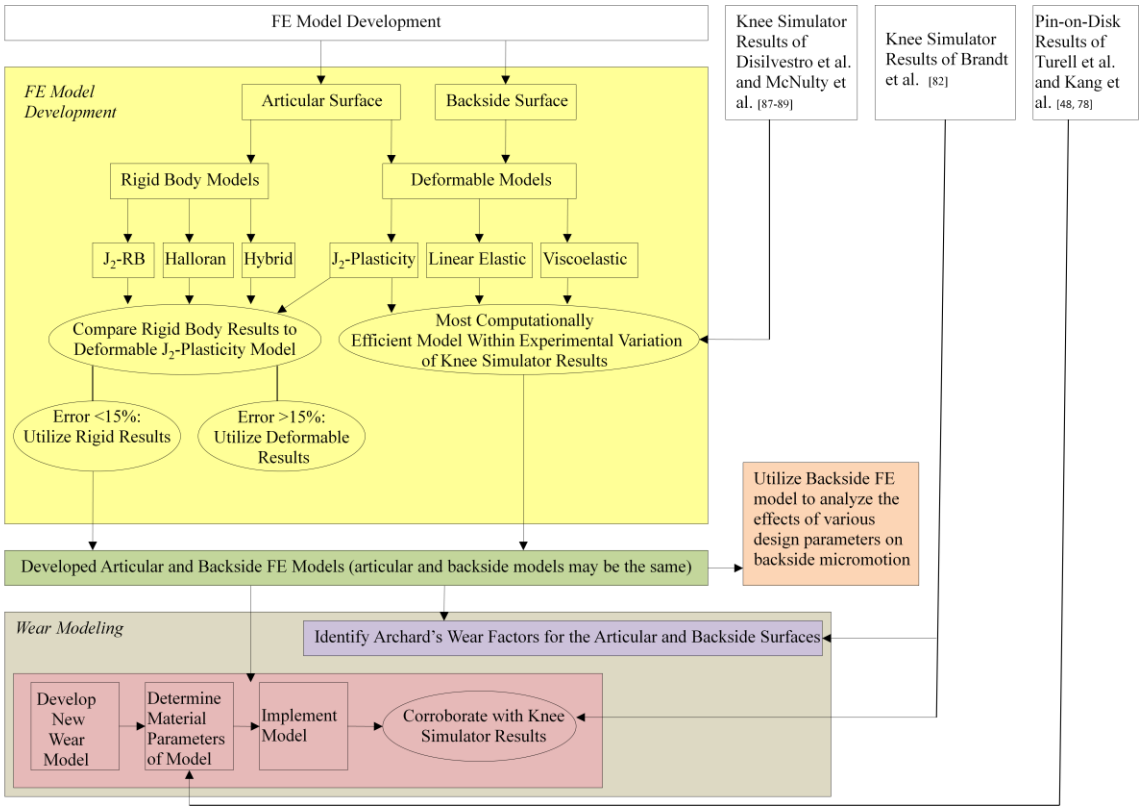

Figure 5: Flow Chart of Overall Process

Chapter 2

Literature Review

2.1 Total Knee Replacement Wear

2.1.1 Polyethylene Wear Theory

PE is a linear homopolymer comprised of carbon and hydrogen molecules (Figure 6). PE, as a thermoplastic, is subject to directional strain hardening [3]. The amorphous molecular chain of PE can become mobile and form oriented crystalline lamella as a result of loading conditions (Figure 7). The direction of the crystalline lamella is referred to as the molecular orientation (MO). The directional strain hardening of a material results in the increased resistance to wear in the direction of the MO, but reduced wear resistance (orientation softening) in the perpendicular direction to the MO [22]. The angle between the MO and the direction of relative sliding displacement is typically referred to as cross shear. Therefore, larger cross shear angles result in greater wear volume. Radiation can be used to cross-link PE and reduce the mobility of the molecular chain to reduce wear.

However, PE irradiation has also been shown to be accompanied by a decrease in the ductility of the material [3].

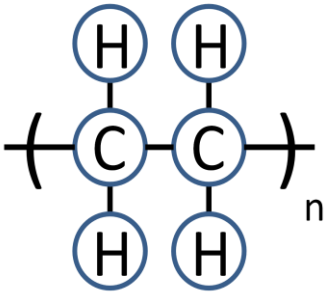

Figure 6: Chemical Structure of Polyethylene (n denotes repetition of structure)

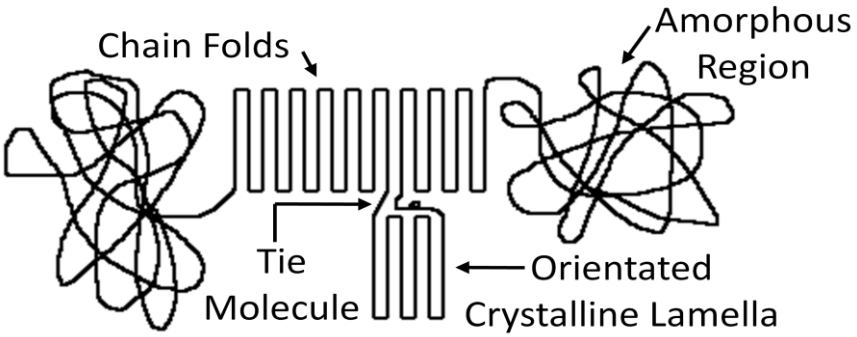

Figure 7: Polyethylene Morphological Features

The articulation between the femoral component and PE insert of TKRs has been suggested to occur predominantly under the boundary lubrication regime [26]. The load between the components is predominantly by the direct contact of asperities. The wear of PE occurs by adhesive, abrasive, tribochemical and fatigue wear. Adhesive wear results from the direct contact of asperities between two sliding surfaces, and occurs as a result of diffusion, electronic and absorption mechanisms [46]. Abrasive wear involves the direct contact and localized plastic deformation of asperities in contact. Abrasive wear in

the case of the TKR involves the harder asperity plastically deforming and removing the softer PE asperity. The articulation between surfaces may also result in chemical reactions which consequently change the chemical properties of the surfaces, resulting in tribochemical wear [46]. Fatigue wear includes both pitting and delamination [47]. The repeated loading of high normal stresses combined with the shear loads from the relative articulation of the components can result in subsurface material failure. This material failure results in crack initiation. The crack may then propagate parallel to the articular surface, resulting in a sheet of material being removed from the component (delamination). Or the crack may propagate perpendicular to the articular surface (pitting), resulting in the release of a PE particle and the creation of a pit. These damage features are typically encountered with gamma-air sterilized PE components, as the free radicals of the material will then oxidize resulting in decreased material strength. Several fatigue models exist for the modeling of fatigue damage over time [48-49] which could be implemented for the simulation of fatigue damage. The focus of this research relates to the adhesive and abrasive wear of PE and therefore wear and wear model hereafter refer to adhesive and abrasive wear or wear modeling.

2.1.2 Relevant Variables Affecting TKR Wear

The wear of PE has been shown to depend on multiple factors. PE wear has been shown to depend on contact pressure, although the relationship does appear to be non-linear [22]. Wear has a strong dependence on sliding distance [22]. Surface finish also has a significant impact on wear, as an increase in roughness results in increased wear rates [23]. Material properties of the hard counterface also have a significant effect on PE

wear, as an increase in hardness reduces PE wear [24], and a change in hydrophobicity results in changed wear rates [26]. Temperature also has a significant effect on wear, and therefore all simulator testing must be conducted at clinically relevant temperatures [3]. Tractive rolling [28], and sliding velocity [29] were both demonstrated to effect the wear rate. The inclusion of dynamic loading results in increased wear [30], and the composition of the lubricant has a significant effect on wear [27]. The directional strain hardening of PE results in increased wear resistance in the direction of the MO and decreased wear resistance in the direction perpendicular to the MO [22].

2.2 The *In Vitro* Simulation of Wear

In vitro simulation is performed for the development and evaluation of TKR designs and materials. There are three main categories of in vitro testing, pin-on-disk (POD) or ball-on-flat (BOF) tests, knee simulator wear tests, and computational wear simulations.

2.2.1 Pin-on-Disk and Ball-on-Flat Wear Tests

POD (Figure 8) and BOF (Figure 9) testing are tribological tests which involve the articulation of the PE bearing material against an opposing counterface (such as CoCr). POD and BOF tests are typically used as screening tests for new materials and have also been implemented for wear model development.

POD testing for TKR materials typically involves a pin which articulates against a flat plate in the presence of a lubricant. Various pin motion paths have been utilized, in-

cluding unidirectional (or reciprocating) [50], circularly translating [50], rectangular motion paths [22, 51-53], random [54] and other varieties [55]. The unidirectional motion does not include cross shear, as the crystalline lamella become orientated in the direction of motion and therefore unidirectional motion paths result in low wear rates in comparison to motion paths which include cross shear. Circularly translating motion paths feature a consistently changing direction of sliding relative to the PE pin, rectangular motion paths include finite sections of unidirectional sliding followed by 90 degree sliding direction changes to form a rectangular shape, random and other paths have also been utilized, all of which include cross shear. Motion paths have been developed to include cross shear, as cross shear is observed within the PE tibial insert of a total knee replacement during the gait cycle and therefore it is important to replicate this tribological condition in POD testing. POD devices have previously been utilized to determine the wear factor of Archard's wear law, as well as derive the effects of additional variables on wear. Wear factors derived from POD testing vary from 5.0×10^{-8} to 1.8×10^{-6} mm^3/Nm [56]. Wear model development (including by use of POD and BOF devices) is discussed in more detail in Section 2.2.3. However, it should be noted that macroscopic POD wear models should not applied directly to TKRs, as the experiments do not replicate the complex surface interactions present in TKRs.

There have been fewer BOF tests investigating PE wear, compared to POD tests [57]. BOF tests have the advantage of greater control over the test conditions, making it possible to implement test conditions more relevant to the TKR such as the inclusion of tractive rolling, dynamic loading and more relevant cross shear angles [57]. Although BOF

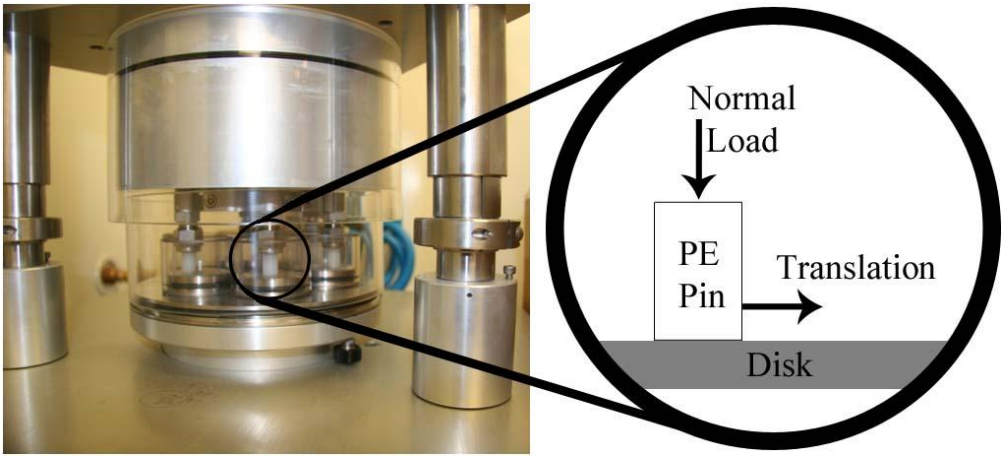

Figure 8: Pin-on-Disk Testing Apparatus (AMTI Orthopod)

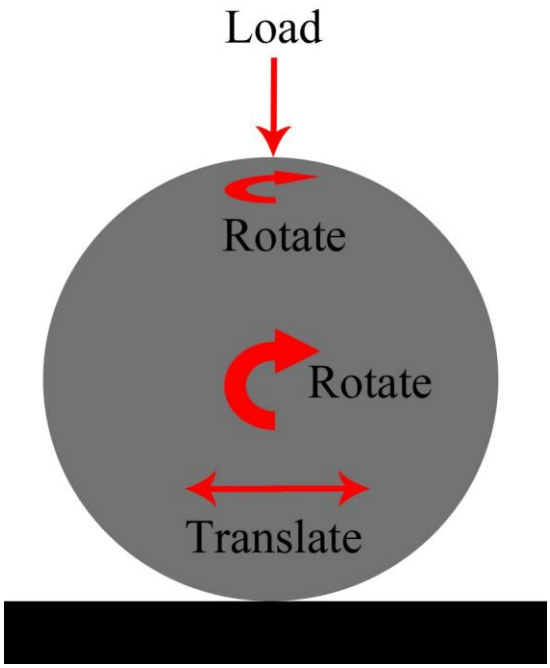

Figure 9: Ball-on-Flat Testing Apparatus

tests have been used to identify the wear factor of Archard's wear law, BOF tests have not been previously utilized to quantitatively derive the effects of any other variables on wear.

2.2.2 Knee Simulator Wear Tests

Knee simulators have been developed to simulate the loading and kinematics of in vivo TKRs (Figure 10). Current knee simulators feature 6-degrees of freedom (3 displacements and 3 rotations of the femoral component relative to the tibial component), and utilize provisions for the inclusion of a heated lubricant to surround the TKR. Knee simulators are utilized to conduct wear tests, either according to the ISO standards for displacement controlled or force controlled testing, or under accelerated wear conditions.

All wear simulation must recreate in vivo motion and loading to be clinically relevant. There are two different approaches to simulating the motions of the knee joint, force controlled and displacement controlled [3]. ISO standards exist for both force controlled (ISO 14243-1) [58] and displacement controlled (ISO 14243-3) [59] methods. Both methods specify the flexion angle and axial loading of the TKR over the gait cycle (Figure 11) [58-59]. The gait cycle begins with the initial contact of the foot with the ground, and ends after the swing phase before the foot contacts the ground again. The displacement controlled method specifies the AP translation and IE rotation over the gait cycle in terms of displacements (

Figure 12) [59]. Conversely, the force controlled method specifies the AP translation force and IE rotational torque over the gait cycle (Figure 13) [58]. Both ISO standards also specify a lubricant of diluted bovine calf serum with a protein concentration of 17.5 ±2 g/l for the simulation of human synovial fluid.

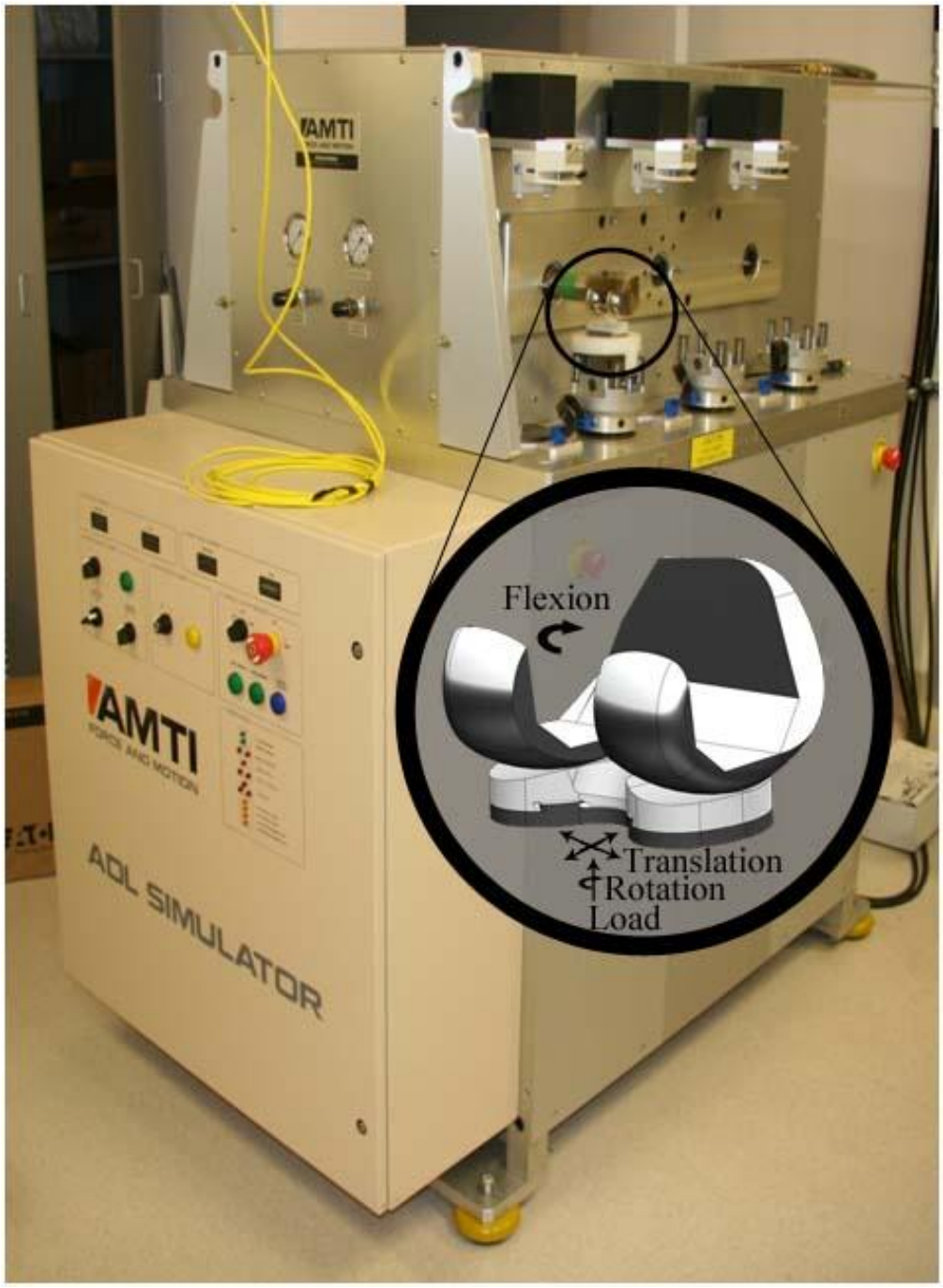

Figure 10: Six Station Knee Simulator (AMTI)

well as cruciate retaining inserts, while the displacement controlled method has the advantage of very consistent and repeatable kinematics, but may only be implemented for

The force controlled method replicates the loads which cause the displacements of human kinematics and can be used with posterior stabilized inserts as cruciate retaining inserts, as the displacements may otherwise cause unrealistic damage to the PE post of posterior stabilized designs.

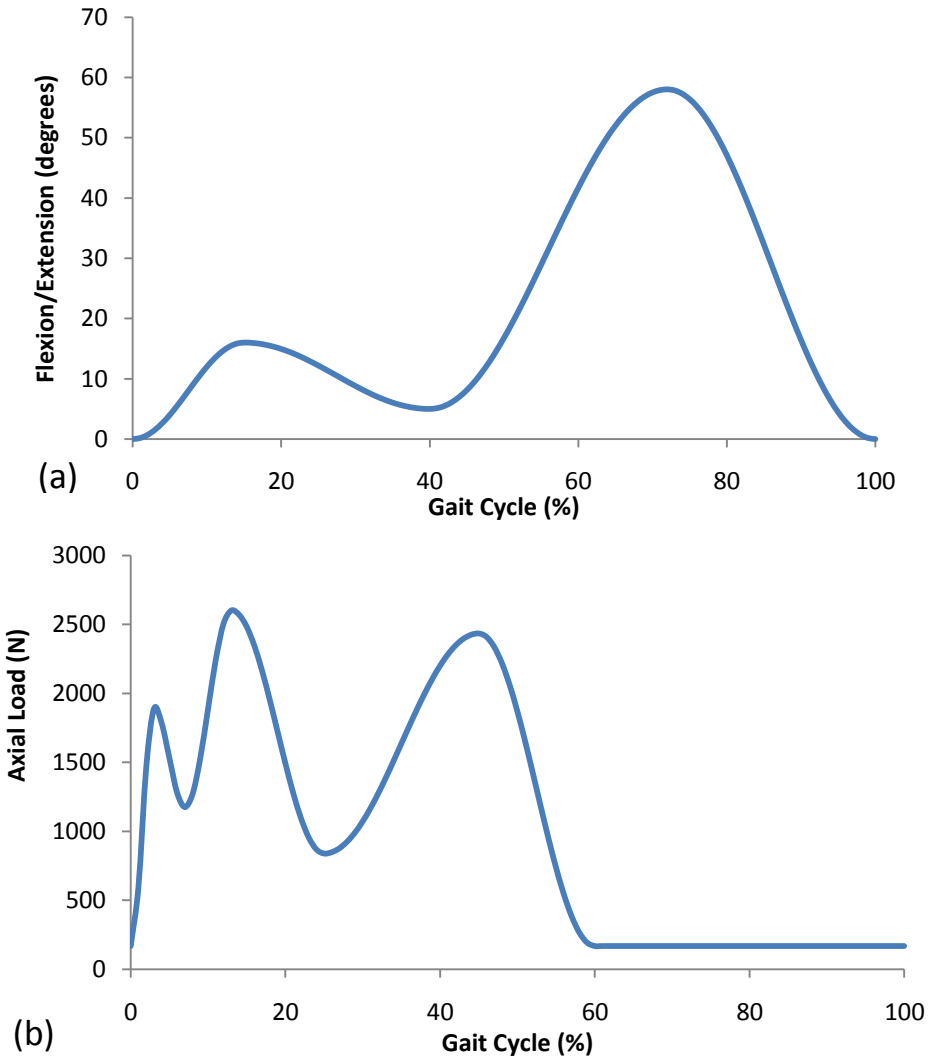

Figure 11: ISO 14243 Standard (a) Flexion/Extension Angle over the Gait Cycle; (b) Axial Loading over the Gait Cycle

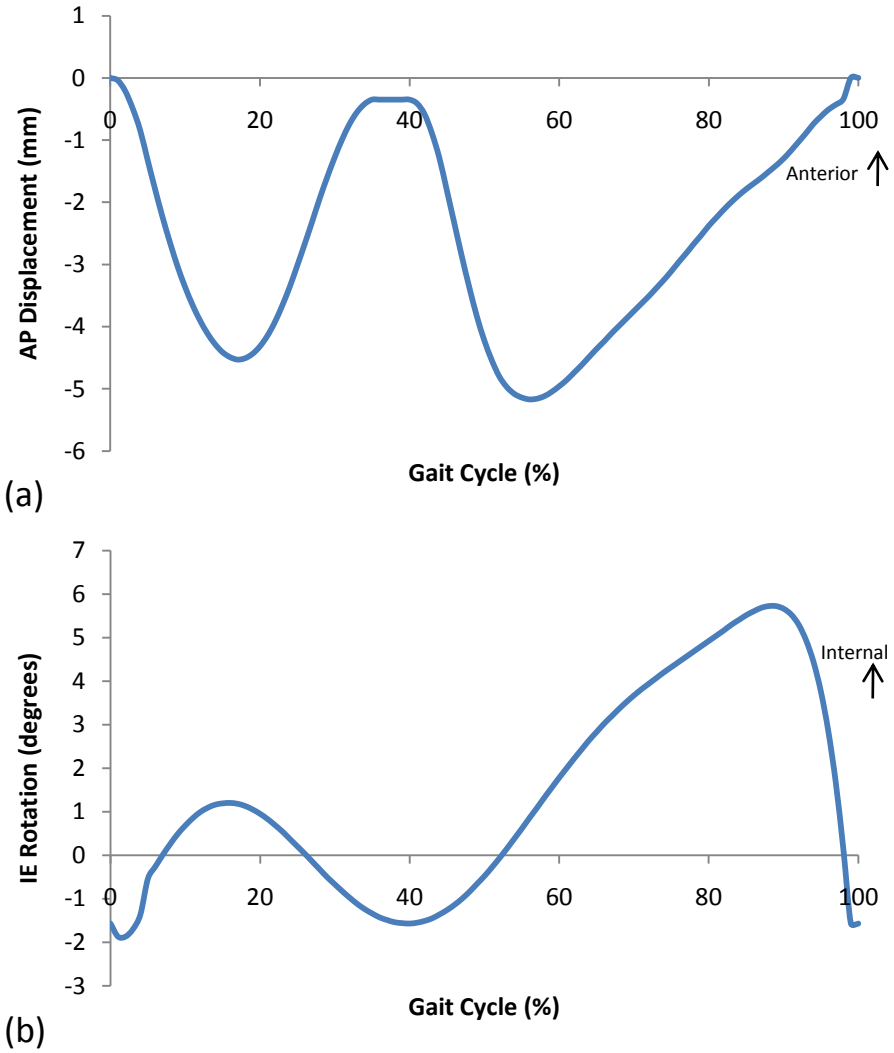

Figure 12: ISO 14243-3 Displacement Controlled (a) Anterior-Posterior Displacement; (b) Internal-External Rotation

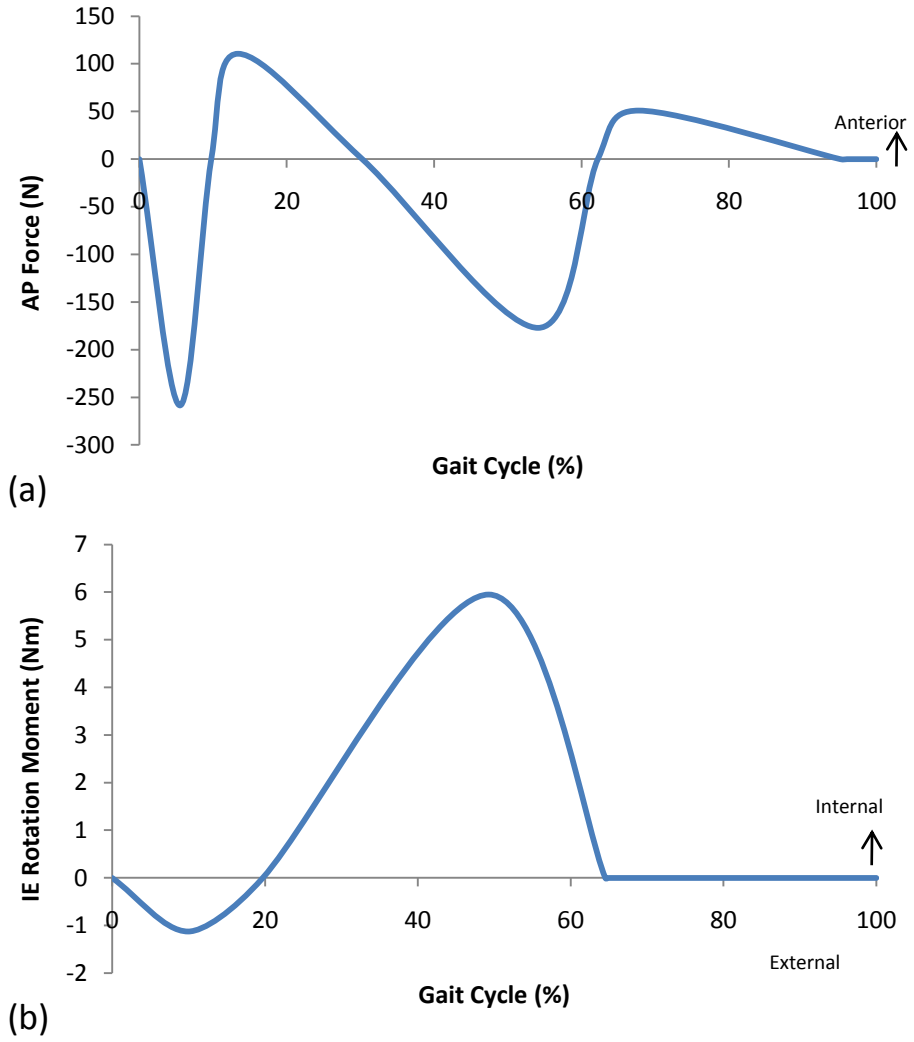

Figure 13: ISO 14243-1 Load Controlled (a) Anterior-Posterior Force; (b) Internal-External Moment

Knee simulators are also utilized to conduct damage mode or accelerated wear tests [3, 60-61]. Damage mode and accelerated wear tests typically feature more severe loading and/or displacement conditions than those of the ISO standard. Damage mode and accelerated wear tests are utilized for the replication of specific damage modes, or for the

simulation of more severe operating conditions than those of the ISO standards [3, 60-61].

Most knee simulator wear testing only considers the overall wear of the PE insert. However, investigating the backside micromotion and wear separately from that of the articular surface can be very beneficial for the optimization of locking mechanisms and implant design [62-65]. In vitro simulation of backside micromotion by use of knee simulators has previously been undertaken to quantify the magnitude of backside micromotion [62-65]. However, the relative micromotion can only be measured around the peripheral surface of tibial inserts during knee simulator experiments, while the micromotion of interest occurs at all locations on the backside surface of PE inserts. This may be regarded as a limitation, as the actual magnitude of micromotion on the backside surface remains unknown. Knowledge of micromotion at each location on the backside surface is necessary for studying the backside wear of existing TKR models and for improving the design of new TKRs.

2.2.3 Computational Simulation

While knee simulators are invaluable for the assessment of TKRs, computational simulations feature improved time and cost efficiency which could potentially enable the analysis of a greater number of variables to be studied than is currently possible with knee simulators alone [66]. The development of a computational model for the prediction of wear may also provide greater insight into the factors affecting wear, such as contact pressures, sliding distances and cross-shear information. The procedure for the computational modeling of TKR wear typically includes the prediction of the contact pressures,

sliding distances and directions by the finite element (FE) method. The FE results are then typically incorporated in a computational wear model, which provides the wear geometry over the specified interval. Typically multiple update intervals are included to account for the effects of geometric changes on the contact pressures and relative sliding between the components (Figure 14).

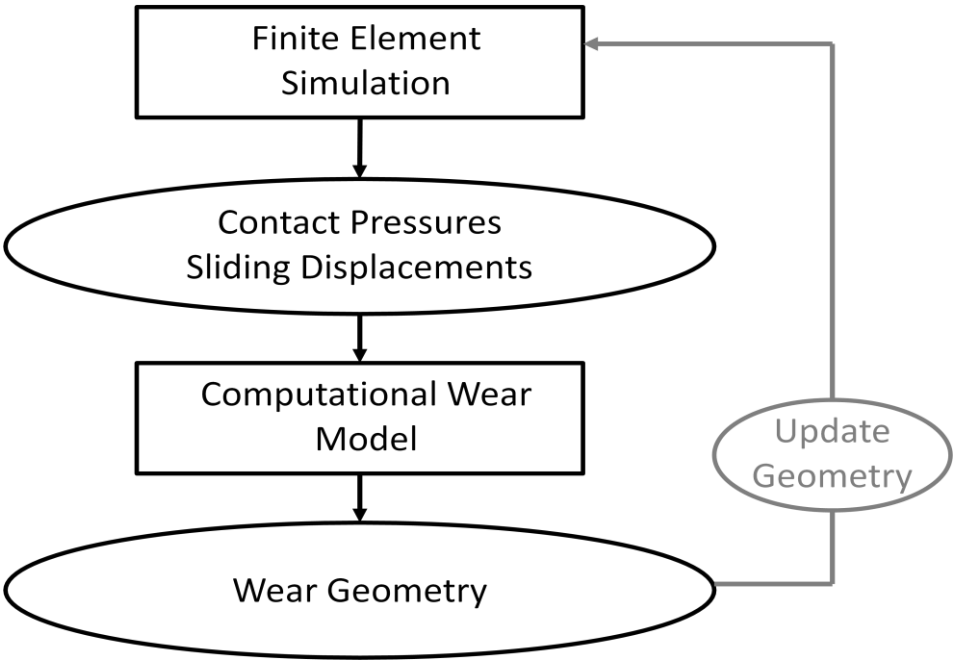

Figure 14: Typical Procedure for the Computational Modeling of TKR Wear [66-73]

The contact pressures and relative sliding distances at each location on the contacting surfaces are required for the analysis of PE wear. Both deformable FE models [66-67, 71], as well as rigid body FE and multibody dynamic (MBD) simulation models [72, 74-79] have previously been implemented for the assessment of the femoral component – PE tibial insert contact interaction.

PE, as a thermoplastic, exhibits a complicated nonlinear response to external loads, thereby increasing the complexity of modeling PE material behaviour. PE behaves viscoelastically at small deformations, followed by distributed yielding, viscoplastic flow, strain hardening at large deformations and finally ultimate failure [3]. The contact pressures and sliding distances at the femoral component – PE tibial insert interface may be predicted by the use of deformable PE models [66-67, 71], or rigid body models [72, 74-79] incorporating the elastic foundation (EF) theoretical formulations or pressure-overclosure relationships to model the penetration of one component into the other.

Material models implemented for the modeling of PE material behavior by deformable FE models, typically include the linear elasticity model, hyperelasticity model, linear viscoelasticity model and the J_2-plasticity model. Linear elastic models offer simplicity as well as computational efficiency and have been previously implemented in TKR wear models [68-69]. Only Young's modulus and Poisson's ratio are required for a linear elastic model. However, the linear elastic model has been shown to be unable to describe the characteristics of PE for medium to large strain values [3]. The hyperelasticity model is valid for applications where the history of deformations, such as yielding, viscoplasticity or time dependant changes (creep) do not need to be taken into account by the material model. However, using this model at higher strain rates would likely result in a lack of Drucker-stability [80]. The Drucker stability postulate specifies that a stress increase which results in additional strain does positive work and is therefore stable, however for the descending branch of a deformation-strain curve, the strain increases with decreasing stress, therefore the additional stress does negative work resulting in instability [80]. Therefore, the lack of Drucker-stability in the computational solution would provide in-

accurate results, and therefore, the uses of this model are also very limited. The linear viscoelasticity model enables the prediction of time-dependence and viscoelastic flow. However, its accuracy is still limited to low strain values, and the strain values in PE tibial inserts under ISO loading have been shown to reach levels higher than the yield strain value of the material [3]. The J_2-plasticity model is typically represented by a modulus of elasticity and a set of tabular stress-strain values obtained from experiments, which are used to construct piecewise linear interpolation between the data points. It has been demonstrated that a J_2-plasticity model exhibits improved accuracy over the linear elastic model while still offering computational efficiency [81]. The J_2-plasticity material model developed by Bergström et al. [81] predicted the mechanical behavior of PE with a coefficient of determination, a measure of how well the FE model predicted the outcome, of 0.877, compared to experimental data of PE under various experimental conditions, including small, intermediate, and large monotonic deformation, as well as cyclic loading.

Alternatively, rigid body models offer improved computational efficiency over deformable models. However the simplification of the model is accompanied by an associated decrease in prediction accuracy. Previous TKR rigid body models have consisted of rigid femoral and PE tibial insert components. The deformation of the PE material is instead simulated by the utilization of EF theory or pressure-overclosure relationships, which permit the penetration of the femoral component into the rigid body PE tibial insert. The EF theory includes the theoretical representation of the deformable component by a set of distributed elastic components “bed of springs” [79], where the contact pressure and deformation of each spring is independent of its neighbouring springs. The contact pressure (p) for each spring is calculated using the equation [82]:

$$\mathrm{p} = \frac{(1-v)E}{(1+v)(1-2v)}\frac{d}{h} \quad (1)$$

where E is the Young's modulus of the PE, v is Poisson's ratio, d is the springs deflection and h is the thickness of the component. The rigid body model supports the use of both linear and nonlinear elastic models [78]. The advantage of implementing rigid body models is the greatly increased computational efficiency over fully deformable models. The rigid body models can reduce computational time to 2% of the time required for deformable models [78]. However, the validation of such models has previously been limited to the analysis of average and maximum contact pressure over the gait cycle [78]. While the correct specification of the spring rates or pressure-overclosure relationships could result in the correct average contact pressures, the contact pressure distribution and contact areas are expected to be inaccurate, as the assumption that each element is not affected by neighbouring elements does not match the behaviour of the PE.

Following the evaluation of contact pressures and the relative sliding at the articular surface, a computational wear model may be applied for the simulation of wear. The majority of the wear models [45, 68, 72-73, 83-85], have been based upon Archard's wear law [86] with a wear factor obtained from POD testing. Archard's wear law specifies that the wear depth is proportional to a wear factor (k) multiplied by the contact pressure (P) and the sliding distance (S) [86].

$$\mathrm{W}_{\mathrm{depth}} = k \cdot P \cdot S \quad (2)$$

There are a wide range of published POD test derived wear factors intended for TKR wear, ranging from 5.0×10^{-8} to 1.8×10^{-6} mm^3/Nm [56]. The majority of previously developed Archard's wear law models were only applied to one implant, or resulted in poor predictability when TKRs of different geometries were implemented [76].

The strong dependence of wear on multidirectional motion (or cross shear) recently became apparent through the results of POD tests [87], and knee simulator wear tests [88]. Therefore, more recent wear models have been developed to include the effect of cross-shear on wear, a relationship also derived from POD test results [46-47]. The majority of wear models have been built upon the existing foundation of Archard's wear law, by specifying the wear factor (k) to be a function of the cross shear. Cross shear (CS) is typically defined to be the magnitude of shear force perpendicular to the primary MO ($W_{cross\text{-}shear}$) divided by the total frictional work (W_{total}) [52].

$$CS=\frac{W_{cross-shear}}{W_{total}} \tag{3}$$

Turell et al. [87] defined the wear factor of Archard's wear law to be related to the aspect ratio of the sliding path for POD tests (Figure 15):

$$k=\frac{A}{A+B} \tag{4}$$

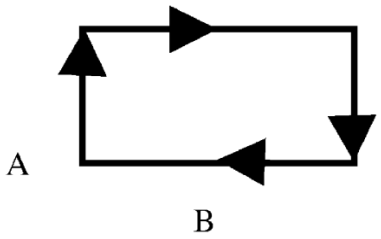

Figure 15: Rectangular Path Motion of POD Device

However, the comparison of this model to the POD results revealed this model to be in-accurate and identified the need for a more complex wear model which would explain why the wear did not peak at an aspect ratio of 0.5 as expected (Figure 16)

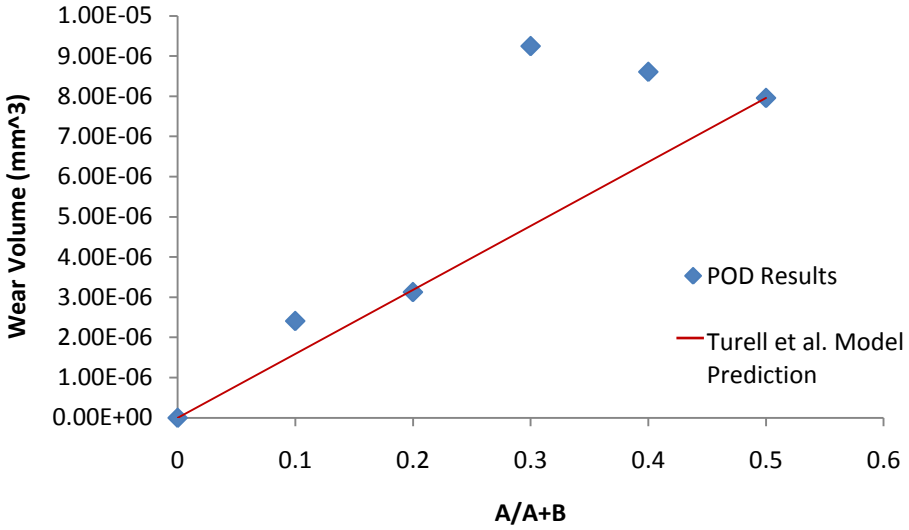

Figure 16: A/A+B Wear Model Prediction of Turell et al. [87] and POD Results

Further experimentation and wear model development was carried out by Kang et al. [22, 51-52]. Extensive POD testing was conducted to develop relationships for both cross shear and contact pressure relative to wear:

$$k(CS, P)=e^{-13.1+0.19*\ln(CS)-0.29P} \quad (5)$$

where k is the wear factor, CS is cross shear and P is contact pressure. The results indicated that increasing cross shear results in increased wear, which is in agreement with the theory of directional strain hardening [22]. However, the results also indicated that increasing contact pressure would lead to a reduction in wear, and that the effect of cross shear on wear reduces with increasing contact pressure, both of which contradict the results of knee simulator wear tests and are contrary to the current understanding of polymer wear [53].

In response to the evident lack of understanding in regards to the effect of contact pressure on wear, recent computational wear models have avoided implementing contact pressure in the wear formation, specifying that wear is only proportional to sliding distance, cross shear and contact area [67]:

$$W_{depth} = S \cdot (8.5 \cdot 10^{-65} + (9.4 \cdot 10^{-60} \cdot CS))^{1/6.7454} \quad (6)$$

In addition, a non-Archard based model has been developed by Wang et al. [53] through the use of hip simulator wear tests and POD tests. However, this model is not relevant for conventional non-crosslinked PE, as the application of the model in the absence of crosslinking would result in the prediction of infinite wear [53]. Furthermore, the extensive hip simulator wear testing is not directly applicable to the prediction of wear in TKRs, as total hip replacement wear occurs dominantly under the mixed lubrication regime [53, 89], as the hip is a ball-socket-type joint. TKR wear occurs dominantly

under the boundary lubrication regime [26] as it is a hinge-type joint with a much smaller area of contact in comparison to hip replacements.

Despite the significant contributions of POD testing to the development of wear models, significant disagreement still exists between the results [22, 53, 67, 87]. There are many issues relating to the application of a macroscopic POD wear model to TKR wear. Although POD testing is useful for material screening, it is questionable whether the results of POD testing should be directly implemented for the modeling of TKR wear as POD experiments are not able to replicate the complex surface interactions present in TKRs. POD experiments used for the development of wear models have not included tractive rolling [28], dynamic loading [48], sliding velocity [35] or replicate the geometric contact conditions of TKR's and therefore do not entirely replicate the conditions of a knee simulator. Therefore, due to the disagreement between the current wear models, and the questionable relevancy of POD developed models to TKRs, the development of a wear model through the use of knee simulator results, rather than from POD testing, was deemed beneficial to ensure the relevancy of the finite element model to TKR wear.

Although there has been much research in regard to the prediction of wear at the articular surface of TKRs, no computational or FE simulation has previously been reported for the simulation of backside micromotion or backside wear. Additional insight into backside micromotion could be gained from a computational or finite element method based simulation. The sliding distances across the surface could be used to investigate the effects of various locking mechanism design changes, as well as to optimize the locking mechanism design for the reduction of backside micromotion and wear. However, the complexity of the physical system increases the difficulty of developing a finite element

model to predict backside micromotion. Backside micromotion is dependent upon several factors, including the material deformation of the insert, the complex contact interactions and reaction forces at both the articular and backside surfaces of the PE insert, as well as the contact and reaction forces at the PE insert and locking mechanism interface.

The reaction forces at each contacting surface of the PE insert are in turn dependent upon a number of variables including the relative motion of each component in contact, the coefficient of friction, and the loading conditions of the contact interaction. The coefficient of friction between the components of the physical system depends upon the lubricant [33], thermal conditions [34], sliding velocity [35], surface finish [23] and the contact pressure at the interface [36]. The loading conditions at each interface depend on the forces transferred through the PE insert from all other interactions. The adopted polyethylene material model has a significant effect on the predicted micromotion, since the material's mechanical properties determine the stress distribution and the deformation of the material. The material model effects the stress distribution, which in turn affects the contact pressure, therefore significantly affecting the coefficient of friction [36] and the resulting reaction forces. The material model also has a significant effect on the results since micromotion occurs due to the deformation of the material. Therefore, the prediction of backside micromotion by the finite element method requires the solving of complex multibody contact interactions and accurate PE constitutive modeling. The complexity of backside micromotion increases the difficulty associated with predicting micromotion. To the author's knowledge, no finite element model has previously been developed to predict the backside micromotion or backside wear of a TKR.

Chapter 3

Methods

The computational prediction of wear requires the contact pressures and sliding displacements of each surface, as well as a computational wear model. A FE model was developed for the prediction of contact pressures and sliding displacements. Next, the Archard's law wear factors relevant to TKRs were identified by utilizing knee simulator results. Finally, a new wear law was developed based on a theoretical understanding of PE wear and assessed by comparing the predicted wear to knee simulator wear test results. The Anatomic Modular Knee (AMK®, DePuy Orthopedics Inc., Warsaw, IN) was selected for the analysis of wear, as it was previously estimated to hold a large percentage of the TKR market [90]. Although the AMK is no longer on the market, a large number of AMKs remain implanted in patients and there is much clinical and experimental data available which can be used for the development and corroboration of the models.

3.1 Knee Simulator Experiments

Knee simulator wear tests were previously conducted from 0 to 3 million cycles (Mc), on six modular TKRs (AMK; DePuy Orthopedics, Warsaw, IN) by Brandt et al. [91]. The wear tests were performed following the loading and displacement conditions recommended by ISO 14243-3:2009 [59]. Incremental gravimetric measurements were performed every 0.5 Mc and converted to volumetric measurements using a PE density of 0.936 mm^3/kg. Approximately 20% of gravimetric wear has previously been shown to occur on the distal surface of the AMK tibial inserts [65], and therefore the articular incremental wear volumes were assumed to be 80% of the measured values, while the backside wear volumes were assumed to be 20% of the measured values. The interval wear volumes for each surface were implemented for the identification of the wear factors of Archard's wear law (Section 3.4), and for the corroboration of a new wear law (Section 3.5).

3.2 Finite Element Models

A FE model was required for the prediction of the contact pressures and sliding displacements of each surface. Three different deformable constitutive models were considered for both the articular and backside surfaces, and three additional rigid body models were considered for the articular surface alone. The ability of the model to accurately predict backside micromotion (backside relative sliding displacements), was anticipated

to be more problematic than the prediction of contact pressures and articular surface sliding distances. Therefore, the models ability to predict backside micromotion was corroborated with knee simulator results to verify the accuracy and predictability of the model. The model was then utilized to investigate the effects of locking mechanism design on backside micromotion.

3.2.1 Finite Element Model of the AMK

A FE model of the AMK was required for the evaluation of the contact pressures and sliding distances at each interface. The solid models of a size 3 femoral component, and a size 3 tibial tray were constructed using Solidworks based on manufacturing drawings obtained from DePuy. A solid model of a size 3-4, 10 mm nominal thickness, cruciate retaining PE insert was also provided by DePuy (Figure 2). A finite element model was developed using Abaqus/Explicit (Figure 17) (Abaqus 6.101, Simulia, Providence, RI).

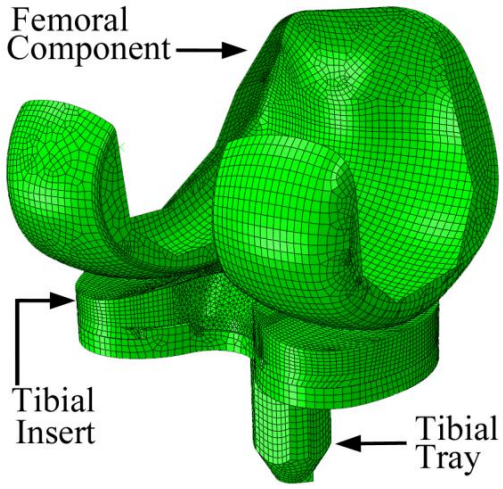

Figure 17: AMK Finite Element Assembly

The PE insert was modeled as a deformable body with a density of 0.936 g/cm^3 [3]. Both the femoral component and tibial tray were modeled as rigid bodies to reduce computational time, since both the CoCr alloy and the Ti alloy have moduli of elasticity far greater than that of the PE insert [3]. The contact interaction between the components was modeled as penalty contact. The CoCr-PE interface included a coefficient of friction of 0.04, a value in agreement with experimental tests [71, 92-93].

Mixed hexahedron-tetrahedron meshes dominated by hexahedrons were adopted in the FE model. The hexahedral elements were implemented for their comparative higher convergence rate and tetrahedral elements for their flexibility in dealing with complex geometry. Mesh densities were determined by a mesh sensitivity study (Table 1) based on a prescribed accuracy requirement of less than 5% variance in peak sliding distance without oscillation between meshes as the mesh density was increased.

Table 1: Mesh Sensitivity Analysis Parameters for the Finite Element Model of the AMK

Mesh Density	Approximate Element Size (mm)	Number of Elements used for components (x10^4)		
		PE Insert	Femur	Tibial Tray
Low	1.397	4.70	0.61	0.84
Medium	0.889	11.0	1.36	1.62
High	0.635	24.8	2.54	2.78

The loading and boundary conditions were applied according to ISO 14243-3:2009. The IE rotation and AP displacement were implemented as boundary conditions on the tibial tray (Figure 17). These boundary conditions were implemented about the reference

point placed at the intersection of the axis of the tibial tray stem and the tray-insert interface. The axial load was applied to the tibial tray, offset in the medial direction from the tibial tray's reference point by 7% of the trays width as per the stated ISO standard. The flexion of the knee was recreated by the rotation of the femoral component, by means of a boundary condition, about a reference axis placed at the ISO specified flexion/extension axis location.

The FE model must replicate the material behaviour to accurately evaluate the contact pressures and sliding distances of the articular and backside surfaces. The articular surface reaction forces, caused by the loading and relative displacement of the femoral component against the PE insert, are transferred through the PE insert to the tibial tray, and produce the deformation of the PE insert and the relative movement between the PE insert and the tibial tray. Since the deformation of the PE insert around the locking mechanism is responsible for permitting the micromotion to occur, the selection of an accurate constitutive model for the PE is critical to the success of the model for the prediction of backside micromotion. Three different deformable constitutive models were implemented, the linear elastic model, viscoelastic model and a nonlinear J_2-plasticity model based on the true stress-strain behaviour of PE (Section 3.2.2). In addition, three rigid body contact models were considered, including the model of Halloran et al. [78], the stress-strain data utilized for the J_2 model, and a Hybrid model (Section 3.2.3).

3.2.2 Deformable Polyethylene Constitutive Modeling

For the accurate prediction of contact pressures and sliding distances, particularly for the prediction of backside micromotion, the implementation of a proper constitutive model is of vital importance. Three deformable constitutive models were considered, a linear elastic model, a viscoelastic model and a non-linear model.

The linear elastic model was considered for its simplicity, computational efficiency, and due to its wide application for the modeling of PE in the literature [68, 92]. The linear elastic constitutive model included a modulus of elasticity of 680 MPa, and a Poisson's ratio of 0.46 [3].

A viscoelastic material model was developed based on the stress relaxation behaviour modeling of Waldman and Bryant [94]. Waldman and Bryant described the stress relaxation behaviour of PE by the equation:

$$\sigma(t) = \left[(-449.6 \cdot 1E^6) + \left(673.1 \cdot 1E^6 \cdot \left(\frac{t + 0.05062}{100}\right)^{-0.05661}\right)\right] \cdot (\varepsilon_0) +$$
$$2 \cdot \left[(30.97 \cdot 1E^6) + \left(-31.84 \cdot 1E^6 \cdot \left(\frac{t + 0.05062}{100}\right)^{-0.00937}\right)\right] \cdot {\varepsilon_0}^2 +$$
$$3 \cdot \left[(215.3 \cdot 1E^6) + \left(-213.4 \cdot 1E^6 \cdot \left(\frac{t+0.05062}{100}\right)^{-0.00505}\right)\right] \cdot {\varepsilon_0}^3 \quad (7)$$

where the time dependant stress is represented by σ(t), time is represented by *t*, and strain is represented by ε_0. Therefore, the Abaqus formulated time domain viscoelastic parameters included a density of 0.935 g/cm^3, modulus of elasticity of 680 MPa, Poisson's ratio

of 0.46 and the normalized shear relaxation modulus (Table 2) calculated from the data of Waldman and Bryant [94].

Table 2: Shear Relaxation Modulus (gR) over Time

Time	gR
5	0.516629
10	0.619048
15	0.681834
20	0.727597
25	0.763759
30	0.79372
35	0.819335
40	0.841726
45	0.861629
50	0.879549
55	0.895854
60	0.910814
65	0.924638
70	0.937489
75	0.949497
80	0.960767
85	0.971385
90	0.981425
95	0.990946

The nonlinear model was implemented by means of the J_2-plasticity theory. The J_2-plasticity material parameters utilized by Bergstrom et al. [81], for the simulation of PE under cyclic loading as well as small, intermediate and large monotonic deformations, were adopted. The J_2-plasticity model included a modulus of elasticity of 1051 MPa, a Poisson's ratio of 0.46 and the non-linear tabular stress-strain values listed in Table 3. The model includes an elastic component defined by the modulus of elasticity and Pois-

son's ratio, as well as a plastic component defined by the linear interpolation functions of the tabular stress-strain values. The model was preconditioned to ensure that the plastic response of the PE insert had stabilized by repeating the step which recreated the conditions of the stated ISO standard until the peak cumulative micromotion converged to within 5% of the previous step's values without any oscillation between results.

Table 3: Non-Linear Stress (σ_y) - Stain (ε^p) values used for the J_2-Plasticity Model

Strain ε^p (%)	0	0.03	0.11	0.55	0.98	1.09	1.34
Stress σ_y (MPa)	12.1	21.4	23.8	44	92.4	135	515

3.2.3 Rigid Body Modeling

As an alternative to deformable FE models, rigid body models utilizing pressure-overclosure relationships, or EF theory, feature greatly improved computational efficiency. However despite the use of such models in the literature [76, 78], the accuracy of rigid body models have not been extensively validated. Halloran et al. [78] quantitatively evaluated the peak contact pressure over the gait cycle of a linear and nonlinear EF model compared to a nonlinear deformable model, however the contact pressure distribution and contact areas over the gait cycle were not quantitatively compared. Contact pressures and contact areas over the gait cycle must be found to be in good agreement between EF and deformable models before the method can be considered validated and utilized for the analysis of TKRs. Therefore three different rigid body models were developed and compared to the deformable J_2-plasticity model for the assessment of the models accuracy

compared to a deformable model. The first model incorporated the nonlinear pressure overclosure relationship which was previously utilized by Halloran et al. [78] as shown in Table 4 (hereafter referred to as Halloran model). The second model (J_2-RB) was based on the linear piecewise tabular stress-stain values optimized for use with the J_2-plasticity model [81] (Table 4). Finally, a new model (Hybrid model) was developed by the author based on the hypothesis that the Halloran model would perform best at low contact pressures while the J_2-RB model would perform best at high contact pressures. The new model utilized the parameters of the Halloran model for pressures of 3 MPa and below, and the parameters of the J_2-RB model above 3 MPa (Table 4).

Table 4: Pressure-Overclosure Relationships for Rigid Body Models

Overclosure (mm)	Pressure (MPa)		
	Halloran	J_2-RB	Hybrid
0	0	0	0
0	0	12.1	0
0.25	13.15	19.03	13.15
0.5	18.33	22.45	18.33
0.75	21.36	24.3	21.36
1	23.51	25	23.51
2	28.69	25.5	28.69
3	31.72	27.9	31.72
5	35.54	52.06	52.06
8	39.05	96.29	96.29
10	40.72	303.52	303.52

The contact of TKR components includes variable levels of conformity between the contacting components. If rigid body modeling were to be deemed acceptable for the wear prediction process, the method must be capable of accurately predicting contact ar-

eas and contact pressures for all design possibilities including designs of both high and low conformity. For this reason, three different scenarios were devised by the author for the evaluation of contact pressures and contact areas in comparison to the deformable models. For the first scenario, a low conformity FE simulation was conducted, including a ball of 70 mm diameter (similar to the sagittal radius of a femoral condyle), which was pressed against a flat PE disk of 10 mm thickness. The second scenario included a 70 mm diameter ball against an 80 mm diameter PE cup with a minimal thickness of 10 mm for the simulation of high conformity. Each of the first two tests were conducted at loads of 225 and 665 N to consider both high and low contact pressures. The third and final scenario for the comparison of models was the AMK under ISO 14243-3:2009.

3.3 Simulation of Backside Micromotion

The prediction of backside wear requires knowledge of the relative sliding displacements between the tibial insert and the tibial tray of a modular TKR. To the author's best knowledge, there has been no previously reported computational, finite element, or physical experiment capable of determining the micromotion at each location of the interface. Knee simulators only permit peripheral measurements to be taken during experimentation. Therefore, a FE model for the simulation of backside micromotion was developed and corroborated with knee simulator peripheral micromotion measurements. Since backside micromotion may be the most complicated outcome to predict, the assessment

of the FE models accuracy with respect to this outcome provides some indication of the FE models overall accuracy in predicting the physical experiment.

3.3.1 Finite Element Model Development

Corroboration of the predicted backside micromotion was achieved by the comparison of the FE models predictions to published knee simulator experiments implementing the AMK. The AMK was of particular interest as it not only held a large percentage of the TKR market [90], but it was considered possible that dovetail type locking mechanisms, such as that of the AMK, might permit a greater amount of backside micromotion to occur, therefore resulting in increased risk of wear particle induced osteolysis. It was found that backside wear of the AMK accounts for over 19% of the total wear volume [65]. The AMK was available with either a grit-blasted Ti6Al4V (Ti) alloy tibial tray or with a polished cobalt-chromium (CoCr) alloy (ASTM-F75) tibial tray. Both trays were of the same geometry, but include different substrate materials and surface finishes. The arithmetic average roughness coefficients of Ra = 1.05 ± 0.06 μm, and Ra = 0.02 ± 0.01 μm were reported for the grit-blasted blasted Ti alloy tibial tray and the polished CoCr alloy tibial tray respectively [95].

Published knee simulator experiments implementing the AMK are also available for the purpose of corroboration. DiSilvestro et al [62] and McNulty et al. [65, 95-96] investigated the effects of surface finish and PE locking mechanism on the AMK. The experiments of DiSilvestro et al [62] and McNulty et al. [65, 95-96], shared the same experimental set up for the measurement of micromotion during knee simulator tests. Miniature differential variable reluctance transducers (DVRTs) were utilized for the measurement

of micromotion, with a resolution of 200 nm and a maximum displacement of 750 μm [62, 65, 95-96]. The DVRTs were placed at the lateral edge of the insert, as well as at the most posterior point of the medial and lateral condyles. The bracket which the DVRTs were attached to was directly fixed to the tibial tray so that micromotion is measured as insert movement relative to the tibial tray [62, 65, 95-96]. The experiments of DiSilvestro et al [62] and McNulty et al. [65, 95-96] incorporated the loading conditions of ISO 14243-3:2009.

DiSilvestro et al. [62] presented the typical average AP micromotion knee simulator results plotted over a single ISO gait cycle for the AMK with a blasted Ti alloy tray, ranging from approximately 0-70 μm. McNulty et al. [95-96] reported the maximum AP micromotion of each condyle during the ISO gait cycle for the AMK with a polished CoCr tray. The results were obtained over two Mc for three TKRs. The resulting maximum AP micromotion with the polished CoCr alloy tibial tray was 510 ± 275 μm and 345 ± 190 μm (magnitude ± variance) for the medial and lateral sides respectively [95-96].

The FE model of the AMK (Section 3.2.1) with the linear elastic, viscoelasticity and J2-plasticity models were implemented for the evaluation of the models ability to predict backside micromotion. The rigid body models were not considered for the modeling of backside micromotion as it was considered unlikely that the simplified rigid body models would be able to predict the micromotion of the backside surface. The AP micromotion was calculated by comparing the most posterior node of each condyle on the peripheral-distal edge of the insert to the tibial tray node directly below it. This method of calculating AP micromotion was selected to be in agreement with the measurement system of the

in vitro knee simulator experiments [62, 95-96]. Similarly the medial-lateral micromotion was calculated at the insert node of the most lateral point, compared to the node of the tibial tray directly below it, also in agreement with the method of the in vitro knee simulator experiments [62, 95-96]. The average AP micromotion was determined by averaging the AP values from each condyle. Since backside wear is proportional to the cumulative relative sliding distances, not the maximum displacement from the initial state, cumulative micromotion was also calculated for each node of the backside surface. Two trays having different surface roughness, a blasted titanium alloy tray and a polished CoCr alloy tray, were studied by finite element simulations and compared to the corresponding knee simulator results for each type of tibial tray.

3.3.2 Titanium Alloy Tray Experiment

The micromotion of the AMK with a blasted Ti alloy tibial tray over the ISO gait cycle was simulated and compared to the knee simulator results. The PE-Ti interface was modeled with a coefficient of friction of 0.5, based on experimental results [97]. The objective of the simulation with the Ti alloy tibial tray was to compare the FE simulation trend of the average AP micromotion over the ISO gait cycle for each constitutive model to that of the knee simulator results [62].

3.3.3 Cobalt Chromium Alloy Tray Experiment

The micromotion was also simulated for the AMK with a polished CoCr alloy tray. The CoCr-on-PE contact interaction included a coefficient of friction of 0.04, a value in

agreement with experimental tests [71, 92-93]. The objective of the CoCr alloy tray simulation was to evaluate the ability of the model to predict the proper maximum micromotion magnitude of each condyle by comparing the FE results to those of McNulty et al. [95-96].

3.3.4 Cumulative Micromotion of Backside Surface

A compression test was conducted to analyze the significance of obtaining micromotion predictions for the entire backside PE surface, compared with relying on the peripheral measurements a knee simulator test would provide. The compression test was conducted by incrementally adding and removing a load of 2600 N, using tabular equally spaced intervals, to the femoral component while the tibial tray remained fixed. The compression of the femoral component against the PE insert was the only relative motion applied during the simulation. The cumulative micromotion of the backside surface during the stated ISO simulated gait cycle was also analyzed to consider the increased amount of backside micromotion information obtained by the FE simulation over knee simulator experimentation alone.

3.3.5 Analyses of Tibial Locking Mechanisms

Two different locking mechanisms were analyzed to assess the influence of the locking mechanism design on backside micromotion. A comparison was conducted between the AMK with a dovetail and pin locking mechanism and the AMK with a modified peripheral locking mechanism. The peripheral locking mechanism was similar to that of the

Press-Fit Condylar knee system (PFC®, DePuy Orthopedics Inc., Warsaw, IN). The PFC-type locking mechanism was applied to the AMK insert in order to enable a direct comparison of the locking mechanism performance without altering the reaction forces of the topside surface. A laser scanner (Ai600 ShapeGrabber, Ottawa, Ontario) was used to generate solid models of the PFC PE insert and tibial tray. The solid models of the AMK insert and the tibial tray were modified to include the PFC-type full peripheral locking mechanism and remove the original dovetail and pin locking mechanism (Figure 18).

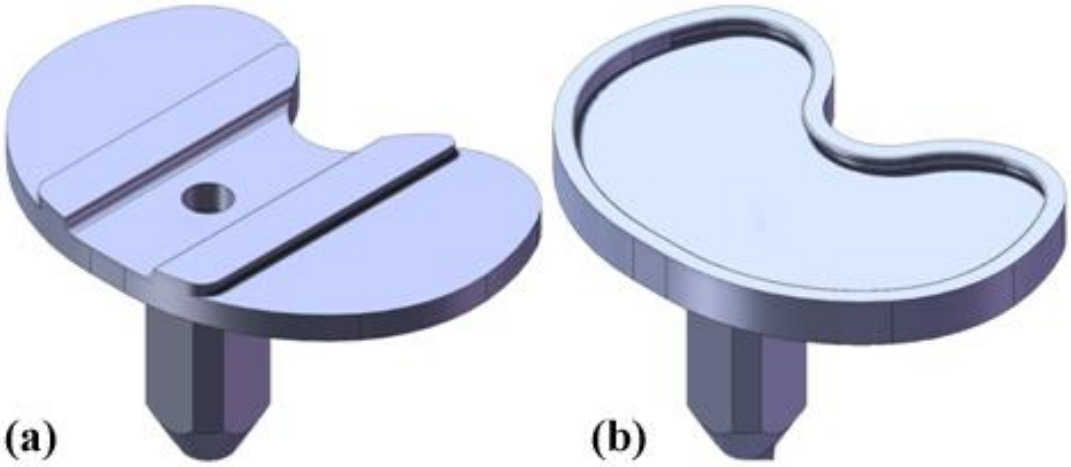

Figure 18: Locking Mechanisms Comparison: (a) AMK Dovetail Design; (b) PFC-type Peripheral Locking Mechanism Design;

The influence of interference fit on backside micromotion was also analyzed. Interference fit (press fit), refers to the amount of geometrical overlap (interference) between two components. Once the two components are pressed together, the PE deforms (resulting in strain) to fit the geometry of the tray and results in pressure between the two components. The measure of interference fit of the AMK with the PFC-type locking mechanism was varied from size-on-size to 0.254 mm. The femoral component and tibial tray were, once again, modeled as rigid bodies for computational efficiency. The PE insert

was modeled with the nonlinear J_2-plasticity model of Bergstrom et al. [81]. Penalty contact was defined between all contacting components, and the CoCr-on-PE contact interaction included a coefficient of friction of 0.04 [71, 92-93]. Loading and boundary conditions were once again applied according to the stated ISO standard. The mesh densities of the PFC-type design were determined by a mesh sensitivity analysis (Table 5).

Table 5: Mesh Sensitivity Analysis Parameters for the Finite Element Model of the Modified AMK including a PFC-type peripheral locking mechanism

Mesh Density	Approximate Element Size (mm)	Number of Elements used for components (x10^4)		
		PE Insert	Femur	Tibial Tray
Low	1.397	1.01	0.61	0.84
Medium	0.889	7.10	1.05	1.06
High	0.635	25.5	2.54	2.78

3.4 Identification of Wear Factors of Archard's Wear Law

The majority of previous TKR computational wear models have utilized Archard's wear law [45, 68, 72-73, 83-85]. Although more complex wear models, incorporating the effects of cross shear, have recently been developed based on POD test results [22], the trends of such models are not in agreement with the results of knee simulator wear tests, such as the decrease in wear with increasing contact pressure [22]. The macroscopic POD wear models previously developed may contradict knee simulator wear test results because POD experiments are unable to replicate the complex surface interactions present

in TKRs. POD experiments used for the development of wear models have not included tractive rolling [28], dynamic loading [30], sliding velocity [29] or replicate the geometric contact conditions of TKRs. The development of a wear model through the use of knee simulator results, rather than from POD testing, was deemed beneficial to ensure the relevancy of the finite element model to TKR wear. The simplicity and versatility of the model also make the model well suited for the development of a wear model for a surface which has never before been modeled, such as the backside surface.

3.4.1 Identification of the Wear Factor of Archard's Wear Law

The FE model previously developed (Section 3.2.1) was utilized to analyze the contact pressures and sliding distances of both the articular and backside surfaces. The knee simulator wear test results previously discussed in Section 3.1 were utilized for the identification of the wear factor of Archard's wear law. A derivation of Archard's wear law was implemented for the wear factor identification process. Archard's wear law specifies that the wear depth at each location can be calculated as follows:

$$W_{depth} = k \cdot p \cdot S \tag{8}$$

where W_{depth} is the wear depth, k is the wear factor, p is the contact pressure and S is the sliding distance between the two components [98]. The volume lost due to wear can be found by integrating the wear depth across the contact zone:

$$V_{wear} = k \int S\, p\, dA \tag{9}$$

where V_{wear} is the volume lost due to wear, and *dA* is a differential of the area. Therefore, the wear factor can be determined, since V_{wear} is known from the knee simulator results [91], and all other variables apart from *k* can be calculated from the finite element results. Since approximately 20% of total wear volume was known to occur at the backside surface [65], the wear volume of the articular surface ($V_{wear\text{-}A}$) was specified as 80% of the knee simulator incremental V_{wear} over the given 0.5 Mc interval. Similarly, the wear volume of the backside surface ($V_{wear\text{-}B}$) for each interval was specified as 20% of the knee simulator incremental V_{wear} over the given 0.5 Mc interval. The articular wear factor (k_A) and the backside wear factor (k_B) were determined for each of the six inserts used in the knee simulator, for each 0.5 Mc interval. Therefore, the equation for the calculation of k_A or k_B can be written as:

$$k_{A,B} = \frac{(V_{wear})_{A,B}}{(\sum_{i=1}^{elements}(\sum_{t=0}^{100}(S_t p_t A_t)_i))_{A,B}} \tag{10}$$

where the denominator is the sum of the products of the sliding distance, contact pressure and area for each time interval over all nodes. This equation was implemented for each surface (articular and backside) for the identification of the wear factors k_A and k_B (Figure 19).

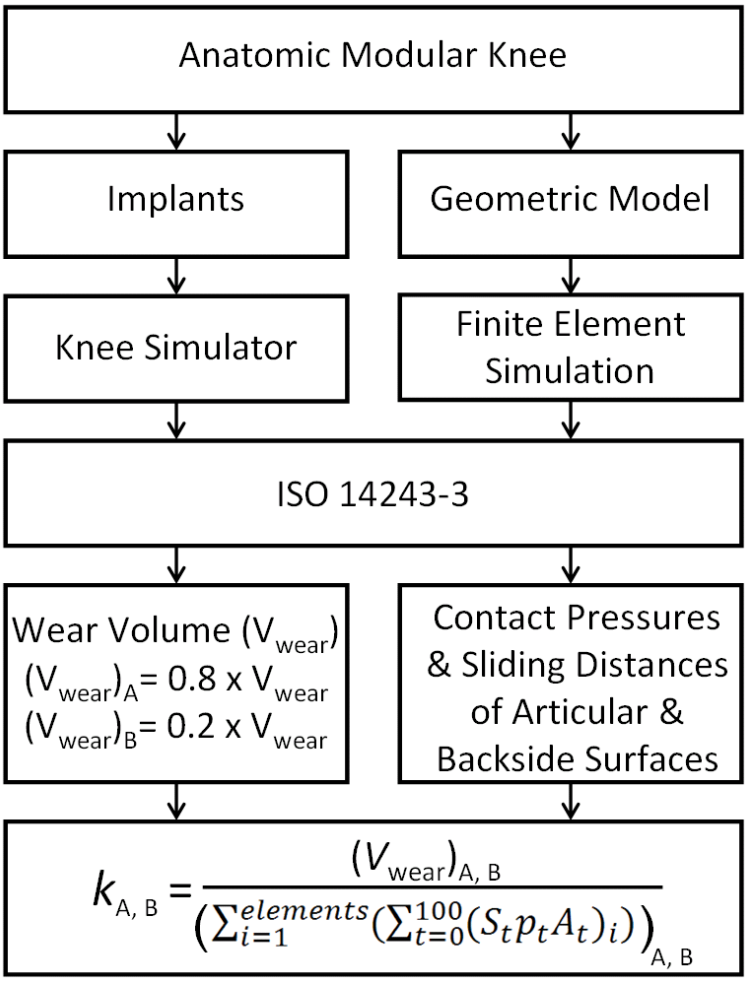

Figure 19: Identification Calculation for the Articular Wear Factor (k_A) and the Backside Wear Factor (k_B) of Archard's Wear Law

A python code was developed to directly interface with Abaqus, which read the contact pressures and sliding distances from the Abaqus output database and calculated the wear depths at each node based on the last known wear factor (or a starting value of 2 x 10^{-7} mm^3/Nm for the first interval). The worn geometry output by the python program was then implemented in a Matlab program (Matlab, Mathworks, Natick, MA), which

was developed to create a polygon mesh over the new surface geometry and calculate the volume. The Matlab program utilized Delaunay Triangulation to create a wrap polygonal mesh around the exterior nodes of the insert and calculate the difference between the new volume and the volume of the insert at the previous wear increment. The Matlab program would then increase or decrease the wear factor by 10%, based on whether the calculated wear volume was higher or lower than that of the knee simulator wear test and repeat the process. Once wear factors resulting in wear values both higher and lower than the knee simulator wear volume were obtained, linear interpolation was conducted to calculate the next iteration for the wear factor. The process continued using the high and low values closest to the knee simulator wear volume until the predicted wear volume became within 1.5% of the knee simulator wear volume. Then the program would proceed to the next wear interval (Figure 20). The program was used to calculate the wear factors k_A *and* k_B, and the use of 0.5 Mc interval increments was verified by an update interval convergence study to limit the error associated with the interval of geometric updating. Archard's wear law has previously been utilized for the simulation of the PE insert articular surface rolling-sliding wear [45, 68, 72-73, 83-85], as well as for the simulation of fretting wear [99].

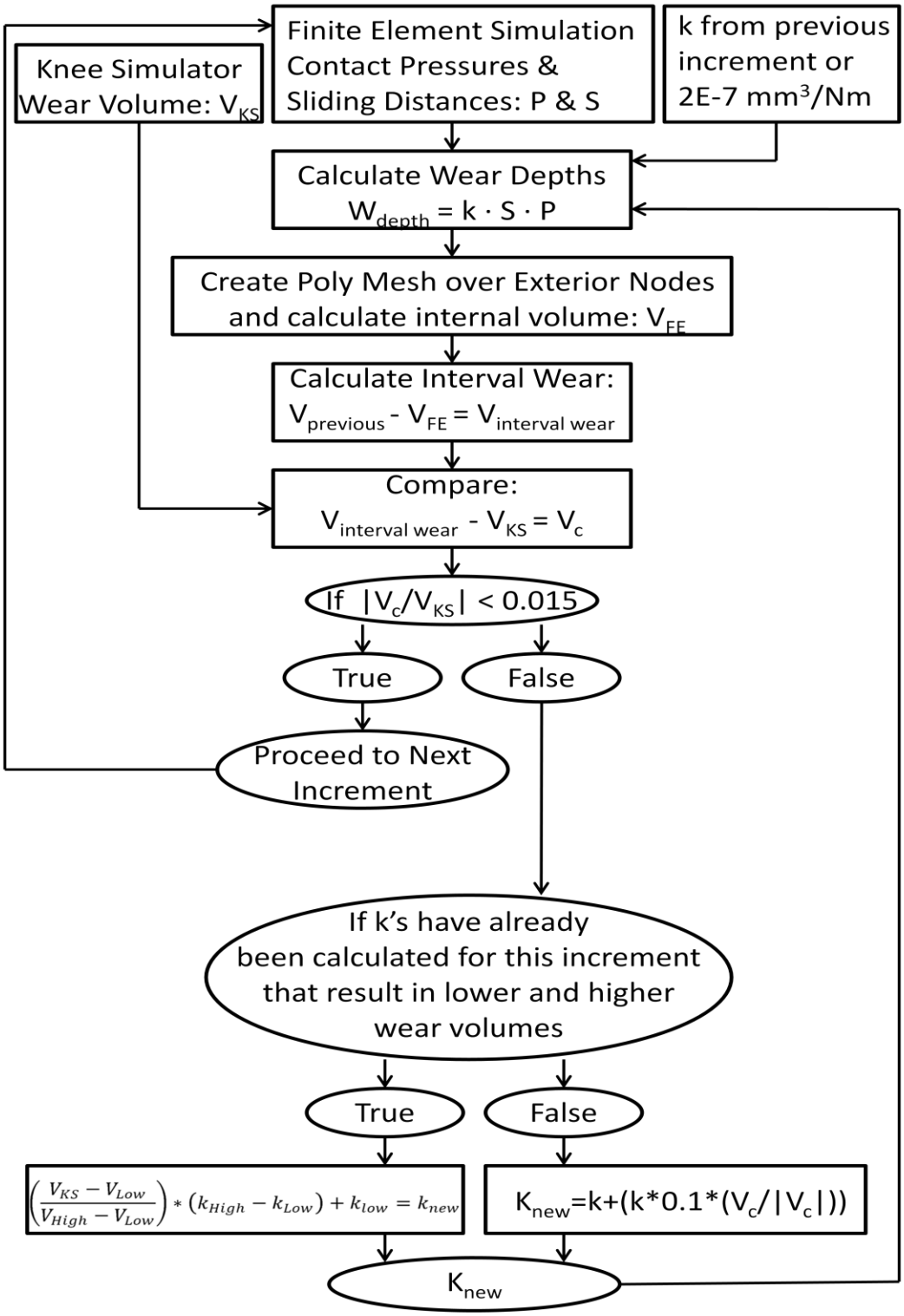

Figure 20: Python and Matlab Program Procedure for the Identification of the Wear Factors

3.5 Development of a Novel Wear Model Based on PE Molecular Structure and Wear Theory

While the development of a wear model based on the Archard's wear law has enabled the investigation of the different tribological conditions between the articular and backside surfaces, such a model would not be able to account for the changes in cross shear that would result from changes in design geometry or knee kinematics. The wear model based on Archard's wear law can only account for the effects of changes in contact pressure, and sliding distances since all other variables are modeled by the wear factor *(k)*. Obtaining the wear factor *(k)* from knee simulator results indicates that the wear factors *(k)* are relevant for the conditions from which they were derived. Therefore any changes to parameters other than contact pressure and sliding distances, such as cross shear, will not be accounted for and the wear calculation will continue to include the parameters of the AMK under the stated ISO standard, since those were the conditions from which the wear factors were derived. Therefore, a more complex model, incorporating the effects of the directional strain hardening of PE was required. Previously developed PE wear models incorporating the effects of cross shear have either poorly predicted PE wear [87], or have shown trends which contradict the results of knee simulator wear testing [22]. Therefore, a new wear model was developed by the author, based on a theoretical understanding of the molecular structure of PE. First, an explanation of the theory and the de-

veloped equations is given. The theory explanation is followed by the identification of the material parameters of the model by use of POD test results. Finally, a discussion of how the new computational wear model was implemented is provided.

3.5.1 Wear Model Theory

Previously developed wear models exist which include provision for cross shear, however the models have been shown to result in poor predictability [76] in comparison to knee simulator wear tests. The previously available wear models suffer from significant theoretical limitations, for instance the model of Turell et al. [87], Wang et al. [53], Kang et al. [22, 51-52], and Abdelegaied et al. [67] all predict constant wear rates extending to infinity with continued sliding in a consistent direction which has been demonstrated to be inaccurate by Dressler et al. [100]. In addition, the model of Turell et al. [87] predicts a linear increase in wear rate with increasing CS to a peak wear rate at an aspect ratio of 0.5, which has been identified through POD testing to be inaccurate, instead the wear follows a curve of exponential decay [22, 51-52, 87]. The model of Wang et al. [53] is not relevant for TKRs as it is based on hip simulator wear testing which occurs dominantly under the mixed lubrication regime [53, 89] while TKRs function dominantly under the boundary lubrication regime [26]. As well, the model of Wang et al. [53] specifies that wear is only resisted by the cross-linked bonds of carbon atoms, which would result in infinite wear for non-crosslinked PE, which is not accurate. The model of Kang et al. [22] predicts decreasing wear with increasing contact pressure which is contrary to knee simu-

lator wear test results [3]. The model of Abdelegaied et al. [67] does not account for the effects of contact pressure on wear which have been shown to be influential through knee simulator wear tests [3].

It has previously been shown that wear occurs to a far greater magnitude when the direction of sliding is perpendicular to the orientation of the molecular chains (orientation softening), and with continued sliding in the same direction, the molecular chains will eventually become orientated in the current direction of sliding and the wear rate will decrease significantly [100]. This demonstrates the importance of the time dependence of the PE molecular structure and the need for modeling the molecular orientation over time. While previous models have only considered the angle between the current direction of sliding and the average direction of sliding, the objective of the current research was to model the molecular interactions within PE over time. The energy dissipated at the interface was considered the driving force of these molecular interactions. The wear of other materials have previously been shown to be proportional to the energy dissipated at the surface interaction (Energy Dissipation Theory) [101]. However in the case of thermoplastics such as PE, the energy not only results in the breaking of intermolecular bonds and generation of wear particles, but also results in the directional strain hardening of the material.

The Primary Molecular Orientation (PMO) has previously been defined as the average (time independent) direction of sliding. Alternatively, the Current Molecular Orientation (CMO) is here defined as the current (time dependant) direction of the highly orientated crystalline lamella, measured relative to the anterior-posterior plane on the tibial in-

sert. While the Cross Shear (CS) has previously been defined as the relative angle between the current sliding direction and the PMO, the Cross Shear Angle (CSA) is here defined as the current (time dependant) angle between the current shear force vector and the CMO.

Energy dissipated at the PE surface either results in molecular changes to the polymer (such as wear and strain hardening), or the energy is dissipated to the external system (such as through the generation of heat or work done on the lubricant). When work is done with a shear force direction other than that of the PE's CMO, the work results in the mobility of the molecular chains (as the chains re-orientate themselves in the direction of shear force), as well as the simultaneous generation of wear particles as molecular bonds within the PE are broken. When work is done with a shear force in the direction of the PE's CMO, the work results in the stretching of the molecular chain and reinforces the current orientation. Previous POD testing indicates that the relationship between molecular orientation, as well as wear generation, over time is not linear [51-52]. The results of Kang et al. [22, 51-52] have demonstrated the relationship between wear and cross shear to be best described by an exponential decay function and the POD test results of Turell et al. [87] further support this modeling strategy. Therefore, the wear volume (V_{wear}) is here proposed to be related to work by the equation:

$$V_{wear} = R_w \cdot \left(1 - e^{-C_w/M_{mc}}\right) \tag{11}$$

where R_w is the materials resistance to wear and is proportional to the maximum magnitude of wear that can be attained during infinite work done with a shear force in a single direction (starting at a 90 degree angle to the initial molecular orientation). C_w is the current work, for a shear force exerted in a single direction over a given time interval. M_{mc} is the shape factor of the exponential curve (Figure 21) and represents mobility of the molecular chain. By using the theoretical material parameters M_{mc} and R_w, for the development the model, the model is applicable to a wide range of PE varies, including PE of all GUR types as well as conventional PE and PE of all crosslink densities. For example, increasing the crosslink density of PE by irradiation would decrease the mobility of the molecular chain, resulting in an increased M_{mc}, as well as an increase in the materials resistance to wear during molecular reorientation, resulting in a decreased R_w. Work done with a consistent shear force direction over a discrete time interval may be represented as:

$$C_w = S \cdot \mu \cdot P \cdot NA \tag{12}$$

where C_w is the work over the current interval, μ is the coefficient of friction and P is the contact pressure over the specified area NA. The CSA may be related to work by the equation:

$$\text{CSA}=\left(e^{-C_w/M_{mc}}\right) \tag{13}$$

for work with a shear force of a consistent direction beginning perpendicular to the CMO. Therefore, the wear volume over time may be calculated according to Equation (12) (Figure 21) and the CSA over time may be calculated according to Equation (13) (Figure 22) for work done on PE with a shear force of a consistent direction, beginning perpendicular to the materials CMO.

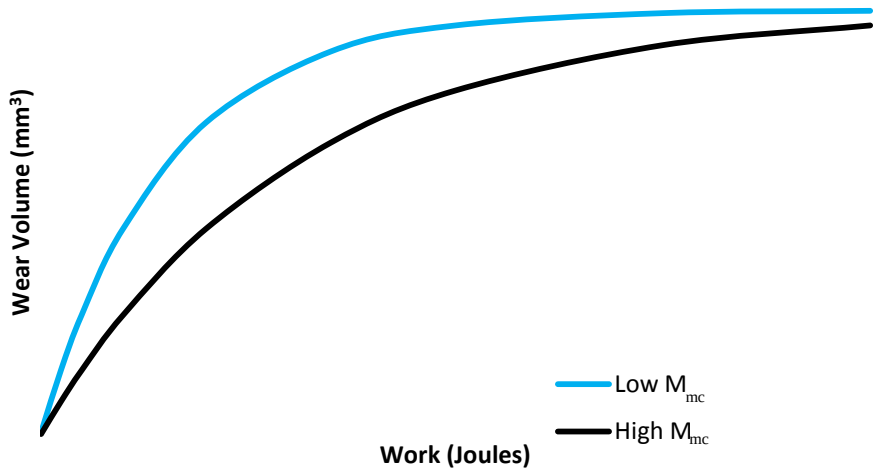

Figure 21: Wear Volume vs Work for PE with Low and High M_{mc} Values

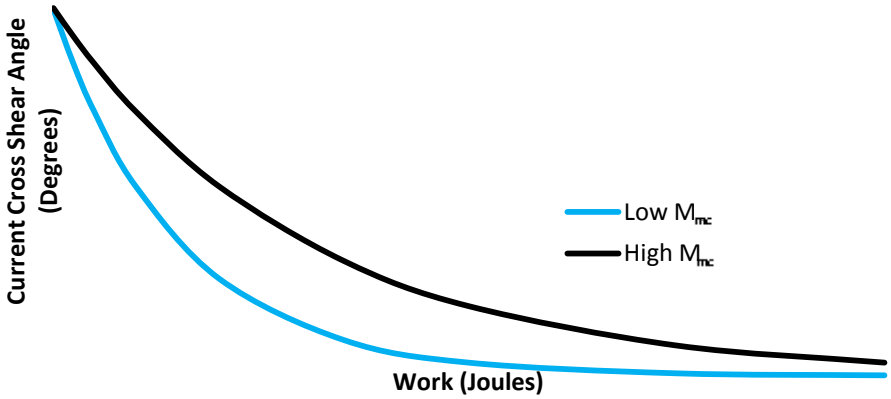

Figure 22: Current Cross Shear Angle vs Work for PE with Low and High M_{mc} Values

The wear of PE rarely begins at 90 degrees of cross shear angle, the theoretical work (B_w) required to reach the current cross shear angle at initiation (CSA_i) of the time interval must be calculated:

$$B_w = -M_{mc} \cdot ln(CSA_i) \tag{14}$$

Then the wear volume (V_{wear}) over the current time interval can be calculated by the equation:

$$V_{wear} = R_w \cdot \left(1 - e^{-(C_w + B_w)/M_c}\right) - \left(1 - e^{-(B_w)/M_c}\right) \tag{15}$$

The cross shear angle at the end of the time interval (CSA_e) can be calculated by the equation:

$$CSA_e = \left(1 - e^{-(C_w + B_w)/M_c}\right) \tag{16}$$

The CSA_e can then be utilized, along with any changes in the direction of shear force and work, for the calculations of the next interval.

While the models of Turell et al. [87], Kang et al. [22, 51-52] and Abdelgaied et al. [67] have been based on extensions of Archard's wear law by adding additional variables for the calculation of Archard's wear factor *(k)*, the wear model developed in the present

thesis is not based on Archard's wear law but on a unique and novel calculation for the time dependant changes to the molecular polymer chain. Furthermore, while the previous wear models have been based on macroscopic POD results, the newly developed wear model is based on a theoretical understanding of PE wear and POD tests are only utilized to evaluate the material parameters of the model.

3.5.2 Assessment of Model Parameters

Before the model could be applied to TKR designs the parameters μ, R_w and M_{mc} were required. The coefficient of friction was specified as 0.04 based on the values in the literature [71, 92-93]. The material parameters R_w and M_{mc} were determined from previously published POD testing [51, 87]. A python program was created which implemented an iterative optimization script to reduce the error between the predicted wear volume and the experimentally determined wear volume utilizing Equations (12)-(16). The resultant parameters were $R_w=1 \times 10^{-6}$ and $M_{mc}=0.055$ which are relevant for the experimental conditions from which the parameters were derived (conventional non-crosslinked GUR 1050 PE operating in diluted bovine serum with a protein concentration of approximately 20 g/l). Additional POD test results could be utilized to develop parameters for PE of different crosslink densities, GUR types as well as for different lubricants.

3.5.3 Implementation and Corroboration of the New Wear Model

A new python program was written to calculate wear based on the newly developed wear model. The FE model previously developed for the AMK was utilized for the assessment of contact pressures, sliding distances and the direction of shear forces at the surfaces of the PE insert.

The area surrounding each node was required for the new wear method to relate the wear volume at each node to the wear depth of the revised geometry. A python program was created to calculate the area surrounding each node and load the value to memory, as well as to a text file which could be loaded to memory at a later time as needed. The program utilized node sets for the topside and backside surfaces to reduce the number of nodes for which processing was necessary. The program looped through the nodes of each set and obtained lists of all elements that each node was associated with. The area contributed to the node by each associated element was calculated by dividing the element area (determined from the elements associated node coordinates) by the number of nodes associated with the element. Therefore, the area of a node may be calculated by the formula:

$$NA=\sum \left(\frac{EA}{NN}\right)_{Associated\ Elements} \quad (17)$$

where EA is the element area, NN is the number of nodes associated with the element, and Associated Elements refers to all elements associated with the node for which area is to be calculated.

Once the nodal areas had been calculated by the nodal areas python program and the contact pressures, sliding distances and shear vectors had been determined by the FE model (Section 3.2.1), the wear of the PE insert could be calculated. The python program for the calculation of wear initially developed a PMO matrix as a starting point. The average direction of shear force for each node was determined by calculating the weighted average based on the magnitude of work and the direction of the shear vector. All shear vectors were converted to occur in the first two quadrants as shear angles of 180 degrees apart are equivalent in terms of molecular orientation. The program utilized the PMO directions as the initial CMO starting point. The program then ran through the gait cycle an additional three times, utilizing Equations (12), (14) and (16), to precondition the CMO. Next, the python program utilized Equations (12)-(16) for the prediction of wear, CMO and CSA's over the gait cycle. The wear volumes were converted to wear depths based on the area surrounding each node (NA). In addition, the effect of creep on implant geometry was accounted for by the new wear model by implementing a creep law based on the curve fitted data of Lee and Pienkowski [102]:

$$CD = 3.491 \cdot 10^{-3} + (7.966 \cdot 10^{-4} \cdot (log(t) - 4) \cdot P \cdot h) \quad (18)$$

where CD is creep deformation (mm), t is time (minutes), P is the contact pressure (MPa), and h is the part thickness (mm) in the direction of loading. The creep was modelled with natural creep recovery, and the surface evolution was equal to the wear depth and creep. The python program would output the wear volume for each surface and create a new .INP file with the revised wear and creep geometry for the next run of the FE model. The procedure was repeated with a geometric update interval of 0.25 Mc which was confirmed to be sufficient by a convergence analysis (Figure 23).

The program considers the polymers of a new tibial insert to initially be orientated in the direction of dominant sliding. This simplification is not accurate, as the polymer chains will be either of a random orientation, or will be orientated based on the manufacturing geometry of the compression moulding process. However, after a short period of time the polymer chains will become re-orientated. Neglecting this initial phase is therefore justified by the fact that a comparatively small amount of wear would be generated during this initial phase.

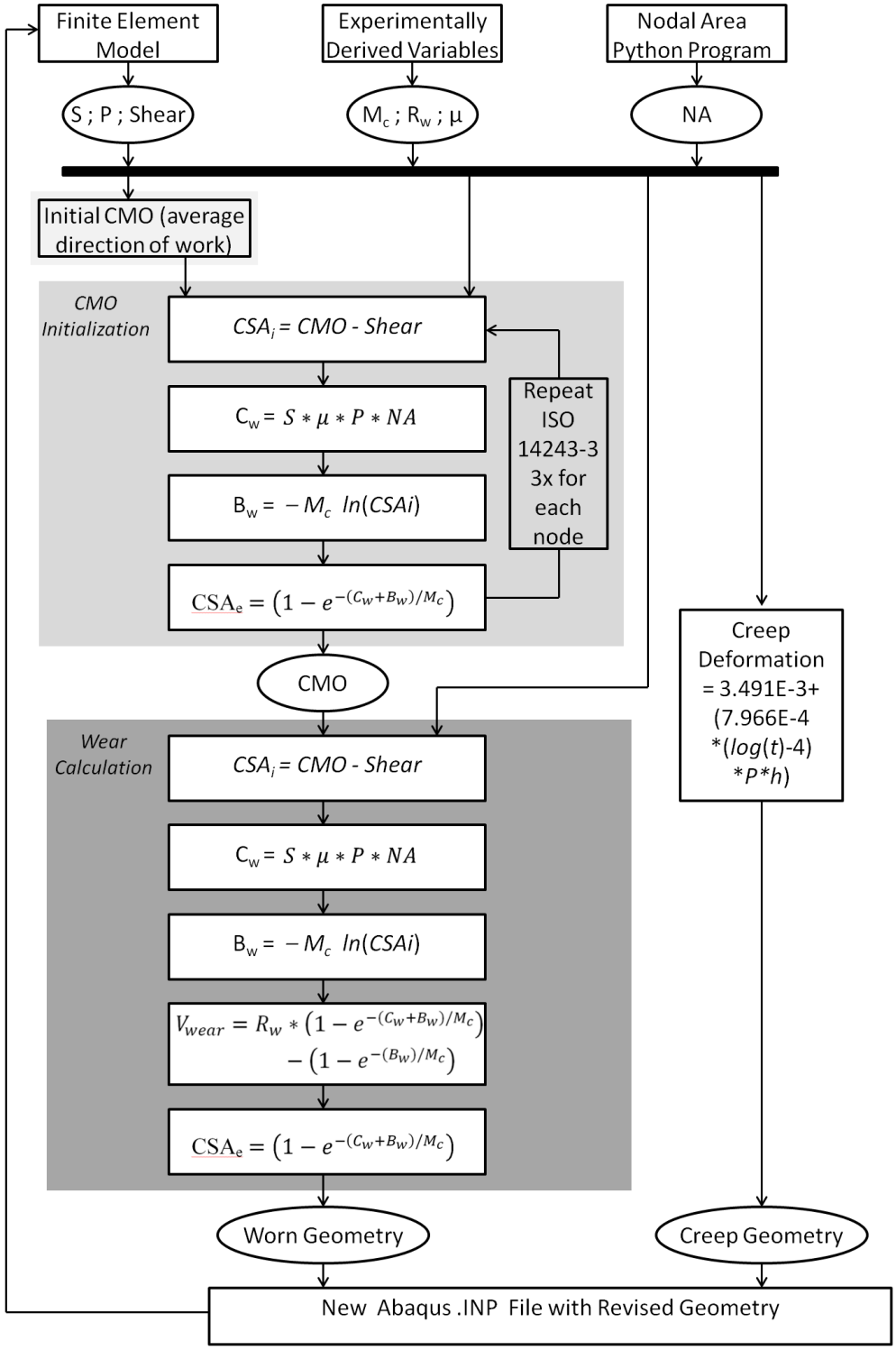

Figure 23: New Wear Model Program Procedure

Chapter 4

Results and Discussion

The prediction of wear requires knee simulator testing for development or verification, a FE model for the assessment of contact pressures and sliding displacements, and a computational wear model for the assessment of wear. Knee simulator results were required, both for the identification of Archard's wear factor, as well as for the corroboration of the new wear model to independent results. The wear volumes of the articular and backside surfaces were obtained from the knee simulator wear tests and are presented in Section 4.1. Convergence studies were performed for the FE models to ensure results convergence prior to utilizing the results (Section 4.2). FE studies were performed with three rigid body models and a deformable model of a known accuracy to evaluate whether the rigid body models were sufficiently accurate for the evaluation of articular contact pressures and areas (Section 4.2). The deformable FE model was utilized to predict backside micromotion and the results were corroborated with knee simulator results to assess the accuracy of the model. Following the verification of the accuracy of the model, the model was utilized to investigate the effects of various design parameters on backside micromotion (Section 4.3). The FE model with verified accuracy was then util-

ized along with the knee simulator results for the identification of the wear factors of Archard's wear law for both the articular and backside surfaces (Section 4.4). Although the results of the model based on Archard's wear law provided useful insight into TKR wear, the model is not sufficient for design optimization as it does not account for the effects of changes in cross shear resulting from geometric or kinematic changes. Therefore, a new wear model was developed based on a theoretical understanding of PE microstructure and wear. The new wear model was utilized for the prediction of wear with the AMK, and the results were corroborated with the independent knee simulator test results to verify the accuracy of the new model (Section 4.5).

4.1 Knee Simulator Experiments

The articular and backside interval wear volumes were calculated from the interval wear volumes of Brandt et al. [91], based on the observation of 80% articular and 20% backside wear (Table 6 and Table 7).

Table 6: Knee Simulator Wear Test Articular Interval Wear Volume (mm^3) for the AMK

Implant Number	Interval (Mc)						
	0-0.5	0.5-1	1-1.5	1.5-2	2-2.5	2.5-3	Average
1	4.669	6.056	8.416	8.407	12.746	10.277	8.428
2	5.228	8.004	8.584	8.989	12.137	10.340	8.880
3	5.436	6.743	7.725	9.827	10.376	8.656	8.127
4	6.631	9.230	9.614	11.211	8.100	8.494	8.880
5	5.456	7.584	8.025	10.061	8.481	7.537	7.857
6	7.164	9.863	11.536	12.066	9.985	9.552	10.028
Average	5.764	7.913	8.983	10.094	10.304	9.143	8.700

Table 7: Knee Simulator Wear Test Backside Interval Wear Volume (mm^3) for the AMK

Implant Number	Interval (Mc)						
	0-0.5	0.5-1	1-1.5	1.5-2	2-2.5	2.5-3	Average
1	1.167	1.514	2.104	2.102	3.186	2.569	2.107
2	1.307	2.001	2.146	2.247	3.034	2.585	2.220
3	1.359	1.686	1.931	2.457	2.594	2.164	2.032
4	1.658	2.307	2.403	2.803	2.025	2.124	2.220
5	1.364	1.896	2.006	2.515	2.120	1.884	1.964
6	1.791	2.466	2.884	3.017	2.496	2.388	2.507
Average	1.441	1.978	2.246	2.523	2.576	2.286	2.175

4.2 Finite Element Models

4.2.1 Finite Element Model of the AMK

Convergence tests were performed to analyze mesh sensitivity and the stabilization of the materials plasticity (Figure 24-Figure 25). The mesh sensitivity analysis revealed an element edge size control of 0.889 mm to be sufficient for the prediction of backside micromotion. The materials plasticity stabilization analysis showed the difference from the second cycle to subsequent cycles to be less than 0.5%. Therefore one preconditioning cycle was implemented and the second cycle was utilized for the analysis of backside micromotion.

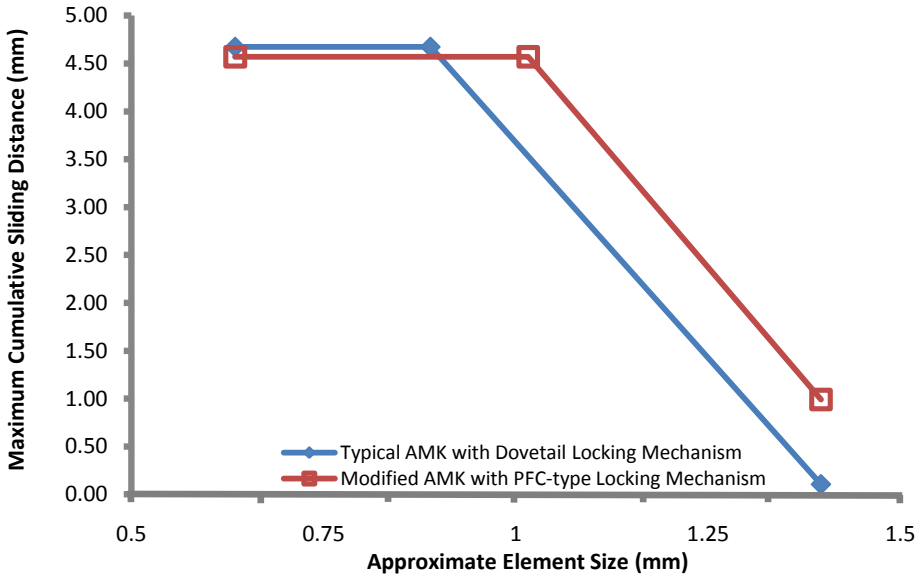

Figure 24: Mesh Sensitivity Analysis of Maximum Cumulative Sliding Distance (µm) over Repeated Cycles for: (a) Typical AMK Tray with a Dovetail Locking Mechanism; (b) Modified AMK Tray with a PFC-type Full Peripheral Locking Mechanism

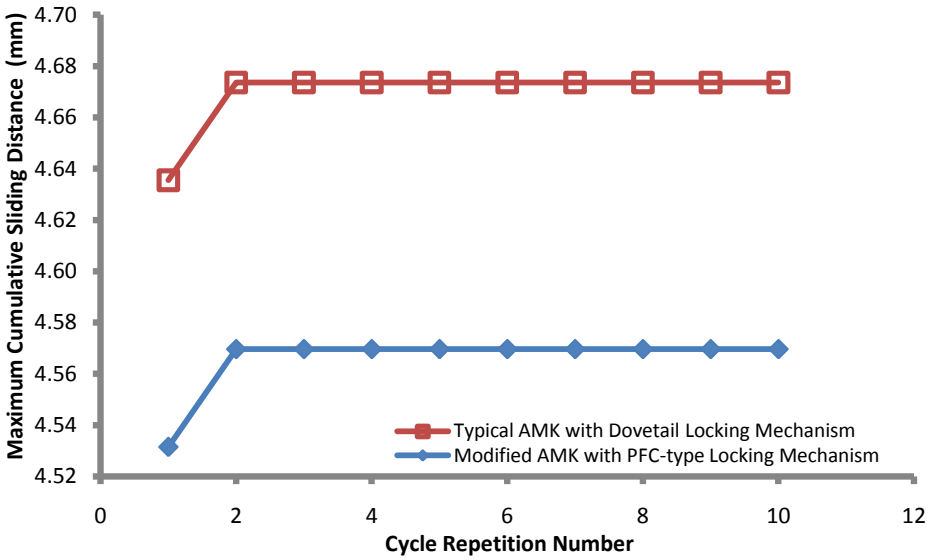

Figure 25: Plasticity Stabilization of Maximum Cumulative Sliding Distance (µm) over Repeated Cycles for: (a) Typical AMK Tray with a Dovetail Locking Mechanism; (b) Modified AMK Tray with a PFC-type Full Peripheral Locking Mechanism

4.2.2 Deformable and Rigid Body Modeling of PE

The PE component was modeled both as a deformable body with three different constitutive models (linear elastic, viscoelastic and J_2-plastic model), and as a rigid body with three different pressure-overclosure relationships (J_2-RB, Halloran and Hybrid model). Two simple FE simulation scenarios of a rigid ball on a PE tray or cup were developed to assess the predictability and computational efficiency of the rigid body models under low and high levels of conformity and with high and low loads (Table 8). Plasticity stabilization was once again confirmed to have occurred by the second step for all FE simulations as the second and third steps resulted in negligible differences (less than 5%) with no oscillation of results. High density meshes were utilized to obtain results of high resolution for comparison. The meshes (0.5 mm approximate element size) were confirmed to have converged as mesh densities of 0.75 mm and 1 mm also resulted in the same solution, however a less dense mesh was not implemented as a high level of contact pressure distribution resolution was required. As well, the AMK was simulated under the ISO 14243-3 loading and displacement conditions to assess each methods' predictability and computational efficiency when simulating a TKR.

Each of the rigid body models were compared to the deformable J_2-placticity model to assess the accuracy of the rigid body models in comparison to a deformable model (Table 8). Unfortunately it was not possible to compare the FE simulation results to a physical test as no test method currently exists which could measure the contact pressure across the surface, however the J2-placticity model was previously determined to have a

Table 8: Rigid Body Model Error with High and Low Conformity
(CP stands for Contact Pressure)

		J_2-RB Model Error (%)			Halloran Model Error (%)			Hybrid Model Error (%)		
Test	Load	Max CP	Avg CP	Area	Max CP	Avg CP	Area	Max CP	Avg CP	Area
Low Conformity	225	130%	61%	300%	65%	4.72%	400%	65%	4.72%	400%
	665	6.7%	49%	150%	2.7%	-3.2%	250%	-18%	-8.1%	250%
High Conformity	225	-26%	-20%	0.0%	-49%	33%	-55%	-49%	-55%	33%
	665	5.0%	-3.3%	0.0%	-46%	-63%	67%	-46%	-63%	67%
Average		42%	34%	113%	41%	26%	193%	45%	33%	188%

coefficient of determination of 0.877 compared to physical test results [81]. Pressure sensitive films would not be sufficient for the measurement as they introduce an additional deformable layer into the analysis and, given the low modulus of elasticity of the PE component, would result in substantial error. Overall, the J_2-RB model featured improved accuracy over the other two models. The J_2-RB derived model resulted in 42%, 34% and 112% average error for the prediction of maximum contact pressure, average contact pressure and contact area respectively. Despite the use the Halloran et al. [78] model in the literature [76, 78] for the prediction of contact pressures and contact areas, the model resulted in 41%, 26% and 193% average error for the prediction of maximum contact pressure, average contact pressure and contact area respectively. The Hybrid model did not offer any improved accuracy over the other rigid body models. The Hybrid model resulted in 45%, 33% and 187% average error for the prediction of maximum contact pressure, average contact pressure and contact area respectively. The rigid body models resulted in maximum contact pressure errors similar to those measured by Halloran et al.

[78]. None of the previous literature had quantitatively investigated the effects of rigid body models on contact area predictions [76, 78]. The rigid body models predicted contact areas of more than 2-times greater than those of the deformable J_2-plasticity model on average.

FE simulations were also conducted with each rigid body model and the deformable J_2-placticity model for the AMK under the ISO displacement controlled knee simulator conditions. The J_2-RB pressure overclosure relationship resulted in a higher level of accuracy than the other rigid body models; however, the predicted contact areas of the J_2 derived model were approximately double those of the deformable model. The maximum and average contact pressures over the gait cycle for the deformable J_2-placiticy model and J_2-RB rigid body models are shown in Figure 26 and Figure 27 (Halloran and Hybrid models have been omitted from the figures for clarity). The rigid body models resulted in similar trends in terms of maximum and average contact pressure, with the tendency to over predict the contact pressure. The rigid body models resulted in significant error, particularly in terms of contact area predictions which were over double those of the deformable models. The significant difference in predicted contact area would affect the wear prediction and introduce additional error. Therefore, despite the improved computational efficiency of rigid body models over deformable models it is recommended that only deformable body models be considered for the simulation of contact pressures and areas.

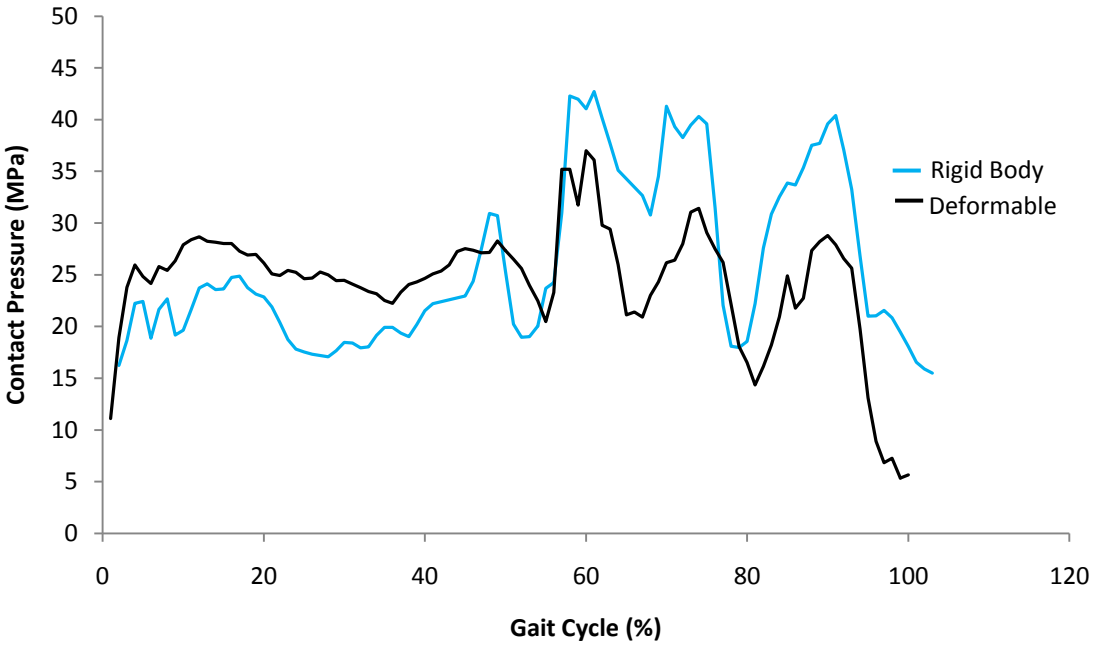

Figure 26: Maximum Articular Contact Pressure for the AMK with the Deformable J_2-plasticity and Rigid Body J_2-RB Models

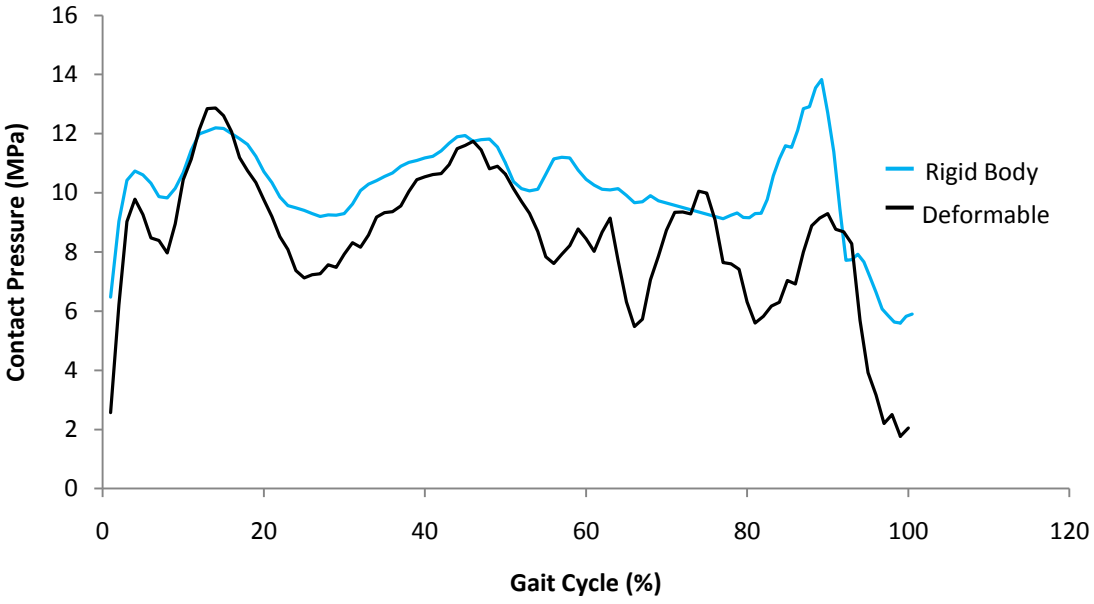

Figure 27: Average Articular Contact Pressure for the AMK with the Deformable J_2-plasticity and Rigid Body J_2-RB Models

4.3 Simulation of Backside Micromotion

The wear prediction process requires contact pressure and sliding displacement results from a FE simulation. It was anticipated that the relative sliding displacements of the backside surface (backside micromotion) would be the most difficult behaviour for the model to predict. Therefore, a FE model was developed with three different deformable constitutive models (linear elastic, viscoelastic and J_2-placticity) for the assessment of backside micromotion. The predicted micromotion values of the FE model were compared to knee simulator results to verify the FE models ability to predict such behaviour. Following the corroboration of the predicted micromotion with knee simulator results, the model was utilized to analyze the effects of various design parameters on backside micromotion.

4.3.1 Finite Element Model Development and Corroboration

FE simulations were conducted for the AMK with both a blasted Ti alloy tray and a polished CoCr alloy tray and the results were compared with corresponding knee simulator results.

For the simulation of the AMK with a Ti alloy tray, the average AP micromotion of the knee simulator results [62], linear elastic model, viscoelastic and the J_2-plasticity model are shown in Figure 28. As can be seen from the results, neither the linear elastic model nor the viscoelastic model predicts the trend as successfully as the J_2-plasticity model. The J_2-plasticity model results in similar micromotion to the knee simulator results during the majority of the ISO gait cycle, but under predicts the micromotion during

the swing phase (from approximately 60-95% of the gait cycle). However, as there is a comparatively small load (approximately 6% of the peak load) on the knee during the swing phase (Figure 11), the wear generated during this phase of the gait cycle is not very significant. Furthermore, the FE results are within reasonable proximity to the knee simulator results for this deviation to be explained by the experimental variation of knee simulator results.

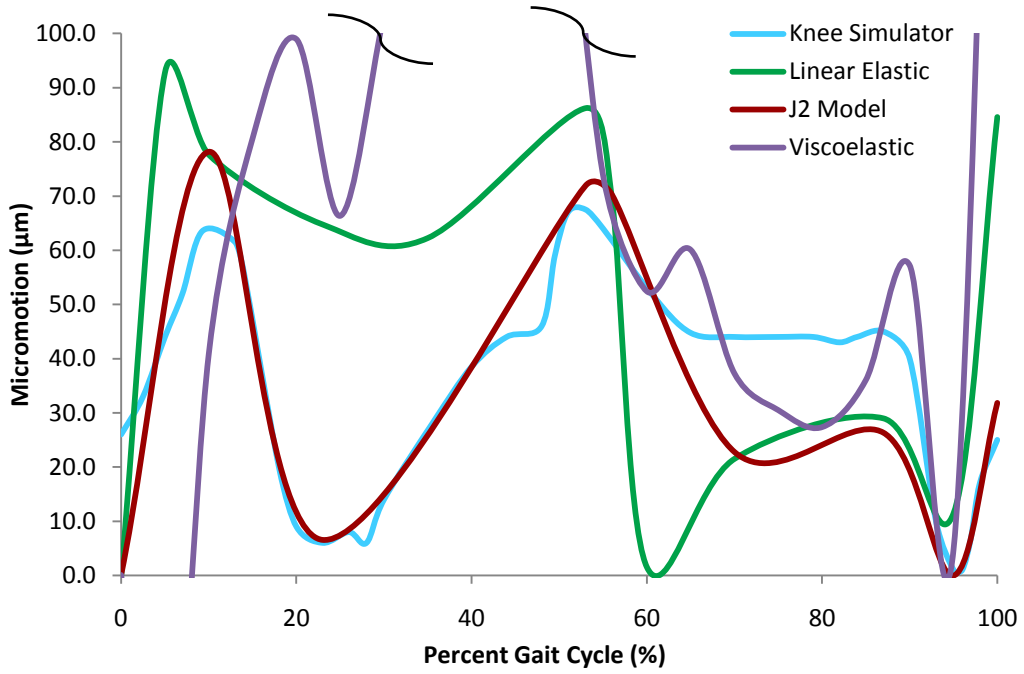

Figure 28: Average Anterior-Posterior Micromotion during one Gait Cycle of ISO 14243-3 for the AMK with a Grit Blasted Ti-alloy Tray

The maximum micromotion at each point of interest on the peripheral surface of the insert was determined for the AMK with a CoCr alloy tray. The FE simulation results obtained with both the linear elastic and the J_2-plasticity model are listed in Table 9, along with the magnitude and variance from the knee simulator results. The maximum AP mi-

cromotion of the medial and lateral condyles of the linear elastic, viscoelastic and J_2-plasticity model fell within the variation of the knee simulator results. However, the linear elastic model and the J_2-plasticity model predicted significantly different results for the ML micromotion and internal-external rotation for the CoCr alloy tray (Table 9).

Table 9: Backside Micromotion Results for the AMK with a polished CoCr Tray

In-vitro Tests	Anterior/Posterior Micromotion [µm]		Medial / Lateral [µm]	Internal/External Rotation [º]
	Lateral Condyle	Medial Condyle		
Knee Simulator	345 ± 190	510 ± 275	N/A*	N/A*
Linear Elastic Model	535	567	270	0.729
J_2-Plasticity Model	357	516	403	1.279

*N/A = not applicable

The maximum AP micromotion of each condyle for the AMK with a polished CoCr tray is shown in (Figure 29). The knee simulator results show a greater amount of micromotion on the medial condyle, as a result of the load being offset towards the medial side as specified by the stated ISO standard. The linear elastic model failed to replicate this medial/lateral difference, and predicted only a small difference between the two condyles (32 µm). Conversely, both the viscoelastic and J_2 models predicted a significant difference between the medial and lateral sides, accurately replicating the behaviour seen from the knee simulator experiments, with the J_2 model being the most similar to the knee simulator results with a medial/lateral difference of 159 µm.

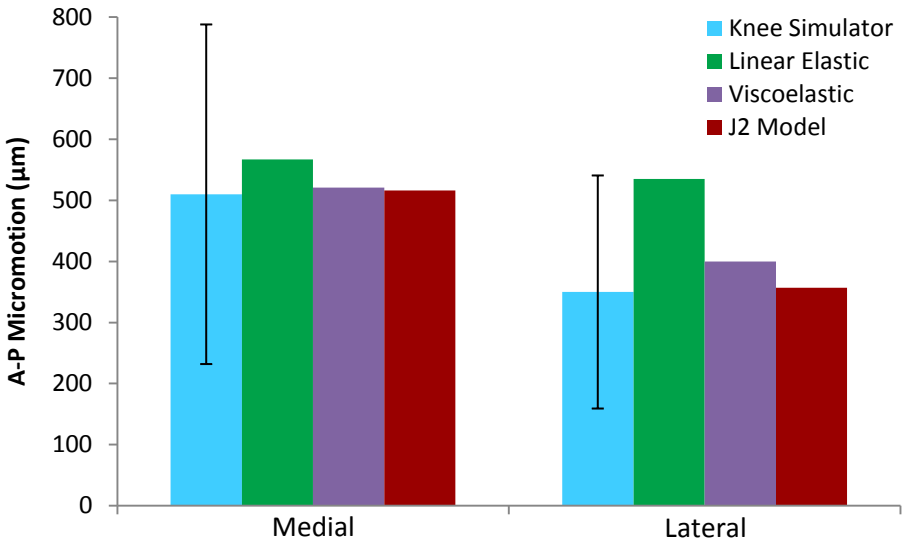

Figure 29: Maximum Anterior-Posterior Micromotion of the Medial and Lateral Condyles for the AMK with a CoCr Tray

The AP micromotion of each condyle over the ISO gait cycle for the AMK with a CoCr alloy tray and the J_2 model is shown in Figure 30. The difference in phase between the two condyles is evident, resulting in the overall internal-external rotation of the polyethylene insert relative to the tibial tray. This rotation is likely responsible for the stippling marks which have been observed for the AMK on components retrieved from patients [65, 103].

The backside micromotion of the AMK was simulated using a FE model with linear elastic, viscoelastic and J_2 models. The J_2 model behaved much more accurately, in comparison to the knee simulator results, than the linear elastic or viscoelastic model. The linear elastic model was investigated for its simplicity, computational efficiency and use in the literature [68, 92]. The linear elastic model was proven to be an oversimplification of the material, and has been previously shown to exhibit accurate material response

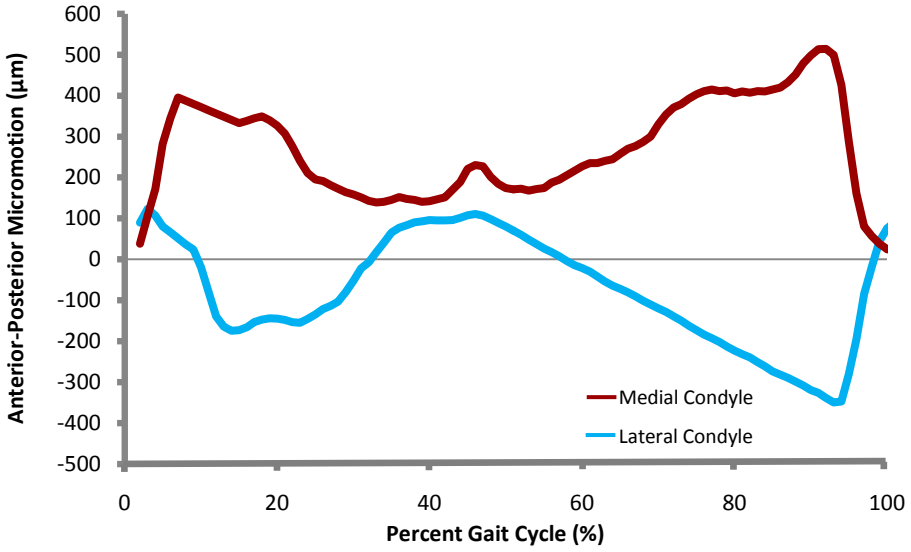

Figure 30: J_2-Plasticity Model Predicted Micromotion of the Medial and Lateral Condyles in the Anterior-Posterior Direction during one gait cycle following ISO 14243-3 for the AMK with a Polished CoCr alloy Tray

only for small strain values [3]. The viscoelastic model has been shown to result in improved accuracy over the linear elasticity model [3], however the viscoelastic model did not result in similar AP micromotion trends to those of the knee simulator wear testing (Figure 28). The third material model implemented the true stress-strain behaviour of PE by means of the J_2-plasticity theory. Although the J_2 model does have several disadvantages compared to more complex models, the J_2 model has an excellent balance of computational efficiency and accuracy [81]. Some of the shortcomings of the J_2-plasticity model include predicted piecewise linear behavior due to the linear interpolation between the points of the tabular stress-strain values. The J_2-plasticity model does not account for

strain-rate dependant behaviour. The model also predicts linear unloading behaviour rather than the nonlinear behaviour of PE [81]. However, the model has been shown to perform well in comparison to physical material testing (r^2=0.877) [81], and accurately predicted the AP micromotion magnitude and trend over the ISO gait cycle. The J_2-plasticity model was well corroborated with the knee simulator results, providing confidence in the accuracy of the FE model. Therefore, all subsequent results relate to the J_2-plasticity model unless otherwise indicated.

4.3.2 Cumulative Micromotion of Backside Surface

FE simulation was utilized to evaluate the cumulative micromotion of the backside surface under a compression load. While knee simulator tests would only be able to provide measurements of the micromotion around the periphery of the insert, FE simulation results are capable of predicting backside micromotion across the entire backside surface (Figure 31). The use of the FE simulation also enabled the quantification of the relative sliding distances at each location on the backside surface during the stated ISO gait cycle (Figure 32). The use of the FE method also enabled the quantification of the relative sliding distances at each location on the backside surface during the ISO simulated gait cycle (Figure 32).

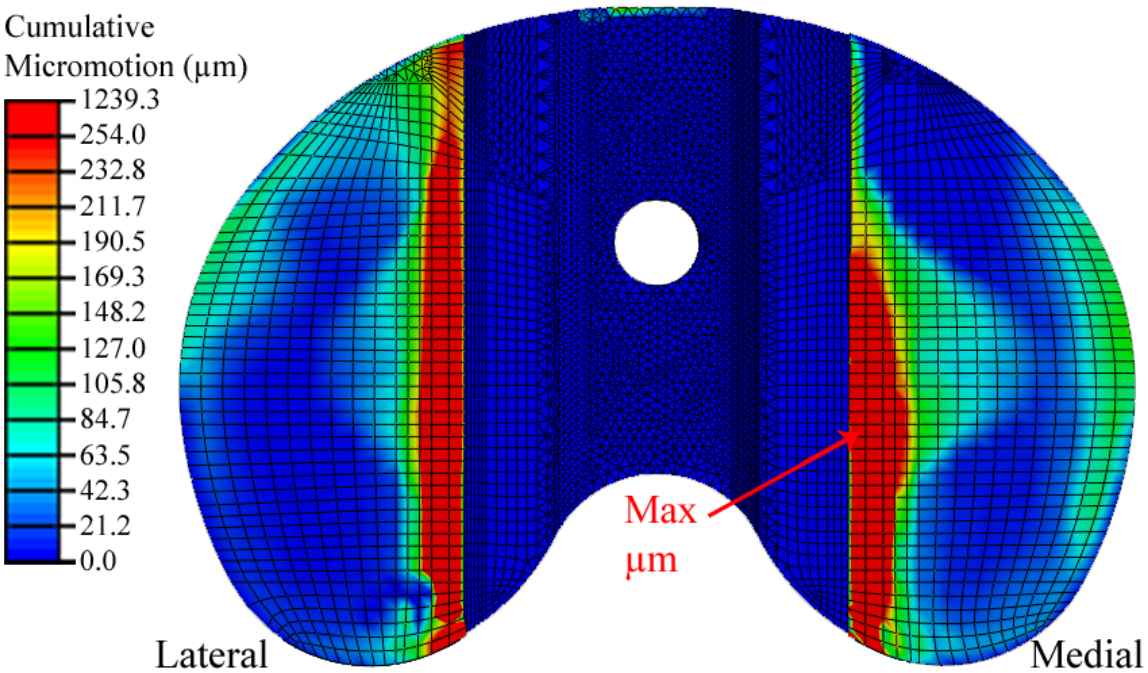

Figure 31: J_2-Plasticity Model Predicted Cumulative Micromotion for the AMK Tibial Insert Backside Surface, with a Polished CoCr alloy Tray, during Compressive Loading Only

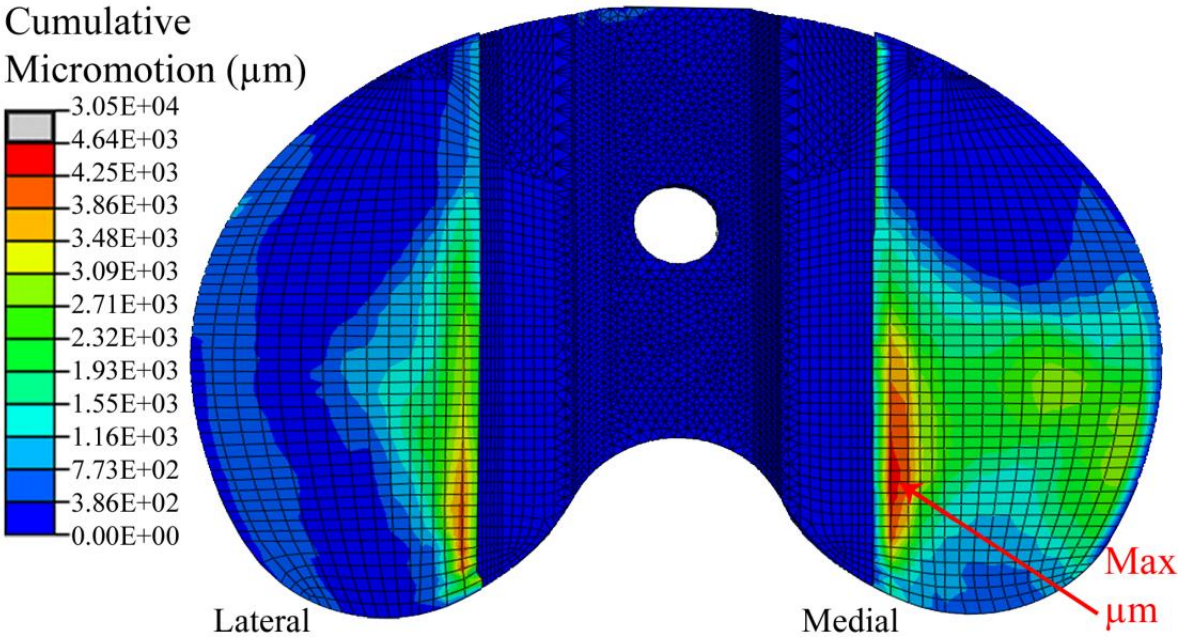

Figure 32: Cumulative Micromotion for the AMK during the ISO Simulated Gait Cycle with the J_2 Model

FE simulation with the proposed model is capable of predicting the micromotion in all regions of the backside surface, where as only peripheral points can be monitored during in vitro knee simulator testing. Peripheral measurements are insensitive to the majority of micromotion which occurs on the backside surface and therefore, provide a poor measure of implant performance with respect to backside micromotion (Figure 31).

During the ISO gait cycle the greatest amounts of micromotion were identified to occur in the region below the femoral condyles and near the interface of the locking mechanism (Figure 32). The evaluation of relative sliding vectors at each location provides micromotion information which is not obtainable through the use of in vitro knee simulators, yet could be used to improve the designs of locking mechanisms.

4.3.3 Analysis of Tibial Locking Mechanisms

The AMK with a CoCr alloy tray was compared with a modified AMK featuring a peripheral locking mechanism modeled after the PFC. In addition, the effect of geometric interference of the locking mechanism on backside micromotion was investigated to consider how the design parameters can affect implant performance with respect to backside micromotion. Convergence analyses were conducted for the PFC-type design. The mesh sensitivity analysis revealed an element edge size control of 1.016 mm to be sufficient for the prediction of backside (Figure 24). The plasticity stabilization analysis revealed once again that only one preconditioning cycle was necessary and the data from the second cycle was used for the analysis (Figure 25).

The dovetail type locking mechanism of the AMK was compared with the peripheral type locking mechanism adapted from the PFC. The PFC-type design resulted in greatly decreased micromotion over the locking mechanism design of the AMK (Figure 32-Figure 33). The majority of micromotion for both designs occurred beneath the medial condyle, and around the locking mechanism interface resulting from the deformation of the PE under loading. The results of the FE simulation are in agreement with the retrieval study results [9-10, 39] which have indicated that peripheral type locking mechanisms reduce backside damage compared to central locking mechanisms.

The methods ability to efficiently analyze various designs was further demonstrated by analyzing the effect of interference fit between the PE insert and the tibial tray for the AMK with the PFC-type locking mechanism (Figure 33-Figure 35). The analysis revealed that increasing the interference fit from size-on-size to 0.254 mm interference reduced cumulative backside micromotion by 9.88%. The location of maximum backside micromotion for the PFC-type design occurred on the medial side of the implant along the PE-Tray locking mechanism interface (Figure 35).

The analysis of locking mechanism interference fit revealed that increasing the amount of interference fit results in increased initial stresses in the PE, providing increased stiffness and therefore decreased relative movement in response to loading (Figure 33-Figure 35). Furthermore, increased interference fit would be beneficial to the design to avoid the introduction laxity between the components as a result of creep and other forms of PE damage over time.

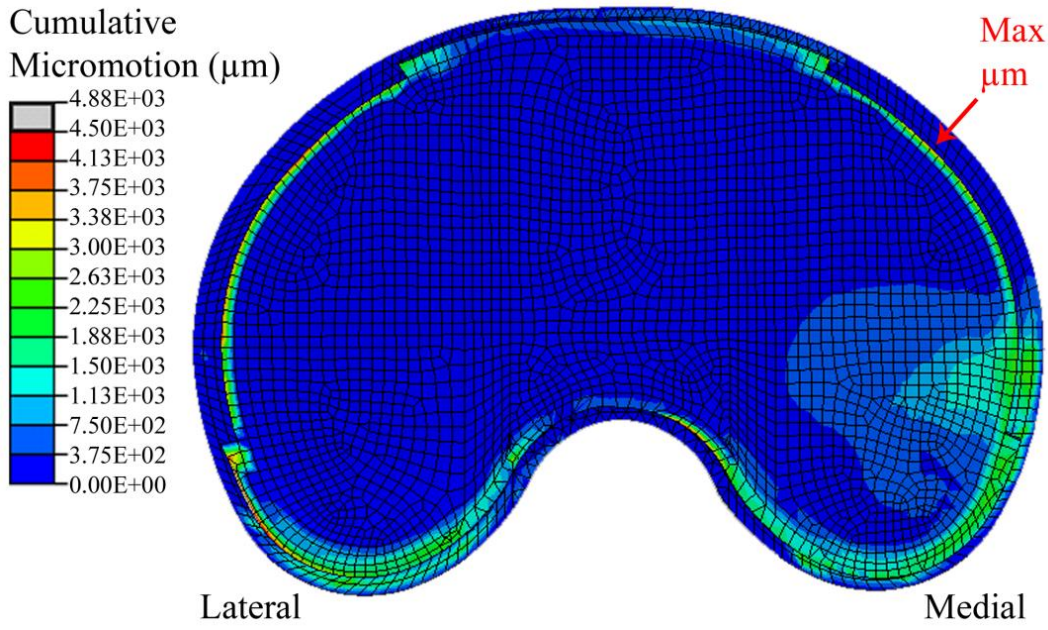

Figure 33: J_2-Plasticity Model Predicted Cumulative Micromotion for the Modified AMK Tibial Insert Backside Surface including a PFC-type Peripheral Locking Mechanism of 0.254mm Interference Fit, with a Polished CoCr alloy Tray, during one gait cycle following ISO 14243-3

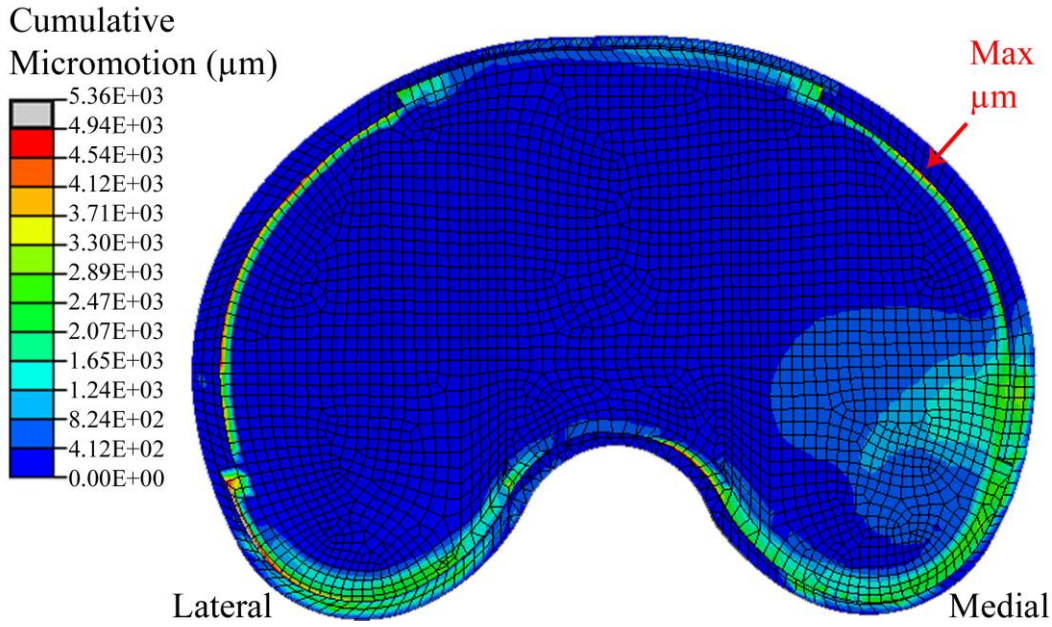

Figure 34: J_2-Plasticity Model Predicted Cumulative Micromotion for the Modified Anatomic Modular Knee AMK Tibial Insert Backside Surface including a PFC-type Peripheral Locking Mechanism of size-on-size Interference Fit, with a Polished CoCr alloy Tray, during one gait cycle following ISO 14243-3

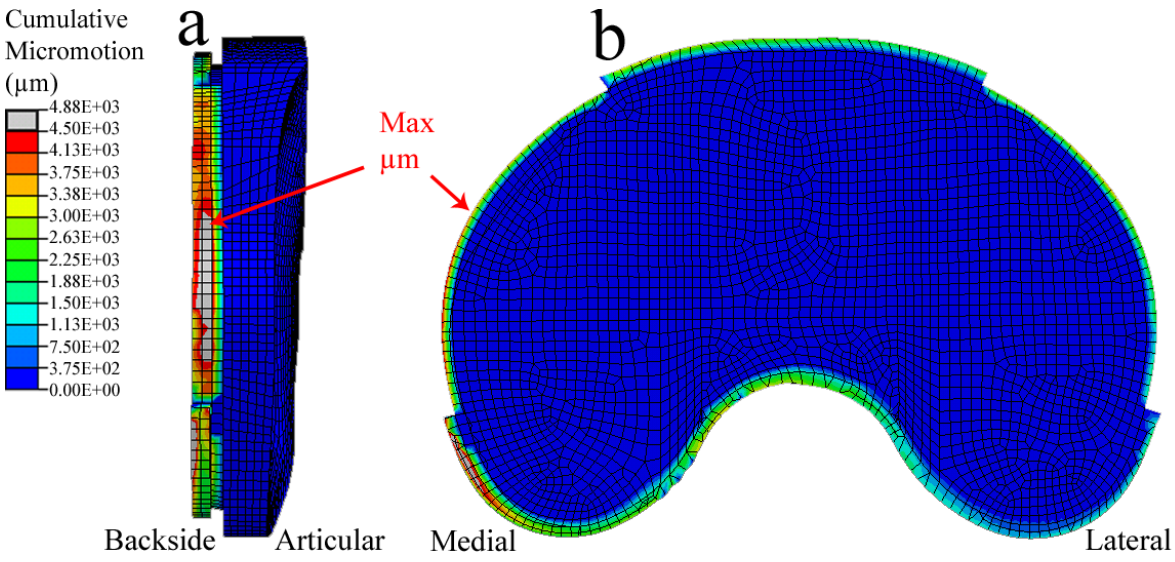

Figure 35: J_2-Plasticity Model Predicted Cumulative Micromotion for the Modified AMK Tibial Insert Backside Interface including a PFC-type Peripheral Locking Mechanism of 0.254mm Interference Fit, with a Polished CoCr alloy Tray, during one gait cycle following ISO 14243-3: (a) Veiw from the Medial Side Showing the Location of Maximum Micromotion; (b) Sectioned View from the Articular SurfaceTowards the Distal Surface

The FE model predicted micromotion results have to be compared with clinical results as part of the development process. Unfortunately, there is limited information available regarding the quantification of in vivo micromotion. Therefore, the results of the present study were compared to clinical results of a different implant design in order to serve as an indication of approximate micromotion magnitude which the TKR may experience in vivo. Tibial trays fixed to the bone by screws include a recess for the screw heads. The plastic flow properties of PE may result in protrusions into the screw hole recesses on the backside surface of PE tibial inserts [104]. The AP micromotion results in the formation of oblong screw hole protrusions, rather than round protrusions, corresponding to the PE tibial insert motion relative to the screw hole recesses [16, 104-105]. These screw hole protrusions have been shown to be as much as 600 μm out of round,

indicating 600 um of maximum displacement [16]. These clinical results are of similar magnitude to the FE model predicted micromotion results for TKRs with a polished CoCr alloy tray (Figure 29), indicating that the FE predicted micromotion is within the range of reported clinical micromotion magnitude.

The FE simulation results corroborated well with the available knee simulator results, although further testing to investigate the effects of different test conditions and different implant designs on the model's accuracy could be conducted. For the evaluation of back-side micromotion it is recommended that the FE simulation be performed in combination with knee simulator testing. In such cases, the micromotion of peripheral points from the knee simulator results could be used to evaluate the models accuracy under the given conditions, while the FE simulation could provide the micromotion results for the entire backside surface.

4.4 Identification of Wear Factors of Archard's Wear Law

The wear factors of Archard's wear law for both the articular and backside surfaces were identified by implementing the results of knee simulator wear tests and finite element simulations to develop an Archard's wear law based wear model relevant for both the articular and backside surfaces of TKRs as an alternative to POD derived wear

models. The FE simulation previously developed and corroborated with knee simulator results, utilizing the J_2 model, was implemented for the evaluation of contact pressures and sliding distances at the articular and backside surfaces (Figure 36). The simulation revealed that the peak contact pressures of the backside surface are much lower than those of the articular surface due to the highly conforming geometry of the backside surface. As well, the cumulative sliding distances of the backside surface are approximately one quarter of the articular surface values (Figure 36). The knee simulator results and the finite element simulation results were implemented in the computational wear factor identification procedure for the identification of the wear factors k_A and k_B for each 0.5 Mc interval (Figure 37 and Figure 38, Table 10 and

Table 11). The wear factors k_A and k_B varied over the test intervals of 0-3Mc, corresponding to the variation in interval PE wear volume over time from the knee simulator wear tests. The wear factors k_A and k_B showed trends of increasing from 0-2 Mc and then decreasing from 2.5-3 Mc. The wear factor (k_A) of the articular surface is significantly greater than the backside wear factor (k_B) despite the lower contact pressures and sliding distances of the backside surface in comparison to the articular surface. The average wear factors for 0-3 Mc were k_A = 1.03 (±0.22) x 10^{-7} mm^3/Nm and k_B = 2.43 (±0.52) x 10^{-10} mm^3/Nm for the articular and backside surfaces, respectively.

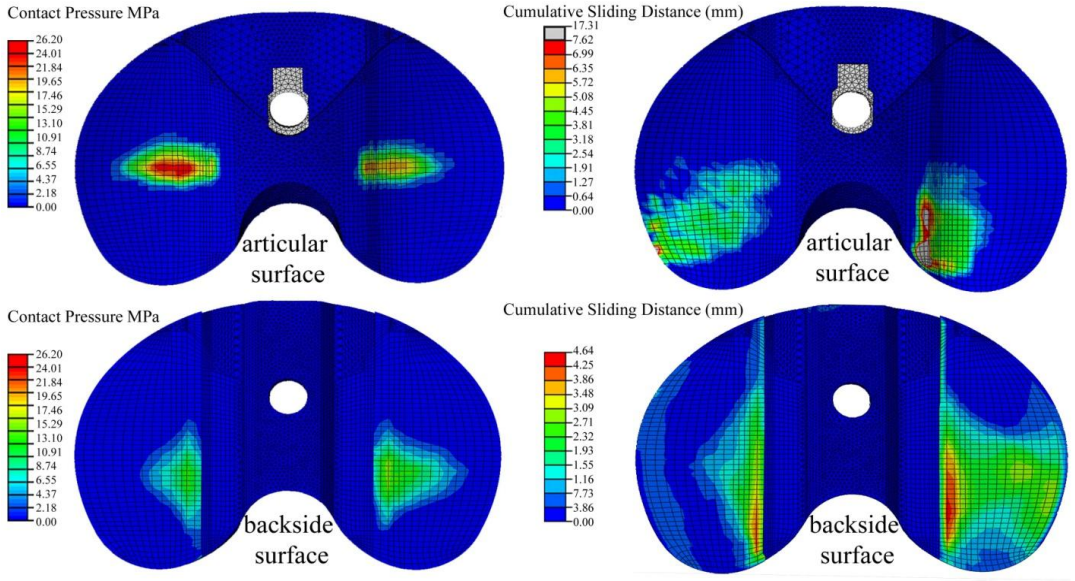

Figure 36: Finite Element Simulation Results of Contact Pressure at 45% of Gait Cycle and the Cumulative Sliding Distances over the Gait Cycle for the Articular and Backside PE Surfaces

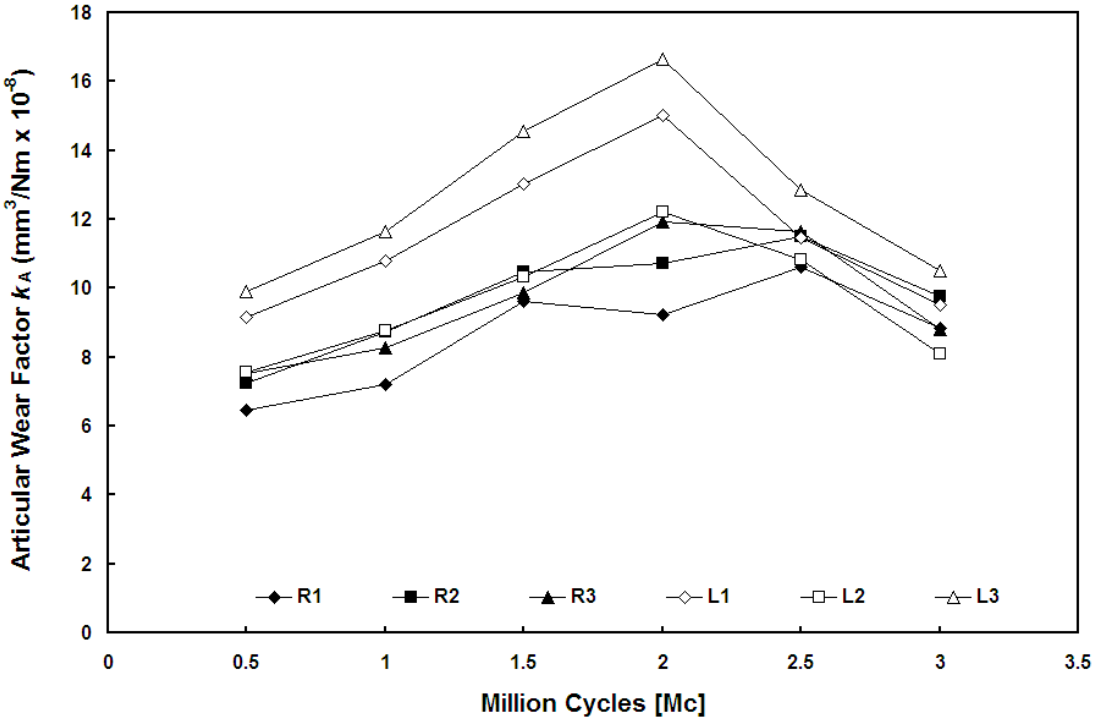

Figure 37: Articular Archard's Wear Factor (k_A) for the R Implants and the L Implants based on the Wear Volume Obtained from Knee Simulator Wear Tests by Brandt et al. [91]

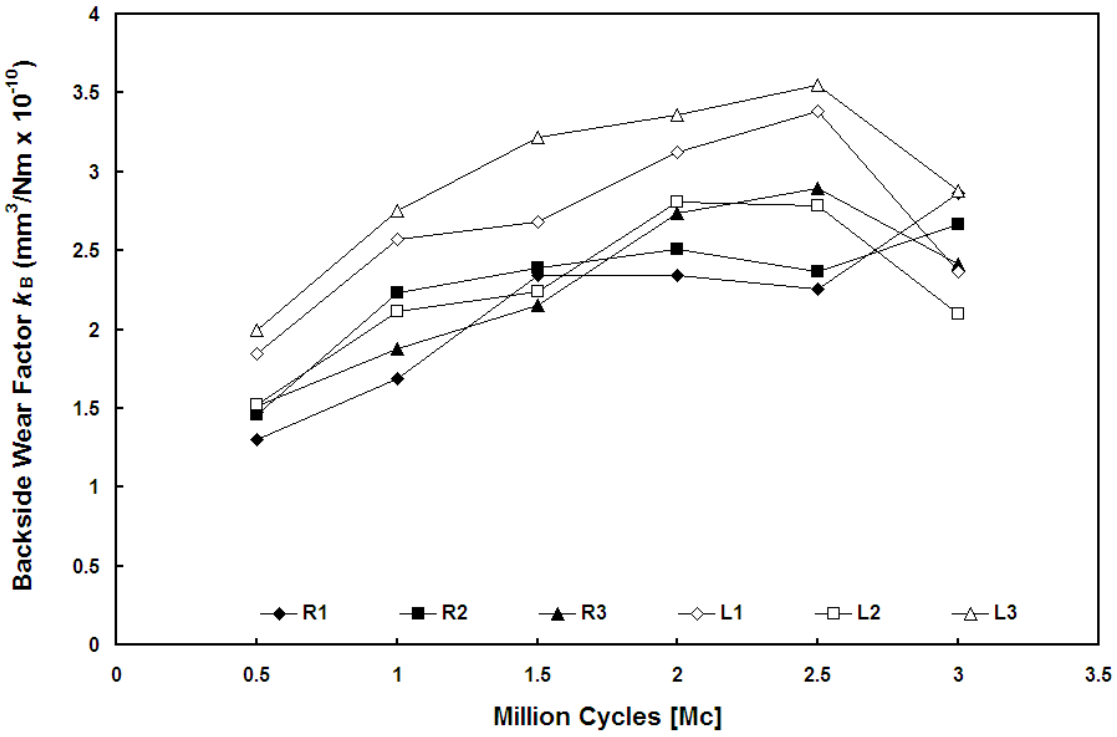

Figure 38: Backside Archard's Wear Factor (k_B) for the R Implants and the L Implants based on the Wear Volume Obtained from Knee Simulator Wear Tests by Brandt et al. [91]

Table 10: Average Articular Wear Volumes, Wear Factors (k_A) and Maximum Wear Depths from 0-3Mc

Articular PE Surface	Wear Testing Interval (Mc)						Mean ± Standard Deviation
	0.5	1	1.5	2	2.5	3	
Interval Wear Volume (mm^3)	4.61	6.33	7.19	8.07	8.24	7.31	6.96 ± 1.22
Articular Wear Factor (k_A) (mm^3/Nm x 10^{-7})	0.80	0.92	1.13	1.26	1.15	0.93	1.03 ± 0.16
Max. Wear Depth (µm)	107	112	114	114	99.1	94.1	107 ± 7.66

Table 11: Average Backside Wear Volumes, Wear Factors (k_B) and Maximum Wear Depths from 0-3Mc

Backside PE Surface	Wear Testing Interval (Mc)						Mean ± Standard Deviation
	0.5	1	1.5	2	2.5	3	
Interval Wear Volume (mm^3)	1.15	1.58	1.80	2.02	2.06	1.83	1.74 ± 0.31
Backside Wear Factor (k_B) ($mm^3/Nm \times 10^{-10}$)	1.61	2.21	2.50	2.81	2.87	2.55	2.43 ± 0.42
Max. Wear Depth ($\mu m \times 10^{-4}$)	0.75	1.03	1.17	1.32	1.34	1.19	1.14 ± 0.2

The wear factor (k) of Archard's wear law was intended to account for all of the variables effecting wear apart from the additional variables included in the wear model, such as contact pressure and sliding distance. Therefore, it is important that the conditions of the experiment utilized for the identification of the wear factors (k), closely match the conditions present in the TKR. The articular wear factor k_A and the backside wear factor k_B were identified for the AMK by implementing the results from knee simulator wear tests combined with the results of the FE simulation in a derivation of Archard's wear law. While POD tests may not be able to match the cross shear, sliding velocity, geometric contact conditions, dynamic loading, and tractive rolling of a TKR, the above derived wear factors k_A and k_B account for such effects, as they were derived directly from knee simulator wear test results. However, if the FE models input parameters were altered, the model would not account for the effects of such a modification, as the model remains linked to the experimental conditions from which it was derived.

The interval wear volumes were obtained from knee simulator commissioning wear tests and include variation in interval wear volumes due to experimental variation, as well

as the exchange of liners between stations [106]. Since the wear factors k_A and k_B were based on the knee simulator wear test results, the variation in interval wear resulted in the variation of the wear factors k_A and k_B. Therefore, the average wear factors k_A and k_B of each surface could be utilized in Archard's Wear Law for the prediction of wear, while the variance provides reference to the experimental variation of the knee simulator wear tests from which the wear factors k_A and k_B were derived. The average wear factor for the articular surface (k_A) fell well within the range of reported wear factors from POD experiments (5.0×10^{-8} to 1.8×10^{-6} mm^3/Nm) [56]. The wear factor k_A of the articular surface was also of similar orders of magnitude (10^{-7}) to the wear factors (k) implemented in other finite element wear simulations, ranging from 2.59 to 2.64×10^{-7} mm^3/Nm [45, 68].

The average backside wear factor (k_B) fell below the usual range of reported wear factors (k) from POD experiments, which was initially unexpected. Although the wear of the articular surface was known to be approximately five-times greater than that of the backside surface [65], the contact pressures and sliding distances of the articular surface were also correspondingly larger than those of the backside surface (Figure 36). Therefore the results indicated that some of the tribological variables, upon which the wear factor (k) is dependent (including cross shear, dynamic loading, wear mechanism and wear mode), were significantly different between the articular and backside surfaces.

Multi-directional motion (cross-shear) has previously been identified as having a significant effect on wear [51-53, 87, 107-108]. The variation in cross-shear magnitude between the articular and the backside surfaces would result in a difference between the respective wear factors (k), however the difference in cross shear between the surfaces is not significant enough to explain the large difference in wear factors (k) observed. An av-

erage backside surface cross shear of 2.86 x 10^{-9} times smaller than that of the articular surface would be required to create the difference in wear factors (k) using the model of Kang et al. [22].

The effect of dynamic loading has also been identified to increase wear over a constant load [22, 30]. The load alternates much more rapidly on the articular surface, as the femoral component moves across the articular surface of the tibial tray, bringing new nodes into contact (introducing a load) and removing contact from others (releasing the load). Conversely, the flat-on-flat contact of the backside surface, and the deformation behavior of the material, result in much more consistent and smooth loading conditions on the backside surface. Although dynamic loading has been shown to as much as double wear [30], it was unlikely to result in the difference between wear factors observed for the two surfaces.

Although cross shear and dynamic loading may both contribute to the differences between the articular and backside wear factors (k), the majority of the difference was likely the result of the differences in wear modes and wear mechanisms. Two-body rolling-sliding wear was the dominant wear mode for the articular surface of TKRs [28], while fretting wear was the dominant wear mode for the backside surface [109]. Furthermore, the active wear mechanism of the articular surface was dominantly abrasive, while the wear mechanism of the backside surface was dominantly adhesive for the articulation of a PE insert against a polished tibial tray [109]. This difference in wear modes and mechanisms results in significantly different tribological conditions, which in turn results in significantly different wear factors (k). Furthermore, the backside wear factor (k_B) does not fall within the range of POD test results as the wear mode and mechanisms of POD

tests are dominantly two-body sliding and abrasive wear. Archard's wear law with FE simulation has previously been demonstrated to be sufficient for the modeling of fretting wear [99], and thus was deemed appropriate for this study.

The computational model does have some limitations as it does not consider the effects of creep, which could have an effect on PE wear due to the resultant changes to the geometry of the tibial insert and molecular PE chain orientation. The implementation of the geometrical models supplied by the manufacturer, or developed based on the manufacturing drawings; avert the limitations in accuracy associated with obtaining the models by computed topography or laser scanning which arise due to the limitations in resolution and accuracy of such systems. However, the use of geometric models not based on the manufactured part does not account for differences which may arise from manufactured parts which fall outside the specified design tolerances of the part. The present computational wear model has been developed based on knee simulator wear test results, and therefore, the validation of the models accuracy when considering different TKR geometric designs would require additional knee simulator wear test results of different TKR designs with the same bearing materials and same lubricant composition. Unfortunately such results are not available in the literature. Although the wear factors (k) are directly relevant to the conditions from which they were derived, the computational wear model does not account for the variation of parameters such as cross shear and sliding velocity that may result from the modification of the FE models input parameters. For example, the computational wear model would not account for changes to variables such as cross shear that may arise from an alteration such as increased internal-external rotation. Nevertheless, the direct identification of the wear factors (k) relevant to the AMK under the

ISO 14243-3 standard has enabled the discovery of the difference in magnitude between the articular wear factor k_A and backside wear factor k_B.

To the authors' knowledge, the proposed computational wear model is the first wear model developed for the analysis of both articular and backside wear. The model is able to assess the effects of changes in contact pressure and sliding distances on wear, which may result from TKR design changes. However, a more complex and comprehensive model, which takes cross shear into account, is required for the design optimization of a TKR.

4.5 Corroboration of Novel Wear Model Based on PE Molecular Structure and Wear Theory

A new, novel wear model was developed based on a theoretical understanding of the microstructure of PE and wear. The new model accounts for the time dependant changes to the molecular structure of PE. Previously available wear models predict a constant wear rate extending to infinity for continued sliding in a consistent direction [22, 51-53, 67, 87] which has been shown to be inaccurate behaviour based on the POD testing of Dressler et al. [100] as the material will eventually become strain hardened in the direction of motion and the wear rate will decrease significantly. The new model not only accurately models the PE behaviour of which other models have been unable to replicate, but also explains the inconsistencies of previous POD wear models which were not pre-

viously understood. The A/A+B model of Turell et al. [87] could not explain why the peak wear volume did not occur at an aspect ratio of 0.5, while the new wear model does explain such phenomenon through the reorientation of the crystalline lamella over time.

The model of Kang et al. [22] demonstrated decreasing wear rate with increasing contact pressure, which is not in agreement with the current understanding of wear and has caused confusion as to the roll of contact pressure in regards to wear [67, 76]. However, the newly developed wear model offers an explanation for this unexpected behaviour. Since the polymer chains are continuously changing based on energy dissipated at the surface with shear forces in directions other than those of the CMO, the material could reach its effective sliding distance during the sliding distances investigated by the study [22], resulting in fully aligned polymer chains for all of the contact pressures investigated, in which case the wear rate of all trials would have been the same. However, the wear model of Kang et al. [22] is a macroscopic POD model, which does not account for the edge loading of the PE pin and only considers the average cross shear across the pin surface as the cross shear ratio. Therefore, as the areas of high cross shear on the pin surface are worn away during the initial wear-in period, the load is transferred to the unworn areas of low cross shear which have a lower wear rate, resulting in additional error which may account for the decrease in wear with increasing contact pressure. Although the model of Kang et al. [22] is useful as a macroscopic POD wear model, the model is not directly applicable to a TKR without consideration for the time dependence of the CMO and the inconsistent contact pressure and cross shear across the surface of the PE pin.

The new model was utilized to predict the interval wear for both the articular and backside surfaces of the AMK. While the predicted wear of the articular surface was in good agreement with the knee simulator results, the predicted wear volume of the backside surface was approximately 20 times greater than the knee simulator results. This result is similar to the findings of the Archard's wear law based model and provides further indication that the differences in wear mode and mechanisms between the two surfaces require the inclusion of an additional variable in the wear equation to account for the differences in wear modes and mechanisms. Therefore, a mode and mechanism factor (MM) was added to equation 12 for the backside surface:

$$C_w = S \cdot \mu \cdot P \cdot NA \cdot MM \tag{19}$$

A MM of 0.05 was implemented for the backside surface to result in the correct wear volume. The simulation was run and the results are presented in Table 12. The new wear model predicted the articular wear volume to within 0.5% of the average wear volume of the independent knee simulator results, which is within the standard deviation of the knee simulator results. The corroboration of the predicted results to the independent knee simulator wear test results demonstrates the accuracy of the model for the articular surface. The addition of the MM factor makes the backside wear prediction no longer independent of the knee simulator results. Therefore, the wear prediction would need to be completed for another design for which knee simulator wear test results exist for the veri-

fication of the backside model, but unfortunately no results of additional TKR models are available at this time.

Table 12: Articular and Backside: Knee Simulator Wear Volumes, Computational Wear Volumes and Wear Depths of the New Wear Model for the AMK

		Interval (Mc)						
		0-0.5	0.5-1	1-1.5	1.5-2	2-2.5	2.5-3	Average
Articular	Knee Sim. Wear Volume (mm^3)	4.61	6.33	7.19	8.07	8.24	7.31	6.96±0.4
	Predicted Wear Volume (mm^3)	7.03	6.91	6.91	6.91	6.91	6.91	6.93
	Deviation from Average	52.5%	9.1%	-3.9%	-14%	-16%	-5.5%	-0.5%
	Max Wear Depth (mm)	0.18	0.18	0.18	0.18	0.18	0.18	0.18
Backside	Knee Sim. Wear Volume (mm^3)	1.15	1.58	1.80	2.02	2.06	1.83	1.74±0.1
	Predicted Wear Volume (mm^3)	1.64	1.69	1.74	1.78	1.79	1.79	1.74
	Deviation from Average	42.2%	7.1%	-3.2%	-12%	-13%	-2.1%	-0.06%
	Max Wear Depth (mm x 10^{-3})	9.6	8.3	7.4	6.8	6.6	6.6	7.5

The new wear model features improved predictability over the previously available wear models [76]. Some of the inaccuracy previously associated with utilizing POD test results for wear model development resulted from neglecting the change in molecular orientation over time which would result in misleading results. Future work should be carried out to increase the amount of data utilized for the development of the model. The model parameters could be determined for different levels of crosslinked PE, GUR types and lubrication compositions. A function could be developed for these parameters, which would calculate the material parameters M_{mc} and Rw, therefore enabling the comparison

of the predicted results to a wider range of knee simulator wear test results, as well as enabling the complete optimization of a TKR, including material composition as well as geometric optimization. While Archard's wear law performs poorly following the change of TKR design or kinematics, the new wear model provides improved robustness and versatility and resulted in an accuracy far higher than the accuracy of other available wear models [76]. For the currently developed materials and lubrication (non-crosslinked GUR 1050 with 25% bovine serum) the model results in less than 0.5% average error for the prediction of wear at the articular surface indicating that the model is promising as a supplementary process to knee simulator wear testing for the optimization of total knee replacements for the reduction of wear.

Chapter 5

Conclusion

The TKR wear modeling process required that finite element models be developed for the prediction of contact pressures and sliding displacements of each surface, articular and backside. Rigid body FE models were considered for the prediction of articular contact pressures and sliding displacements for their computational efficiency and use in the literature [74, 76, 78, 110]. A total of five FE simulation scenarios were conducted to evaluate the accuracy of rigid body FE simulations with three different pressure overclosure relationships. However, the rigid body models performed poorly compared to the deformable J_2-plasticity model. The J_2-RB model resulted in lower overall error than the other rigid body models and resulted in average errors of 42%, 34% and 113% for maximum contact pressure, average contact pressure and contact area respectively. Due to the high error associated with the rigid body models, such models are not recommended for the prediction of contact pressure and sliding distances.

A FE model was developed for the AMK using a deformable PE component, with boundary and loading conditions to recreate the conditions of ISO 14243-3. The FE model was required to predict the contact pressures and sliding distances of the articular

and backside surfaces. It was anticipated that the prediction backside sliding displacements (backside micromotion) would have the lowest accuracy, of all the FE predicted behaviour, when compared to a physical experiment as the accurate prediction of backside micromotion requires the accurate replication of the contact pressures and reaction forces at both the articular and backside surfaces as well as accurate PE deformation behaviour. Three different deformable constitutive models were implemented, a simple linear elastic model, a viscoelastic model and a non-linear J_2-plasticity model. The predicted micromotion of the J_2-plasticity model corroborated well with knee simulator results and provided improved accuracy over the linear elastic and viscoelastic models.

Following the verification of the FE models accuracy for the prediction of backside micromotion, the model was utilized to analyze the effects of various design parameters on backside micromotion. The peripheral locking mechanism of a PFC-type design was compared to the dovetail locking mechanism of the AMK. The PFC-type design greatly reduced the backside micromotion over the dovetail locking mechanism of the AMK. The influence of interference fit between the locking mechanisms of the tibial insert and the tibial tray was also demonstrated using the FE simulation method. The FE model simulation of backside micromotion features improved time and cost efficiency over in vitro knee simulators for the prediction of backside micromotion. The method also has the ability to predict the micromotion at every location of the backside surface, while only peripheral measurements can be obtained during use of an in vitro knee simulator. The method enables the efficient parametric analysis of design variables for the reduction of backside micromotion. Therefore, the method is promising as a supplemental procedure to improve TKR designs for the reduction of backside micromotion and wear. It is

recommended that the FE micromotion simulation procedure be implemented in combination with knee simulator experimentation for the evaluation of backside micromotion, and the design of new locking mechanisms. The completion of a well corroborated FE model enables backside wear to be predicted by utilizing the contact pressure and sliding predictions of the FE model.

Archard's wear law has been the most frequently implemented wear model in the literature, and commonly uses wear factors taken from POD results [45, 68, 72-73, 83-85]. An identification approach was adapted to determine the wear factors applicable to the AMK by implementing the FE model results along with knee simulator results as an alternative to POD derived wear factors. The average wear factors ($k_{A,B}$) were determined to be 1.03 (±0.22) x 10^{-7} and 2.43 (±0.53) x 10^{-10} mm^3/Nm for the articular and backside surfaces, respectively. The articular wear factor (k_A) was approximately 400 times greater than the backside wear factor (k_B), and this difference in magnitude was suggested to mainly result from the differences in wear modes and mechanisms between the two bearing surfaces. Although, the modeling of wear by use of Archard's wear model enabled the discovery of the significantly different wear factors between the articular and backside surfaces, the model was not sufficient to use for TKR design optimization, since changes to the TKR design or kinematics would result in cross shear angle changes which would not be accounted for by the model. Therefore, a different wear model was required which could account for changes in cross shear angle as well as contact pressure and sliding displacements.

A new novel wear model was developed based on a theoretical understanding of the time dependant molecular structure of PE. The new wear model considers the time de-

pendent behaviour of the molecular structure of PE and relates the molecular changes and wear to the energy dissipated at the surface of the PE tibial insert. The new wear model was demonstrated to accurately predict the articular surface wear volume of the AMK to within the standard deviation of the independent knee simulator results. The newly developed model offers improved predictability over the previously available models and could be utilized for the optimization of total knee replacements. A comparison of the previous leading wear models and the new novel wear model is shown in Table 13.

Table 13: Wear Model Comparison

	Model					
	Archard	Turell	Wang	Kang	Abdelegaid	O'Brien
Time Dependant Molecular Orientation	×	×	×	×	×	✓
Increasing Wear with Increasing Pressure	✓	✓	✓	×	×	✓
Account for Cross Shear	×	✓	✓	✓	✓	✓
Account for Geometric Design Changes	✓	✓	✓	✓	✓	✓
Theoretical Based	✓	×	✓	×	×	✓
Applicable to all GUR Types and XPE Densities	✓	×	×	×	×	✓

There are five main areas of contribution of the present thesis. Firstly, the rigid body models which have previously been used in the literature for wear prediction [74, 76, 78] without validation of the models ability to predict contact area have been identified to be insufficient for the prediction of articular contact pressure, area and sliding distances through the comparison of the deformable J_2-placticity model to the rigid body models during five FE simulation scenarios. The assumption that the deformation of each node does not affect the neighbouring nodes (zero shear stiffness) and does not have a significant effect on the results has been shown to be an invalid assumption and therefore, only deformable models should be considered for the prediction of contact pressures and slid-

ing distances. The second contribution of this research is the identification of the J_2-plasticity model to be model of choice over linear elastic and viscoelastic models.

The third major contribution of this research was the development of an FE model for the prediction of backside micromotion. Previously, there has not been any method for the prediction or measurement of backside micromotion across the contact surface. The newly developed FE model predicts micromotion at all locations of the backside surface and the models accuracy has been verified to be within the standard deviation of the knee simulator results. The development of the verified model also enables backside wear to be predicted by combining the FE simulation with a computational wear model.

Then fourth contribution was the identification of the wear factors of Archard's wear law for the articular and backside surfaces. The identified wear factors revealed the significant difference between the articular and backside surfaces which had not been previously reported. The difference between the articular and backside wear factors was attributed to the difference in wear mode and mechanism between the two surfaces, dominantly two-body sliding and abrasive for the articular surface and dominantly fretting and adhesive for the backside surface with a polished tray. The identification of this difference also indicates that a more relevant test method is required for backside surface wear, as the two-body sliding abrasive testing of POD tests are not directly relevant to the fretting wear and adhesive conditions of the backside surface.

The fifth contribution of the present thesis was the development of a new, novel wear model. Unlike the previously available wear models, which were an extension of Archard's wear law by the addition of a cross shear variable obtained through POD wear testing [22, 51-52, 55, 67, 76, 87], the newly developed wear model is based on a theo-

retical understanding of the time dependant molecular structure of PE. The new model specifies the energy dissipated at the surface as the driving force of time dependant molecular changes within PE. Since the model is based on a theoretical understanding of PE wear, the model is relevant for all PE varieties (including conventional PE, crosslinked PE and all GUR types), only the models material parameters (M_{mc} and R_w) need be determined for the specific PE variety. The model's material parameters for conventional, non-crosslinked, GUR 1050 PE have been determined by utilizing the results of published POD tests [51, 87] and the models accuracy was found to be within 0.5% error for the articular surface of the AMK. The newly developed wear model, combined with the FE model for the prediction of both articular and backside contact pressures and sliding displacements have particular significance, as together they can be used to conduct design optimization of a total knee replacement for the reduction of adhesive and abrasive wear.

The FE model and newly developed wear model feature improved time and cost efficiency over knee simulators. The FE model can assess the contact pressures and backside micromotion at all areas of the backside surface while only peripheral measurements can be obtained during knee simulator wear testing. The efficiency of the novel wear model enables a far greater range of design variables to be considered than with knee simulators alone. Therefore, it is recommended that the finite element simulation and the newly developed computational wear model be performed in combination with knee simulator wear tests for the evaluation and development of TKR designs.

Chapter 6

Future Work

The newly developed wear model is relevant for PE of all varieties with respect to crosslinking and GUR type, but requires the material parameters M_{mc} and R_w to be determined. The identification of these parameters for multiple levels of crosslinking and GUR types may enable the development of a function relating the effects of crosslinking and GUR types to the material parameters. The material parameters for each PE variety could be identified from existing published POD test results or from further POD or BOF testing.

The newly developed wear model features improved material behaviour prediction and accuracy over previously available wear models. However, the model could be improved further by considering the effects of additional variables such as the effects of the lubricant on PE wear through the computational modeling of the boundary lubrication [111-112]. The wear model could also be improved through the additional consideration of the thermal modeling of the system. It would also be beneficial to compare the results of the model for additional TKR designs and kinematics to knee simulator results for a more thorough evaluation of the models overall accuracy.

The scope of the newly developed wear prediction method is limited to adhesive and abrasive wear modeling. However, fatigue wear, such as pitting and delamination is also an active wear mechanism for TKRs. The newly developed adhesive/abrasive wear model could be combined with an existing fatigue model [48-49] and fracture failure model [113] for the complete analysis of PE damage over time. Such a model would then be well suited to optimize material composition and geometric design for the reduction of PE damage.

Bibliography

[1] S. Kurtz, *et al.*, "Projections of Primary and Revision Hip and Knee Arthroplasty in the United States from 2005 to 2030," *J Bone Joint Surg Am,* vol. 89, pp. 780-785, April 1, 2007 2007.

[2] Canadian Joint Replacement Registry, "Hip and Knee Replacements in Canada," 2006.

[3] S. Kurtz, *UHMWPE Biomaterials Handbook: Ultra High Molecular Weight Polyethylene in Total Joint Replacement and Medical Devices*: Elsevier/Academic Press, 2009.

[4] M. Skolnick, *et al.*, "Unicompartmental polycentric knee arthroplasty: description and preliminary results.," *Clinical Orthopedics,* pp. 208-14, 1975.

[5] W. Jones, *et al.*, "Unicompartmental knee arthroplasty using polycentric and geometric hemicomponents," *Journal of Bone and Joint Surgery America,* vol. 63, pp. 946-54, 1973.

[6] M. L. Ecker, *et al.*, "Long-term Results after Total Condylar Knee Arthroplasty: Significance of Radiolucent Lines," *Clinical Orthopaedics and Related Research,* vol. 216, pp. 151-158, 1987.

[7] D. Bartel, *et al.*, "Performance of the tibial component in total knee replacement," *J Bone Joint Surg Am,* vol. 64, pp. 1026-33, 1982.

[8] J. Lewis, *et al.*, "A comparative evaluation of tibial component designs of total knee prostheses," *J Bone Joint Surg AM,* vol. 64, pp. 129-35, 1982.

[9] T. Akisue, *et al.*, ""Backside" polyethylene deformation in total knee arthroplasty," *The Journal of Arthroplasty,* vol. 18, pp. 784-791, 2003.

[10] M. G. Azzam, *et al.*, "Second-Generation Locking Mechanisms and Ethylene Oxide Sterilization Reduce Tibial Insert Backside Damage in Total Knee Arthroplasty," *The Journal of Arthroplasty,* vol. 26, pp. 523-530, 2011.

[11] M. S. J. Brandt J.-M., Bourne R.B., Medley J.B., "Retrieval analysis of modular total knee replacements: factors reducing backside surface damage," *The Knee,* vol. (in press), 2011.

[12] M. A. Conditt, *et al.*, "Backside Wear of Modular Ultra-High Molecular Weight Polyethylene Tibial Inserts," *J Bone Joint Surg Am,* vol. 86, pp. 1031-1037, May 1, 2004 2004.

[13] G. A. Engh, *et al.*, "Clinical Results of Modular Polyethylene Insert Exchange with Retention of Total Knee Arthroplasty Components," *J Bone Joint Surg Am,* vol. 82, pp. 516-, April 1, 2000 2000.

[14] G. A. Engh, *et al.*, "In Vivo Deterioration of Tibial Baseplate Locking Mechanisms in Contemporary Modular Total Knee Components," *J Bone Joint Surg Am,* vol. 83, pp. 1660-1665, November 1, 2001 2001.

[15] M. R. O'Rourke, *et al.*, "Osteolysis Associated with a Cemented Modular Posterior-Cruciate-Substituting Total Knee Design : Five to Eight-Year Follow-up," *J Bone Joint Surg Am,* vol. 84, pp. 1362-1371, August 1, 2002 2002.

[16] R. C. Wasielewski, *et al.*, "Tibial Insert Undersurface as a Contributing Source of Polyethylene Wear Debris," *Clinical Orthopaedics and Related Research,* vol. 345, pp. 53-59, 1997.

[17] D. D. R. Naudie, *et al.*, "Wear and Osteolysis Around Total Knee Arthroplasty," *Journal of the American Academy of Orthopaedic Surgeons,* vol. 15, pp. 53-64, January 1, 2007 2007.

[18] J. H. Lonner, *et al.*, "Prodromes of failure in total knee arthroplasty," *The Journal of Arthroplasty,* vol. 14, pp. 488-492, 1999.

[19] P. F. Sharkey, *et al.*, "Why Are Total Knee Arthroplasties Failing Today?," *Clinical Orthopaedics and Related Research,* vol. 404, pp. 7-13, 2002.

[20] M. Jasty, *et al.*, "Localized osteolysis in stable, non-septic total hip replacement," *J Bone Joint Surg Am,* vol. 68, pp. 912-919, July 1, 1986 1986.

[21] Puloski SKT, *et al.*, "Tibial post wear in posterior stabilized total knee arthroplasty. An unrecognized source of polyethylene debris.," *J Bone Joint Surg Am,* vol. 83, pp. 390-397, 2001.

[22] L. Kang, *et al.*, "Enhanced computational prediction of polyethylene wear in hip joints by incorporating cross-shear and contact pressure in additional to load and sliding distance: Effect of head diameter," *Journal of biomechanics,* vol. 42, pp. 912-918, 2009.

[23] V. Saikko, *et al.*, "Effect of counterface roughness on the wear of conventional and crosslinked ultrahigh molecular weight polyethylene studied with a multi-directional motion pin-on-disk device," *Journal of Biomedical Materials Research,* vol. 57, pp. 506-512, 2001.

[24] M. Spector, *et al.*, "Wear performance of ultra-high molecular weight polyethylene on oxidized zirconium total knee femoral components," *The Journal of bone and joint surgery. American volume,* vol. 83A, 2001.

[25] Y. S. Liao, *et al.*, "The effect of frictional heating and forced cooling on the serum lubricant and wear of UHMW polyethylene cups against cobalt-chromium and zirconia balls," *Biomaterials,* vol. 24, pp. 3047-3059, 2003.

[26] M. P. Heuberger, *et al.*, "Protein-mediated boundary lubrication in arthroplasty," *Biomaterials,* vol. 26, pp. 1165-1173, 2005.

[27] J.-M. Brandt, "Wear and Boundary Lubrication in Modular Total Knee Replacements," Doctor of Philosophy in Mechanical Engineering, Mechanical Engineering, University of Waterloo, Waterloo, 2008.

[28] M. A. Wimmer and T. P. Andriacchi, "Tractive forces during rolling motion of the knee: Implications for wear in total knee replacement," *Journal of biomechanics,* vol. 30, pp. 131-137, 1997.

[29] T. Schwenke, *et al.*, "The influence of slip velocity on wear of total knee arthroplasty," *Wear,* vol. 259, pp. 926-932, 2005.

[30] P. S. M. Barbour, *et al.*, "The influence of stress conditions on the wear of UHMWPE for total joint replacements," *Journal of Materials Science: Materials in Medicine*, vol. 8, pp. 603-611, 1997.

[31] W. J. Maloney, "Management of Osteolysis after Total Knee Replacement," *J Bone Joint Surg Br*, vol. 92-B, pp. 90-a-91, March 1, 2010 2010.

[32] M. E. Berend, *et al.*, "The Chetranjan Ranawat Award: Tibial Component Failure Mechanisms in Total Knee Arthroplasty," *Clinical Orthopaedics and Related Research*, vol. 428, pp. 26-34 10.1097/01.blo.0000148578.22729.0e, 2004.

[33] S. K. Gupta, *et al.*, "Review Article: Osteolysis After Total Knee Arthroplasty," *The Journal of Arthroplasty*, vol. 22, pp. 787-799, 2007.

[34] K. Hirakawa, *et al.*, "Relationship between wear debris particles and polyethylene surface damage in primary total knee arthroplasty," *The Journal of Arthroplasty*, vol. 14, pp. 165-171, 1999.

[35] S. M. Gabriel, *et al.*, "Polyethylene wear on the distal tibial insert surface in total knee arthroplasty," *The Knee*, vol. 5, pp. 221-228, 1998.

[36] T. P. Schmalzried, *et al.*, "Polyethylene wear debris and tissue reactions in knee as compared to hip replacement prostheses," *Journal of Applied Biomaterials*, vol. 5, pp. 185-190, 1994.

[37] M. Horikoshi, *et al.*, "Comparison of Interface Membranes Obtained From Failed Cemented and Cementless Hip and Knee Prostheses," *Clinical Orthopaedics and Related Research*, vol. 309, pp. 69-87, 1994.

[38] R. D. Crowninshield, *et al.*, "An Assessment of Polyethylene Backside Wear in a Modular Tibial Total Knee System," *J Bone Joint Surg Br*, vol. 87-B, pp. 337-c-338, September 1, 2005 2005.

[39] J. M. Brandt, *et al.*, "Retrieval analysis of modular total knee replacements: factors reducing backside surface damage," *The Knee*, vol. (in press), 2011.

[40] S. Swope, "Wear of Non-Modular and Modular Total Knee Tibial Components," in *Society for Biomaterials*, 2005.

[41] M. B. Collier, *et al.*, "Radiographic Assessment of the Thickness Lost from Polyethylene Tibial Inserts That Had Been Sterilized Differently," *Journal of Bone and Joint Surgery*, vol. 90, pp. 1543-1552, July 1, 2008 2008.

[42] M. B. Collier, *et al.*, "Osteolysis after Total Knee Arthroplasty: Influence of Tibal Baseplate Surface Finish and Sterilization of Polyethylene Insert," *Journal of Bone & Joint Surgery, American Volume*, vol. 87, pp. 2702-2708, 2005.

[43] PULOSKI, *et al.*, *Tibial post wear in posterior stabilized total knee arthroplasty : An unrecognized source of polyethylene debris* vol. 83. Boston, MA, ETATS-UNIS: Journal of Bone and Joint Surgery Incorporated, 2001.

[44] P. Ellison and J. Fisher, "Assessment of the damage in retrieved patellar components," *Journal of long-term effects of medical implants*, vol. 20, pp. 57-72, 2010.

[45] Knight L. A., *et al.*, "Comparison of long-term numerical and experimental total knee replacement wear during simulated gait loading," *Journal of biomechanics*, vol. 40, pp. 1550-1558, 2007.

[46] B. Bhushan, *Introduction to tribology*: John Wiley & Sons, 2002.

[47] J. P. Collier, *et al.*, "Impact of gamma sterilization on clinical performance of polyethylene in the knee," *The Journal of Arthroplasty,* vol. 11, pp. 377-389, 1996.

[48] D. L. McDowell and F. P. E. Dunne, "Microstructure-sensitive computational modeling of fatigue crack formation," *International Journal of Fatigue,* vol. 32, pp. 1521-1542, 2010.

[49] T. Elguedj, *et al.*, "A mixed augmented Lagrangian-extended finite element method for modelling elastic–plastic fatigue crack growth with unilateral contact," *International Journal for Numerical Methods in Engineering,* vol. 71, pp. 1569-1597, 2007.

[50] V. Saikko, "A multidirectional motion pin-on-disk wear test method for prosthetic joint materials," *Journal of Biomedical Materials Research,* vol. 41, pp. 58-64, 1998.

[51] L. Kang, *et al.*, "Wear simulation of ultra-high molecular weight polyethylene hip implants by incorporating the effects of cross-shear and contact pressure," *Proceedings of the Institution of Mechanical Engineers, Part H: Journal of Engineering in Medicine,* vol. 222, pp. 1049-1064, 2008.

[52] L. Kang, *et al.*, "Quantification of the effect of cross-shear on the wear of conventional and highly cross-linked UHMWPE," *Journal of biomechanics,* vol. 41, pp. 340-346, 2008.

[53] A. Wang, "A unified theory of wear for ultra-high molecular weight polyethylene in multi-directional sliding," *Wear,* vol. 248, pp. 38-47, 2001.

[54] V. Saikko and J. Kostamo, "RandomPOD—A new method and device for advanced wear simulation of orthopaedic biomaterials," *Journal of biomechanics,* vol. 44, pp. 810-814, 2011.

[55] M. A. Hamilton, *et al.*, "Quantifying Multidirectional Sliding Motions in Total Knee Replacements," *Journal of Tribology,* vol. 127, pp. 280-286, 2005.

[56] T. McGloughlin, *et al.*, "A machine for the preliminary investigation of design features influencing the wear behaviour of knee prostheses," *Proceedings of the Institution of Mechanical Engineers, Part H: Journal of Engineering in Medicine,* vol. 218, pp. 51-62, 2004.

[57] V. Saikko and O. Calonius, "Simulation of wear rates and mechanisms in total knee prostheses by ball-on-flat contact in a five-station, three-axis test rig," *Wear,* vol. 253, pp. 424-429, 2002.

[58] International Organization for Standardization, "Implants for surgery -- Wear of total knee-joint prostheses," in *Loading and displacement parameters for wear testing machines with load control and corresponding environmental conditions for test* vol. 14243-2:2004, ed, 2009.

[59] International Organization for Standardization, "Implants for surgery -- Wear of total knee-joint prostheses," in *Part 3: Loading and displacement parameters for wear-testing machines with displacement control and corresponding environmental conditions for test* vol. 14243-3:2004, ed, 2009.

[60] O. K. Muratoglu, *et al.*, "Aggressive Wear Testing of a Cross-Linked Polyethylene in Total Knee Arthroplasty," *Clinical Orthopaedics and Related Research,* vol. 404, pp. 89-95, 2002.

[61] O. K. Muratoglu, *et al.*, "Knee-simulator testing of conventional and cross-linked polyethylene tibial inserts," *The Journal of Arthroplasty,* vol. 19, pp. 887-897, 2004.

[62] M. R. DiSilvestro, *et al.*, "The design and development of a measurement system for the investigation of dynamic micromotion in total knee joint replacements," *Instrumentation and Measurement, IEEE Transactions on,* vol. 54, pp. 1126-1132, 2005.

[63] D. McNulty, *et al.*, "Influence of Tray Surface Finish on Modular Tibial Tray Micromotion and Wear," in *51st Annual Meeting of the Orthopaedic Research Society*, Washington DC, USA, 2005.

[64] D. McNulty, *et al.*, "Comparison of Static and Dynamic Micromotion Test Methods for Blasted Ti-6-4 and Polished CoCr Modular Tibial Total Knee Components," in *Society for Biomaterials,* 2004.

[65] D. McNulty and S. W. Swope, "Wear of nonmodular and modular total knee tibial components," in *Proceedings of the 31st Annual Meeting of the Society for Biomaterials*, Memphis, TN, USA, 2005.

[66] L. A. Knight, *et al.*, "Comparison of long-term numerical and experimental total knee replacement wear during simulated gait loading," *Journal of biomechanics,* vol. 40, pp. 1550-1558, 2007.

[67] A. Abdelgaied, *et al.*, "Computational wear prediction of artificial knee joints based on a new wear law and formulation," *Journal of biomechanics,* vol. 44, pp. 1108-1116, 2011.

[68] B. J. Fregly, *et al.*, "Computational wear prediction of a total knee replacement from in vivo kinematics," *Journal of biomechanics,* vol. 38, pp. 305-314, 2005.

[69] A. C. Godest, *et al.*, "Simulation of a knee joint replacement during a gait cycle using explicit finite element analysis," *Journal of biomechanics,* vol. 35, pp. 267-275, 2002.

[70] Laz P., *et al.*, "Probabilistic finite element prediction of knee wear simulator mechanics," *Journal of biomechanics,* vol. 39, pp. 2303-2310, 2006.

[71] R. Willing and I. Y. Kim, "A holistic numerical model to predict strain hardening and damage of UHMWPE under multiple total knee replacement kinematics and experimental validation," *Journal of biomechanics,* vol. 42, pp. 2520-2527, 2009.

[72] D. Zhao, *et al.*, "Predicting Knee Replacement Damage in a Simulator Machine Using a Computational Model With a Consistent Wear Factor," *Journal of Biomechanical Engineering,* vol. 130, pp. 011004-10, 2008.

[73] D. Zhao, *et al.*, "Computational Wear Prediction of UHMWPE in Knee Replacements," *Journal o f ASTM International,* vol. 3, pp. 45-50, 2006.

[74] M. A. Strickland, *et al.*, "Could passive knee laxity be related to active gait mechanics? An exploratory computational biomechanical study using probabilistic methods," *Computer Methods in Biomechanics and Biomedical Engineering,* vol. 12, pp. 709-720, 2009/12/01 2009.

[75] M. A. Strickland, *et al.*, "Targeted computational probabilistic corroboration of experimental knee wear simulator: The importance of accounting for variability," *Medical Engineering & Physics,* vol. 33, pp. 295-301, 2011.

[76] M. A. Strickland and M. Taylor, "In-silico wear prediction for knee replacements—methodology and corroboration," *Journal of biomechanics,* vol. 42, pp. 1469-1474, 2009.

[77] M. A. Strickland, *et al.*, "A multi-platform comparison of efficient probabilistic methods in the prediction of total knee replacement mechanics," *Computer Methods in Biomechanics and Biomedical Engineering,* vol. 13, pp. 701-709, 2010/12/01 2010.

[78] J. P. Halloran, *et al.*, "Comparison of Deformable and Elastic Foundation Finite Element Simulations for Predicting Knee Replacement Mechanics," *Journal of Biomechanical Engineering,* vol. 127, pp. 813-818, 2005.

[79] Y. Bei and B. J. Fregly, "Multibody dynamic simulation of knee contact mechanics," *Medical Engineering & Physics,* vol. 26, pp. 777-789, 2004.

[80] J. Lubliner, *Plasticity Theory*: Dover Publications, 2008.

[81] J. S. Bergström, *et al.*, "Constitutive modeling of ultra-high molecular weight polyethylene under large-deformation and cyclic loading conditions," *Biomaterials,* vol. 23, pp. 2329-2343, 2002.

[82] K. L. Johnson, *Contact mechanics*: Cambridge University Press, 1987.

[83] P. S. M. Barbour, *et al.*, "The influence of contact stress on the wear of UHMWPE for total replacement hip prostheses," *Wear,* vol. 181-183, pp. 250-257, 1995.

[84] T. A. Maxian, *et al.*, "A sliding-distance-coupled finite element formulation for polyethylene wear in total hip arthroplasty," *Journal of biomechanics,* vol. 29, pp. 687-692, 1996.

[85] S. Pal, *et al.*, "Probabilistic computational modeling of total knee replacement wear," *Wear,* vol. 264, pp. 701-707, 2008.

[86] J. F. Archard and W. Hirst, "The wear of metals under unlubricated conditions," *Proceedings of the Royal Society A,* vol. 236, pp. 397–410, 1956.

[87] M. Turell, *et al.*, "Quantification of the effect of cross-path motion on the wear rate of ultra-high molecular weight polyethylene," *Wear,* vol. 255, pp. 1034-1039, 2003.

[88] T. S. Johnson, *et al.*, "The effect of displacement control input parameters on tibiofemoral prosthetic knee wear," *Wear,* vol. 250, pp. 222-226, 2001.

[89] D. Jalali-Vahid, *et al.*, "Prediction of lubricating film thickness in UHMWPE hip joint replacements," *Journal of biomechanics,* vol. 34, pp. 261-266, 2001.

[90] R. Y. L. Liow and D. W. Murray, "Which primary total knee replacement? A review of currently available TKR in the United Kingdom," *Ann R Coll Surg Engl,* vol. 79, pp. 335-340, 1997.

[91] J.-M. Brandt, *et al.*, "Commissioning of a displacement-controlled knee wear simulator and exploration of some issues related to the lubricant," *Proceedings of the Institution of Mechanical Engineers, Part H: Journal of Engineering in Medicine,* June 24, 2011 2011.

[92] Godest A. C., *et al.*, "Simulation of a knee joint replacement during a gait cycle using explicit finite element analysis," *Journal of biomechanics,* vol. 35, pp. 267-275, 2002.

[93] Halloran J. P., *et al.*, "Explicit finite element modeling of total knee replacement mechanics," *Journal of biomechanics,* vol. 38, pp. 323-331, 2005.
[94] S. D. Waldman and J. T. Bryant, "Nonlinear Viscoelastic Behaviour of Irradiated Ultra-High Molecular Weight Polyethylene at 37 degrees Celcius," in *ASTM International*, 1994.
[95] McNulty D., *et al.*, "Influence of Tray Surface Finish on Modular Tibial Tray Micromotion and Wear," in *51st Annual Meeting of the Orthopaedic Research Society*, Washington DC, USA, 2005.
[96] McNulty D., *et al.*, "Comparison of Static and Dynamic Micromotion Test Methods for Blasted Ti-6-4 and Polished CoCr Modular Tibial Total Knee Components," in *Society for Biomaterials*, 2004.
[97] C. Allen, *et al.*, "Sliding wear behaviour of ion implanted ultra high molecular weight polyethylene against a surface modified titanium alloy Ti-6Al-4V," *Tribology International,* vol. 29, pp. 527-534, 1996.
[98] Archard J. F. and Hirst W., "The wear of metals under unlubricated conditions," *Proceedings of the Royal Society A,* vol. 236, pp. 397–410, 1956.
[99] I. R. McColl, *et al.*, "Finite element simulation and experimental validation of fretting wear," *Wear,* vol. 256, pp. 1114-1127, 2004.
[100] M. R. Dressler, *et al.*, "Predicting wear of UHMWPE: Decreasing wear rate following a change in direction," *Wear,* vol. 271, pp. 2879-2883, 2011.
[101] M. Z. Huq and J. P. Celis, "Expressing wear rate in sliding contacts based on dissipated energy," *Wear,* vol. 252, pp. 375-383, 2002.
[102] K.-Y. Lee and D. Pienkowski, "Compressive creep characteristics of extruded ultrahigh-molecular-weight polyethylene," *Journal of Biomedical Materials Research,* vol. 39, pp. 261-265, 1998.
[103] A. R. Rao, *et al.*, "Tibial Interface Wear in Retrieved Total Knee Components and Correlations with Modular Insert Motion," *J Bone Joint Surg Am,* vol. 84, pp. 1849-1855, October 1, 2002 2002.
[104] R. C. Wasielewski, "The Causes of Insert Backside Wear in Total Knee Arthroplasty," *Clinical Orthopaedics and Related Research,* vol. 404, pp. 232-246, 2002.
[105] R. C. Wasielewski, *et al.*, "Wear Patterns on Retrieved Polyethylene Tibial Inserts and Their Relationship to Technical Considerations During Total Knee Arthroplasty," *Clinical Orthopaedics and Related Research,* vol. 299, pp. 31-43, 1994.
[106] J. M. Brandt, *et al.*, "Commissioning of a displacement-controlled knee wear simulator and exploration of some issues related to the lubricant," *Proc Inst Mech Eng H,* vol. 225, pp. 736-52, Aug 2011.
[107] A. Galvin, *et al.*, "Wear of crosslinked polyethylene under different tribological conditions," *Journal of Materials Science: Materials in Medicine,* vol. 17, pp. 235-243, 2006.
[108] A. Wang, *et al.*, "Lubrication and wear of ultra-high molecular weight polyethylene in total joint replacements," *Tribology International,* vol. 31, pp. 17-33, 1998.

[109] J.-M. Brandt, *et al.*, "Retrieval analysis of modular total knee replacements: Factors influencing backside surface damage," *The Knee*.
[110] J. P. Halloran, *et al.*, "Explicit finite element modeling of total knee replacement mechanics," *Journal of biomechanics*, vol. 38, pp. 323-331, 2005.
[111] H.-W. Fang, *et al.*, "Conformational and adsorptive characteristics of albumin affect interfacial protein boundary lubrication: From experimental to molecular dynamics simulation approaches," *Colloids and Surfaces B: Biointerfaces*, vol. 68, pp. 171-177, 2009.
[112] Y. C. Kong, *et al.*, "The molecular dynamics simulation of boundary-layer lubrication," *Molecular Physics*, vol. 92, pp. 7-18, 1997/09/01 1997.
[113] J.-H. Song, *et al.*, "A comparative study on finite element methods for dynamic fracture," *Computational Mechanics*, vol. 42, pp. 239-250, 2008.